

# Upper Mantle Discontinuities beneath South Africa

Results of the analysis of P-to-S  
converted phases.

---

Paul Andrew Cattermole

A Dissertation Submitted to the Faculty of Science  
University of the Witwatersrand, Johannesburg  
for the Degree of Master of Science

Johannesburg 1994

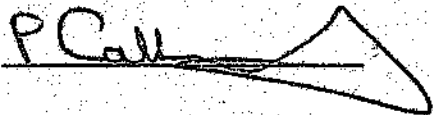
## ABSTRACT.

This dissertation investigates the upper mantle discontinuities beneath South Africa by analysing seismic waves converted from P to Sv recorded at an array of broad-band seismometers. Events, with desirable characteristics recorded at each station are transformed to a suitable coordinate system, normalised, and stacked to enhance the weak converted phases. Additional low pass filters are also applied to improve the signal to noise characteristics of the data.

No data suitable for processing were found for stations outside the Kaapvaal Craton. Despite additional problems related to the application of sub-optimum numerical routines to a limited data base, by combining results with those from an independent study two models were derived for the '400 km' and '670 km' discontinuities beneath the Craton. Models for the '670 km' discontinuity accord with a simplified global earth model while models for the '400 km' discontinuity indicate the presence of a low shear velocity layer not supported in a global earth model. Additional broad band seismic data must be acquired to investigate this phenomenon further.

## DECLARATION.

I declare that this dissertation is my own, unaided work. It is being submitted for the degree of Master of Science in the University of the Witwatersrand, Johannesburg. It has not been submitted before for any degree or examination in any other University.

A handwritten signature in black ink, appearing to read 'P.A. Cattermole', with a large, sweeping flourish extending to the right.

P.A. Cattermole

21 day of January, 1994.

## ACKNOWLEDGEMENTS.

As is normal with a document of this nature, it is impossible to acknowledge everyone who has offered assistance or advice during its compilation. The following people and organisations do, however, warrant special mention:

Dr R W E Green, my supervisor without whose help and advice this document would never have been completed. Special thanks are extended to him for supplying me with copies of various papers awaiting publication.

Dr A Clchowicz, my co-supervisor who got me started and assisted me during the project.

Other staff members associated with the Lithosphere Project. These include:

Ms E Peberdy who compiled invaluable information about events recorded during the project while doing her own research; Mr M Cronje who assisted with the hardware; and his wife whose efforts in compiling the final data base cannot be underestimated.

The staff of the Geophysics Department at the University of the Witwatersrand, especially Dr R J Durrheim for his encouragement and Mr G Cooper for his patience and assistance with Fortran programming during the early days of this research.

The Anglo American Corporation of South Africa who allowed me the time and financial assistance to commence the project. Special thanks are extended to Mr E O Kostlin and Mr K Biesheuvel in this regard.

The Anglo American Prospecting Services' Klerksdorp Office for their understanding while the project was being completed. In particular I would like to thank Mr P J Brirckman who allowed me to avail myself of the office's drafting and printing facilities; Mr W H B Steenkamp for his assistance; the ladies of the drafting office notably Mrs B Enslin who completed the final figures and Mrs L Roets and the secretarial staff for their help.

Finally, I would like to thank Svenja Miller and Monique Smith who proof read the final draft.

This document was produced on a 386 DX personal computer and HP Laserjet Series III printer using Wordperfect 5.1 software.

To my family for their support and to my friends who endured me during the final write-up.

## TABLE OF CONTENTS.

1) INTRODUCTION. . . . .	5
1.1) The Lithosphere Project. . . . .	5
1.2) Geological Setting. . . . .	8
1.3) Seismic Investigations of Upper Mantle Structure. . . . .	12
2) THEORY. . . . .	15
2.1) General Seismic Theory. . . . .	15
2.1.1) Reflection and refraction of seismic waves . . . . .	15
2.1.2) Travel time considerations . . . . .	18
2.2) Theory of the Analysis of P-to-S Converted Phases. . . . .	20
3) DATA ACQUISITION AND PROCESSING. . . . .	27
3.1) PC Based Field Recording System. . . . .	27
3.2) Preprocessing. . . . .	32
3.3) Data Processing. . . . .	33
3.4) Selection of Processed Events. . . . .	45
4) RESULTS. . . . .	48
4.1) Results for Station BPI. . . . .	50
4.2) Results for Station DOU. . . . .	55
4.3) Results for Station JAN. . . . .	60
4.4) Results for Station PIL. . . . .	65
4.5) Results for Station KLI. . . . .	70
4.6) The 400 km Discontinuity Revisited. . . . .	75
4.7) Summary of Results. . . . .	77
5) DISCUSSION. . . . .	78
5.1) Methodology. . . . .	78
5.2) Implications for the Upper Mantle Discontinuities. . . . .	85
5.2.1) The importance of the upper mantle discontinuities. . . . .	85
5.2.2) Current thinking on upper mantle rheology - a simplified model. . . . .	87
5.2.3) Upper mantle discontinuities beneath South Africa. . . . .	91
6) CONCLUSIONS. . . . .	95
7) REFERENCES. . . . .	98

## LIST OF ILLUSTRATIONS.

Figure 1.1.1 - Location of broad-band field stations utilised for the Lithosphere Project. . . . .	6
Table 1.1.1 List of broad-band field stations showing full station name, geographic coordinates and operation dates. . . . .	7
Figure 1.2.1 - The geological provinces of South Africa (simplified from Tankard et al (1982). . . . .	9
Figure 1.2.2 - Geological evolution of southern Africa (after Tankard et al 1982). . . . .	11
Figure 2.1.1 - Two Media ( $M$ and $M'$ ) in welded contact separated by a plane boundary. . . . .	16
Figure 2.1.2 - Seismic ray in a multilayered earth . . . . .	19
Figure 2.2.1 - Three component seismometer in a Cartesian coordinate system. . . . .	21
Figure 2.2.2 Relationship between the vertical, radial, principle and transverse $H$ components . . . . .	22
Figure 2.2.3 - Relationship between the normalised $H(t)$ and $L(t)$ components and $t_{p_0}$ . . . . .	24
Figure 3.1.1 - Three components rotated to the correct polarities for an event at SSI on 09/05/90 recorded at Douglas. The clarity of the P arrivals for all three components is noted. . . . .	31
Figure 3.3.1 - Output from filon of velocity data for an event in the South Sandwich Islands . . . . .	37
Figure 3.3.2 - Filtered versions of the velocity records shown in figure 3.3.1 . . . . .	38
Figure 3.3.3 - Radial and transverse components of the velocity records shown in figure 3.3.1 . . . . .	39
Figure 3.3.4 - $H(t)$ and $L(t)$ components calculated from the components displayed in figure 3.3.3 and the emergent angle $e$ determined in calce. . . . .	40
Figure 3.3.5 - Normalised, cross correlated components $\hat{H}$ and $\hat{L}$ . . . . .	41
Table 3.3.1. - Theoretical angles of incidence for P waves at the base of the crust (after Ben-Menahem and Singh, 1981). Intermediate values	



obtained by linear interpolation. . . . .	42
Table 3.3.2. - Simplified IAPeI 91 velocity model (after Kennett, 1991). . . . .	43
Table 3.3.3. - Table showing phasing depth, travel time delay and normalised travel time delay $\delta t$ . Time delays corresponding to phasing depths of 400 km and 670 km are pertinent to this study. . . . .	44
Table 3.4.1 - List of suitable events used for stacking at stations BPI, DOU, SAN, PIL and KLI. . . . .	47
Figure 4.1 - Relationship between the near surface converted phases. . . . .	49
Figure 4.1.1 - Result of broad-band stack from station BPI. . . . .	51
Figure 4.1.2 - Result of intermediate period stack from station BPI. . . . .	52
Figure 4.1.3 - Result of long period stack from station BPI. . . . .	53
Figure 4.1.4 - Near surface conversions for station BPI. . . . .	54
Figure 4.2.1 - Result of broad-band stack from station DOU. . . . .	56
Figure 4.2.2 - Result of intermediate period stack from station DOU. . . . .	57
Figure 4.2.3 - Result of long period stack from station DOU. . . . .	58
Figure 4.2.4 - Near surface conversions for station DOU. . . . .	59
Figure 4.3.1 - Result of broad-band stack from station SAN. . . . .	61
Figure 4.3.2 - Result of intermediate period stack from station SAN. . . . .	62
Figure 4.3.3 - Result of long period stack from station SAN. . . . .	63
Figure 4.3.4 - Near surface conversions for station SAN. . . . .	64
Figure 4.4.1 - Result of broad-band stack from station PIL. . . . .	66
Figure 4.4.2 - Result of intermediate period stack from station PIL. . . . .	67
Figure 4.4.3 - Result of long period stack from station PIL. . . . .	68
Figure 4.4.4 - Near surface conversions for station PIL. . . . .	69
Figure 4.5.1 - Result of broad-band stack from station KLI. . . . .	71
Figure 4.5.2 - Result of intermediate period stack from station KLI. . . . .	72

Figure 4.5.3 - Result of long period stack from station KLI. . . . .	73
Figure 4.5.4 - Near surface conversions for station KLI. . . . .	74
Figure 4.6 - Additional stacks produced for the 400 km discontinuity. . . . .	76
Figure 5.1.1 - Broad-band stack at station KLI after Vinnik(1992). . . . .	79
Figure 5.1.2 - Long period stack at station BPI after Vinnik(1992). . . . .	80
Figure 5.1.3 - Long period stack at station PIL after Vinnik(1992). . . . .	81
Figure 5.1.4 - Result of broad-band stack for two events recorded at BPI. . . . .	82
Figure 5.2.1 - Calculated compressional velocities plotted against depth for a variety of mantle minerals. . . . .	86
Figure 5.2.2. - Phase diagram of the olivine system showing the stability fields of various stable phases. . . . .	87
Figure 5.2.3 - Phase relations in pure $MgSiO_3$ . . . . .	88
Table 5.2.1 - Simplified global model pertaining to the 400 km and 670 km discontinuities. . . . .	90
Table 5.2.2 - Summary of results and models related to the upper mantle discontinuities beneath South Africa. . . . .	94

# 1) INTRODUCTION.

## 1.1) The Lithosphere Project.

The deep structure of the lithosphere is a contentious issue with many of its properties yet to be determined properly; for example the depth to the base of the lithosphere, the degree of vertical and horizontal heterogeneity and the nature of the interface with the underlying asthenosphere. This dissertation uses data from the South African Lithosphere Project, an industry sponsored project initiated to answer questions such as these and to define the deep structure of the Kaapvaal cratonic lithosphere and asthenosphere and their relationships to the surrounding mobile belts.

The Lithosphere Project employed the 25 South African Geological Survey (SAGeo) seismic stations and 8 broad-band field stations specially designed for the project (see section 3.1). These formed a combined array, covering most of the Kaapvaal craton extending into the Namaqua-Natal mobile belt, to record seismic events. In general teleseismic events were of greater utility to the project than local (mine induced) seismic events. All data discussed in this dissertation pertain to teleseisms recorded by the broad-band field stations which were operational between May 1988 and December 1991 when the project was terminated. The operation dates of the eight stations are presented in table 1.1.1 while the locations are shown in figure 1.1.1.

Although the data recording aspect of the project has terminated, at the time of writing this dissertation, progress was still being made with processing and interpreting data to complement work that has already been completed. Completed work includes use of the spectral ratio method to define crustal parameters for each of the eight field stations (Muller, 1991), a study of velocity anisotropy using wave polarisation characteristics from three component ground motion (Vinnik et al, 1993a), and studies involving P and PKP travel time residuals (Green, 1991a). P-to-S

converted phases were also investigated independently and concurrently with the present study - results are presented in Vinnik et al (1993b) and in an internal University of the Witwatersrand document (Vinnik, 1992).

Although Jordan(1975) indicated that the lithosphere may extend to a depth of approximately 400 km, it is more generally accepted that it extends to a depth of only about 200 km. Therefore the current study falls outside the main brief of the lithosphere project as it investigates upper mantle structures at depths of approximately 400 km and 670 km.

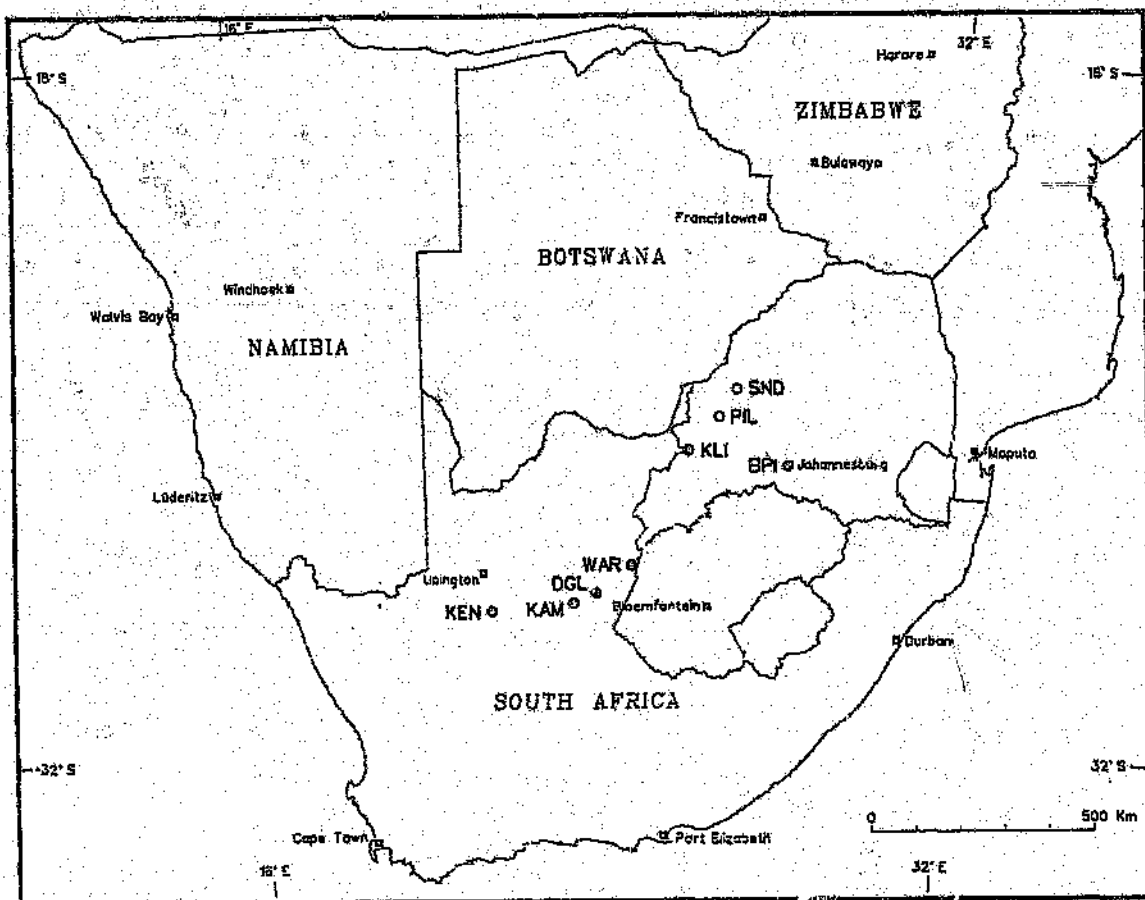


Figure 1.1.1 - Location of broad-band field stations utilised for the Lithosphere project.

STN.	NAME	LAT.	LONG.	ELEV. (m)	Date On	Off.
PIL	Pilanes -burg	25.221S	27.101E	1218	Apr 90	Dec 90
BPI	Johanne- sburg	26.175S	28.030E	1700	Jul 89	Dec 90
DOU	Douglas	29.115S	23.804E	1109	May 88	Dec 90
KEN	Ken -hart	29.742S	21.095E	872	Jul 88	Jan 89
KLI	Klipveld	25.853S	26.266E	1576	Jan 89	Dec 90
KAM	Kameel -puts	29.135S	23.125E	1173	Jul 89	Dec 90
SAN	Sand -rivier	24.626S	27.617E	950	Feb 90	Dec 90
WAR	Warr -enton	28.377S	24.891E	1173	Jul 88	Jan 90

Table 1.1.1 List of broad-band field stations showing full station name, geographic coordinates and operation dates.

## 1.2) Geological Setting.

Since this project is concerned with an investigation of features below the accepted depth of the lithosphere/asthenosphere boundary, an in-depth understanding of the surface geological setting of the eight seismic stations is not required. However, since the research is partly concerned with investigating if variations in the structures of interest - upper mantle discontinuities at depths of approximately 400 km and 670 km - correspond to variations in the gross surface geology, a general overview of this geology after Tankard et al(1982) is presented.

Traditionally the Precambrian tectonic units that make up the structural framework of Southern Africa have been designated as mobile belts or cratons. Mobile belts were defined as younger, linear metamorphic belts which surround ancient cratons. However, it has since been realised that the Limpopo mobile belt is older than the adjacent Zimbabwe and Kaapvaal cratons and is not a belt in the true sense. Tankard et al(1982) believe that cratons are the final stage in the life span of a mobile belt - in other words a craton is a mobile belt in an advanced evolutionary stage - and prefer the use of the nongenetic term "province" to describe the various tectonic units. A geological map showing these provinces is presented in figure 1.2.1.

In terms of the present study, however, the difference between a mobile belt and a craton is critical. The Kaapvaal Craton is an archaean craton while the Namaqua Natal Mobile Belt is an example of proterozoic orogenic activity. Each of these has its own geological and geophysical characteristics as would be expected from crustal evolutionary models (Windley, 1984). For example, evidence from heat flow data (Jones 1987, 1988) suggests a reduced lithospheric thickness for the Namaqua Mobile Belt with respect to the Kaapvaal Craton. The Kaapvaal Craton and the surrounding mobile belts must therefore be considered in terms of their differing geological and geophysical properties. This is part of the reason why the seismic array transected both the Kaapvaal Craton and the Namaqua Natal Mobile Belt. Another aim of the present study is to examine whether differences in the lithospheric mantle correspond to any differences at depths corresponding to the upper mantle discontinuities.

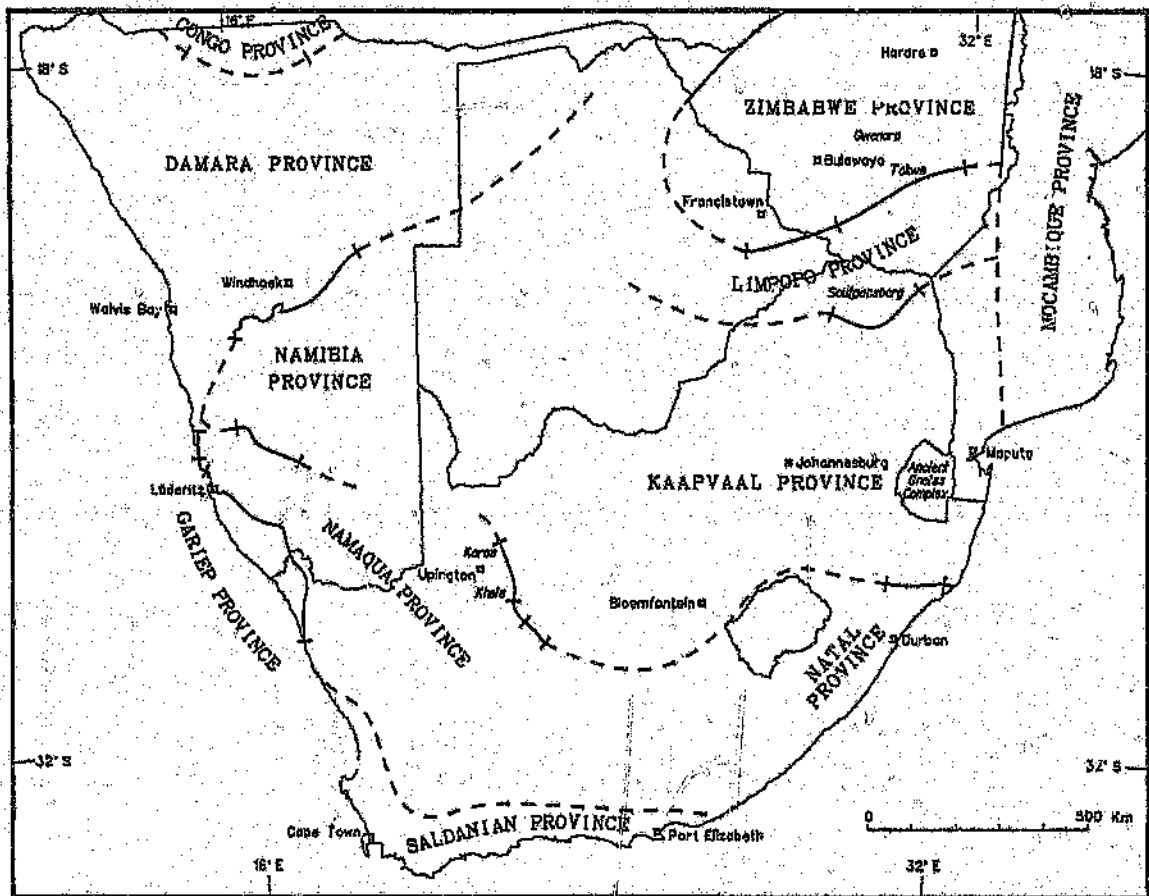


Figure 1.2.1 - The geological provinces of South Africa (simplified from Tankard et al (1982).

Tankard et al(1982) believe that the southern African crust has passed through the five well defined evolutionary stages discussed below. A more detailed chronology of the crustal evolution of Southern Africa is reproduced in figure 1.2.2.

- 1) Archaean pre-crustal development which gave rise to crystalline massifs represented by the Kaapvaal, Limpopo and Zimbabwe provinces;
- 2) During the early Proterozoic this basement was buried beneath the largely sedimentary cover of for example the Pongola, Witwatersrand and Transvaal Supergroups. The Archean-Proterozoic boundary is characterised by a period of cratonic stabilization which resulted from a decreased heat flow and an increased thickness of continental crust. The intrusion of the Igneous Bushveld Complex also occurred during this period.
- 3) A stage of Proterozoic orogenic activity characterised by intense orogeny in the southern and western parts of the subcontinent. This period persisted until the start of the Phanerozoic and gave rise to the Namaqua and Natal provinces.
- 4) The Gondwana era is marked by a period of abortive rifting and continental sedimentation which resulted in the Cape and Karoo Supergroups.
- 5) The period after the Gondwana era is marked by massive scale continental rifting and the development of limited Cenozoic marine sedimentary deposits.

Station KEN was situated on the granitic gneisses of the Namaqua province formed during phase 3. All of the other stations were situated in the Kaapvaal Province in geological environments formed during phases 2, 3 and 4. BPI was sited on the Witwatersrand Supergroup sediments, DOU and WAR were situated on the Ventersdorp Lavas, KLI and SAN were situated on Pretoria Group dolomites, KAM was situated on Karoo Dwyka and PIL was situated within the Pilanesburg Complex (phase 3).



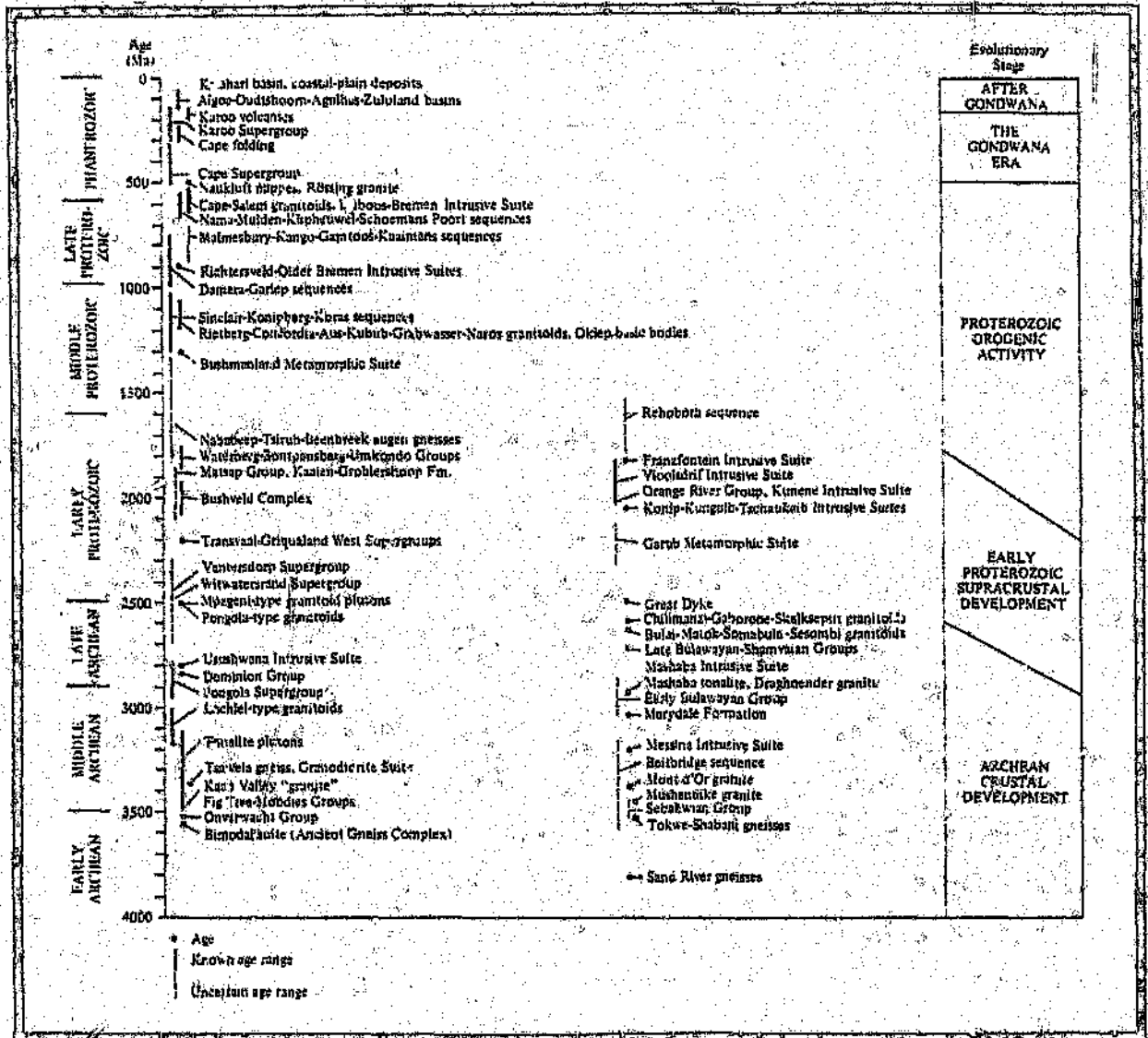


Figure 1.2.2 - Geological evolution of southern Africa (after Tankard et al 1982).

### 1.3) Seismic Investigations of Upper Mantle Structure.

Much progress has been made during this century in defining the structure of the earth at depth with seismic techniques having played a major role in this regard. Present day studies are centred around examining the fine scale structure of the earth's four main structural components which are the crust, the mantle, the outer core and the inner core.

Evidence for the possible existence of upper-mantle discontinuities above 1000 km beneath the earth's surface has existed since the 1920's. For example Byerly(1926) produced evidence for a change in the slope of the travel time curve of P waves at an epicentral distance of approximately  $20^\circ$  in 1926. Later analyses of P wave travel data by Byerly(1935) revealed discontinuities at epicentral distances of approximately  $17^\circ$  and  $28^\circ$ .

The results of additional studies yielding evidence for upper-mantle discontinuities from this time to the mid-1960's; when the existence of two discontinuities, one at a depth of approximately 400 km and the other at approximately 670 km was confirmed ((Nazari and Anderson(1965), Green and Hales(1968), Julian and Anderson(1968), Archambeau et al(1969)); are summarised by Anderson(1965). Today these discontinuities are generally referred to as the '400 km' and '670 km' discontinuities as these are the depths ascribed to them by most reference earth models, for example the Preliminary Reference Earth Model (PREM), (Dziewonski and Anderson, 1981). An understanding of the nature of these discontinuities is crucial in the understanding of mantle convection and its implications for many branches of the earth sciences.

All of the studies during the 1960's cited above employed seismological techniques involving an analysis of P wave travel times. Because of this the '400 km' and '670 km' discontinuities were referred to as seismological or velocity discontinuities. If these discontinuities manifest themselves geophysically there has to be some geological transition occurring at these depths - in other words there has to be an

inherent change in mantle material rheology across the boundaries.

Much research has been conducted in an attempt to establish whether these boundaries are characterised by simple phase transitions of a single bulk mantle material (which implies a chemically homogeneous upper mantle) or whether the actual chemistry of the material at these boundaries changes either with, or without, an associated phase change. Work in this field, which includes relating observed laboratory results of phase and chemical transitions of assumed mantle materials (experimental petrology) to seismic observations, includes that of Anderson(1976), Lees et al(1983), Bass and Anderson(1984), Weidner(1985), Anderson and Bass(1986), Meade and Jeanloz(1990) and Shearer(1991).

The success of any such analyses depend not only on the accuracy of the laboratory measurements but also on the accuracy of the seismic data and the analysis thereof. The major breakthrough in the field of seismic data acquisition is the advent of high resolution, broad-band, digital seismograph networks as discussed by Romanowicz and Dziewonski(1987) and in a South African context by Green(1992).

The global inversion of travel time and surface wave observations (seismic tomography), although relying on accurate global seismic data, is a significant development in the field of seismic data analysis in that it allows for three dimensional inversion and modelling of the earth's structure. The results of such inversions include those of Dziewonski and Anderson(1984), while Woodhouse and Dziewonski(1984) and Anderson(1987), refer more specifically to the upper mantle.

The properties of the upper mantle discontinuities which are pertinent to this study (depth, order and lateral variation) cannot be derived from the limited data of long range profiles, however, "To meet demands for higher resolution and accuracy, a technique of seismic probing using long-period waves converted from P to S within the mantle transition zone was developed and applied to a few sets of seismic records" (Fuchs et al,1987). This method was originally described by Vinnik(1977) and Vinnik et al(1983) and involves the following processing procedures:

- 1) Events with suitable characteristics recorded at each station are transformed to an orthogonal coordinate system containing the principal axis.
- 2) Each event is normalised by cross-correlating the component containing the vertically polarised shear energy with the pulse corresponding to the P onset.
- 4) Normalised events are stacked to enhance the weak converted phases.
- 5) Additional low pass filters may be applied to improve the data's signal to noise characteristics.

Other papers which describe use of the method (with possible modifications) for a variety of applications include Paulssen(1985), Qiyuan and Kind(1986), Souriau(1986), Wajeman and Souriau(1987), and Kind and Vinnik(1988). P-to-S converted phases have also been studied previously in South Africa by Cichowicz (personal communication) and by Vinnik (1992).

This dissertation describes how data acquired over a three year period by the Lithosphere Project broad-band stations were used to investigate P-to-S converted phases from depths of 400 km and 670 km with an aim to gain insight into the nature of discontinuities at these depths for a variety of geographical locations. It is stated at the outset that the processed data discussed in this dissertation are of limited utility in understanding the nature of these discontinuities. This will become evident in the presentation of the results (section 4) while reasons for this will be discussed in section 5.

## 2) THEORY.

### 2.1) General Seismic Theory.

An understanding of P to S converted phases at any seismic boundary requires an understanding of some elementary physics pertaining to the reflection and refraction of elastic waves. Detailed descriptions and derivations of equations related to the theory of transmission of seismic waves across a boundary surface of elastic media are presented in most standard texts on seismic theory, for example Bullen and Bolt(1985) and Ben-Menahem and Singh(1981). The purpose of this section is not to repeat these descriptions but rather to highlight some of the important concepts.

#### 2.1.1) Reflection and refraction of seismic waves

Consider two homogeneous media M and M' (after the notation of Bullen and Bolt, 1985) in welded contact separated by a plane boundary which is taken to be horizontal (fig 2.1.1). Consider the laws of reflection and refraction for plane waves (for example a P wave) propagating through the medium M towards this boundary. O is the origin at any point on the boundary  $Ox_1$ , and  $Ox_2$  points normally into the medium M'. Let  $V_{p_1}$ ,  $V_{p_2}$ ,  $V_{s_1}$  and  $V_{s_2}$  be the respective compressional and shear wave velocities in the two media.

If the angle between the normal to the incident wave front and the normal to  $Ox_1$  is  $i_1$  (the angle of incidence) then the angle between the normal to the wave front and the normal to  $Ox_1$  for the reflected P wave is also  $i_1$ , while that of the reflected S wave will be  $i_1'$ . The corresponding angle for the refracted P wave (propagating in medium M') is  $i_2$  and for the refracted S wave  $i_2'$ . The reflected S wave and refracted P and S waves are a result of the mathematical conditions which state:

$$\sum u_1 = \sum u_2 \quad \sum w_1 = \sum w_2$$

where  $u_i$  and  $w_i$  are the components of particle motion parallel to and perpendicular to the boundary respectively (Howell, 1959). These conditions imply displacement continuity - that is the sum of the motions both parallel and perpendicular to the boundary on either side are equal.

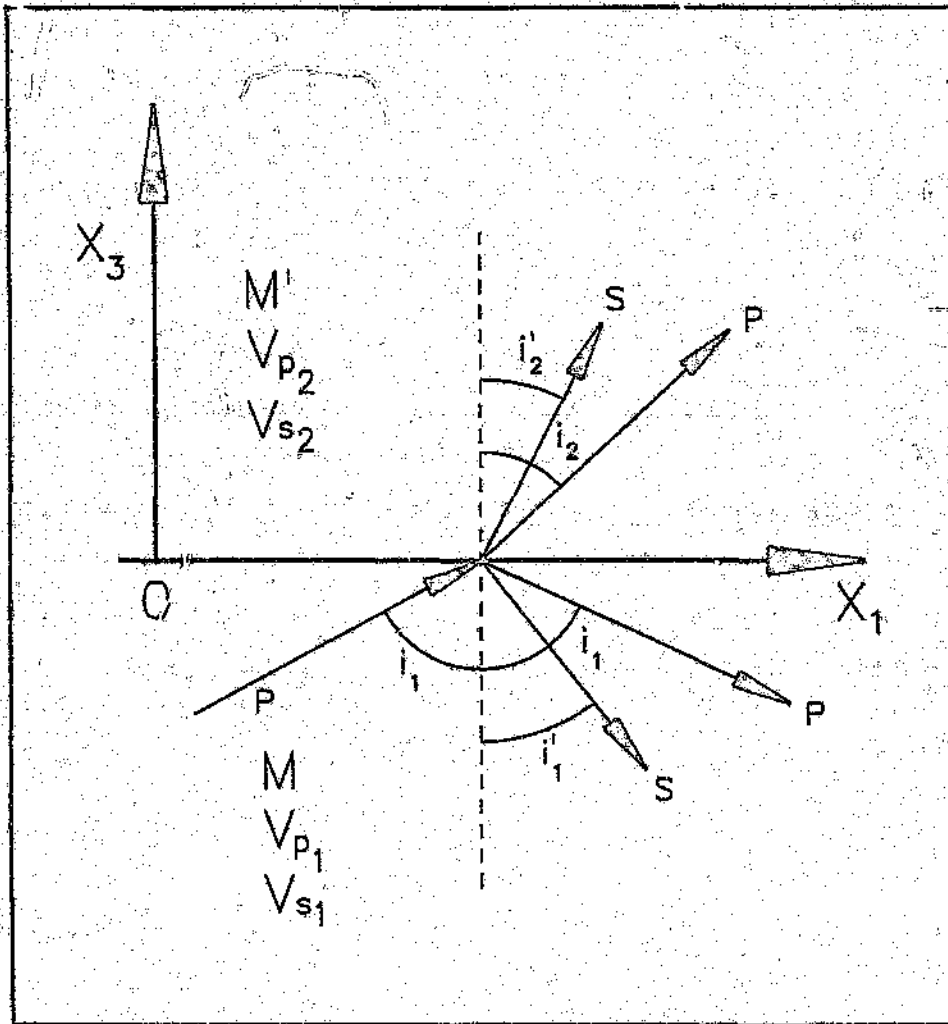


Figure 2.1.1 - Two Media (M and M') In welded contact separated by a plane boundary.

By considering Fermat's principle, or more simply Huygens principle, a relationship is derived which relates the compressional and shear velocities in media M and M' to the angle that the respective ray path of the seismic wave makes to the normal of Ox<sub>1</sub>. This relationship is referred to as Snell's law which states:

$$\frac{\sin i_1}{V_{P_1}} = \frac{\sin i_2}{V_{P_2}} = \frac{\sin i_1'}{V_{S_1}} = \frac{\sin i_2'}{V_{S_2}} \quad 2.1.1$$

The partition of the energy of the incident wave front at an interface must be considered. This partition of energy (or amplitudes) is described by the Zoeppritz equations. Solutions of these equations generally yield the amplitude of the reflected or refracted wave relative to the amplitude of the incident wave. Many papers which present solutions of the Zoeppritz equations for incident P and S waves as a set of simultaneous equations, for example McCamy et al(1962), have been published. However, as noted by Young and Brille(1976), many of these solutions contain errors or ambiguities in the sign conventions used. The problem was resolved by Hales and Roberts(1974) and the solutions as stated, for example by Ben-Menahem and Singh (1981) are assumed to be correct. With respect to the present study it is sufficient to note that the solutions to the equations (and consequently the relative amplitudes and energies of the reflected and refracted phases) are dependant only on the parameters listed in equation (2.1.1) and the densities of the two media across the boundary.

Theoretical equations can be derived for the compressional and shear propagation velocities in a medium. One such expression for these equations, as stated by Bullen and Bolt (1985) is as follows:

$$V_P = \sqrt{\frac{k + 4/3\mu}{\rho}} \quad V_S = \sqrt{\frac{\mu}{\rho}} \quad 2.1.2$$

where k is the bulk modulus of the medium,  $\mu$  the rigidity and  $\rho$  the density. Since these parameters are all related to the nature and the rheology of the material constituting the medium, it is easy to understand why the angles of reflection and

refraction, and the relative amplitudes of the various wave phases across a seismic discontinuity are dependant on the geological conditions at such a boundary.

The above discussion pertains to two homogeneous media separated by a sharp seismic discontinuity where the characteristics of medium M change abruptly to those of M' at the boundary  $Ox_1$ . This is called a first order seismic discontinuity. A second order seismic discontinuity is one where the properties of one medium change gradually to the properties of another medium over a vertical depth interval. The partition of the amplitude of the incident wave front across a second order discontinuity can be analyzed by considering a number of discrete, juxtaposed seismic layers or by numerical techniques like the finite element method. For the present discussion the following features of the two types of discontinuity are relevant:

- the amplitudes of the transmitted phases at a first order boundary are independent of the frequency of the phase,
- second order boundaries transmit lower frequencies preferentially. The more gradual the transition the greater the attenuation of the high frequency component of the seismic wavefront.

### 2.1.2) Travel time considerations

A multilayered earth as shown in figure 2.1.2. is now considered. Starting with equation 2.1.1 it is easy to show that:

$$\frac{r_1 \sin i_1}{V_{P_1}} = \frac{r_2 \sin i_2}{V_{P_2}} = \frac{r_3 \sin i_3}{V_{P_3}} = \dots = p \quad 2.1.3$$

where  $r$  is the radius from the centre of the earth to any point on the seismic ray and  $p$  is a constant for that ray known as the ray parameter. If  $T$  is the travel time for a seismic ray over an arc (epicentral) distance  $\Delta$  then



$$p = \frac{dT}{d\Delta}$$

2.1.4

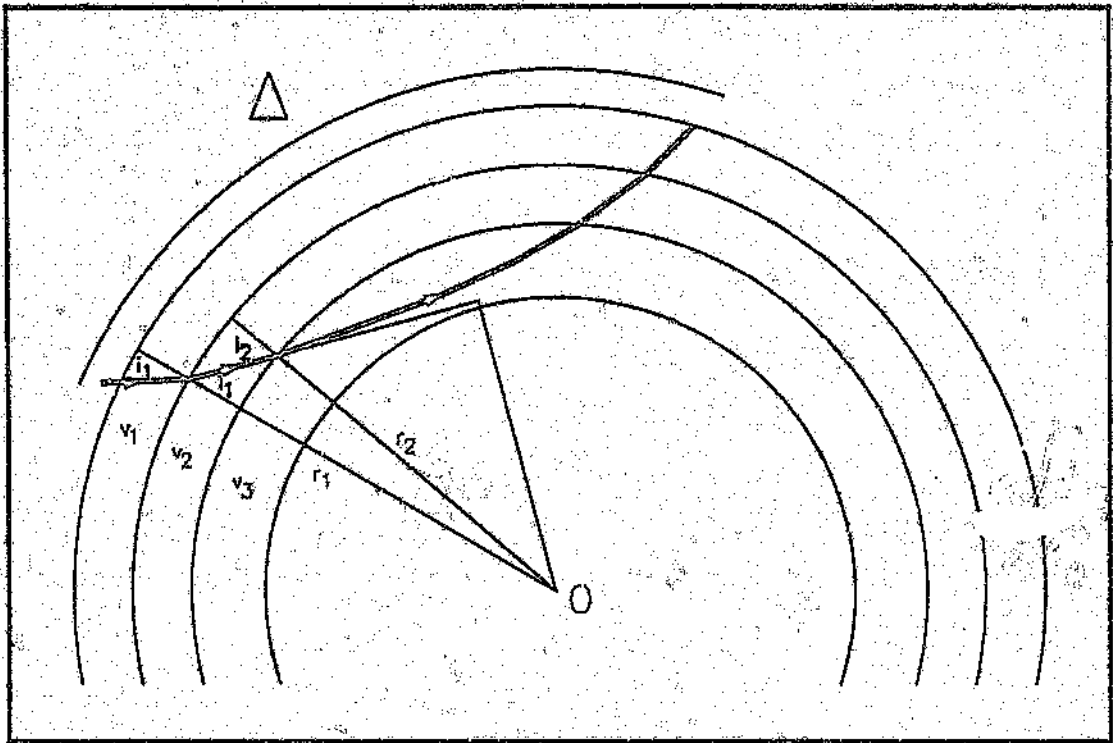


Figure 2.1.2 - Seismic ray in a multilayered earth

Using the definition of  $p$  in equation 2.1.4, integral expressions relating  $T$  and  $\Delta$  can be derived. One such expression (Bullen and Bolt, 1985) relating travel time to epicentral distance is as follows:

$$T = p\Delta + 2 \int_{r_p}^{r_s} r^{-1} (\eta^2 - p^2)^{1/2} dr \quad 2.1.5$$

where

$$\eta = \frac{r}{v} \quad 2.1.6$$

$v$  is the velocity of the seismic phase,  $r_p$  is the radial distance to any point on the ray and  $r_0$  is the earth's radius. Using definition 2.1.6, equation 2.1.5 can be rewritten in the following form:

$$T = p\Delta + 2 \int_{r_p}^{r_0} \left( \frac{1}{v^2} - \frac{p^2}{r^2} \right)^{1/2} dr \quad 2.1.7$$

## 2.2) Theory of the Analysis of P-to-S Converted Phases.

In section 2.1 the phenomenon of the polarisation of the reflected or transmitted S wave was ignored. If the stress vector associated with the displacement across a boundary is considered, it is apparent that an incident P wave generally gives rise to reflected and transmitted Sv waves (Ben-Menem and Singh, 1981). The notation Sv signifies a shear wave that is polarised in the vertical plane.

Hence, an analysis of seismic waves converted from P to S at either the 400 km or 670 km discontinuity involves the detection of long period waves converted from P to Sv at the receiver side of the raypath from a distant earthquake. Since the P-Sv phase is generally a weak phase (with energies of a few percent of that of the P-wave) it is necessary to enhance the signal-to-noise ratio by rotating the records to an H and L coordinate system as discussed below. It is also necessary to stack the standardised H-component records of many events received at the same seismograph station (Vinnik, 1977).

Consider a three component seismometer in a Cartesian coordinate system (figure

2.2.1).

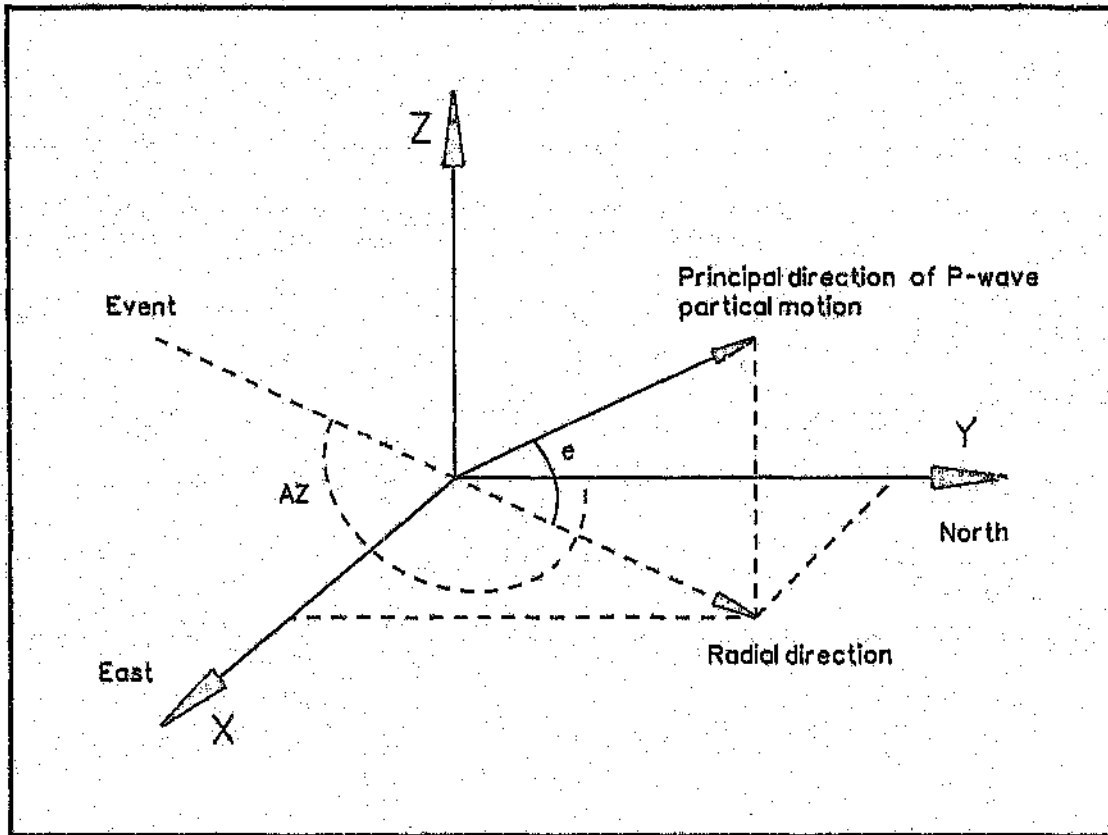


Figure 2.2.1 - Three component seismometer in a Cartesian coordinate system.

Components X, Y, and Z correspond to the east/west, north/south and vertical components respectively. Sv waves are best detected by projecting the particle motion onto an axis which lies in the vertical plane containing the principle direction of the P-wave motion and which is perpendicular at the same time to the principle direction (figure 2.2.2) (Vinnik, 1977). The denotation for this component is  $H(t)$  while that along the principle direction is  $L(t)$ . If the emergent angle (the angle between the principle direction and the radial component in the horizontal plane) is  $\phi$  then:

$$H(t) = R(t) \sin(e) - Z(t) \cos(e) \quad 2.2.1$$

$$L(t) = Z(t) \sin(e) + R(t) \cos(e) \quad 2.2.2$$

where  $R(t)$  is the radial component calculated from the following equation and  $AZ$  is the back azimuth of the event:

$$R(t) = -X(t) \cos(AZ) - Y(t) \sin(AZ) \quad 2.2.3$$

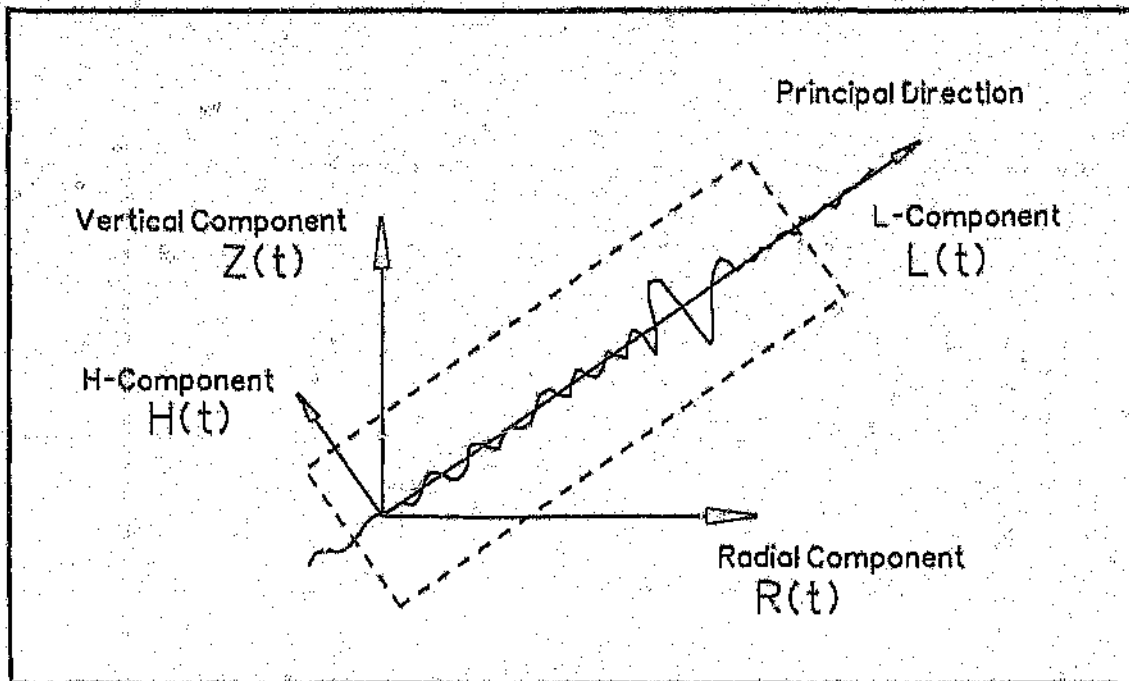


Figure 2.2.2 Relationship between the vertical, radial, principle and H components

The principal direction, discussed in connection with equations 2.2.1 and 2.2.2 is essentially the direction of the P-wave ray path. The emergent angle  $\theta$  can be approximated from tables, for example that of Ben-Menahem and Singh(1981) (see figure 3.3.6) in conjunction with an appropriate crustal correction factor. It is desirable, however, to calculate this angle automatically for each seismic event using the method of Husebye et al (1975) as quoted in Vinnik et al (1983):

$$\theta = \arctan\left(\frac{\langle R(t)Z(t) \rangle}{(\lambda - \langle Z^2(t) \rangle)}\right) \quad 2.2.4$$

where  $\langle \rangle$  denotes averaging over the time period of the P-wave duration. This time period is easily estimated by examining the velocity record of the event.  $\lambda$ , is the bigger root of the equation:

$$(\langle Z^2(t) \rangle - \lambda)(\langle R^2(t) \rangle - \lambda) - \langle R(t)Z(t) \rangle^2 = 0 \quad 2.2.5$$

The  $H(t)$  component must be standardised to account for the differences in the magnitudes and the source functions of the various events being analysed (Vinnik et al, 1983). The standardised  $H(t)$  component can be expressed as follows:

$$\hat{H}(t) = \frac{\int_{t_1}^{t_2} H(t + \tau) * L(\tau) d\tau}{\int_{t_1}^{t_2} [L(\tau)]^2 d\tau} \quad 2.2.6$$

where  $t$  is now the time delay of the cross-correlation between  $H$  and  $L$  and  $t_1$  and  $t_2$  correspond to the first-arrival time and the end of the P-wave train respectively.

If it is assumed that the form of the converted Ps-wave train is similar to that of the P-wave train then local maxima of the function  $\hat{H}$  equal the amplitude ratio  $P_s/P$  and the value of  $t$ , ( $t_{ps}$ ) which corresponds to each maximum is equal to the time interval between the P and the Ps arrivals (Kind and Vinnik, 1988). Zero time on the crosscorrelated records is the time corresponding to the maximum of the autocorrelation of  $L(t)$ . This time is determined by examining the normalised autocorrelation function of  $L(t)$ :

$$\hat{L}(t) = \frac{\int_{t_1}^{t_2} L(t + \tau) * L(\tau) d\tau}{\int_{t_1}^{t_2} [L(\tau)]^2 d\tau} \quad 2.2.7$$

Examination of figure 2.2.3 will clarify the concepts related to equations 2.2.6 and 2.2.7.

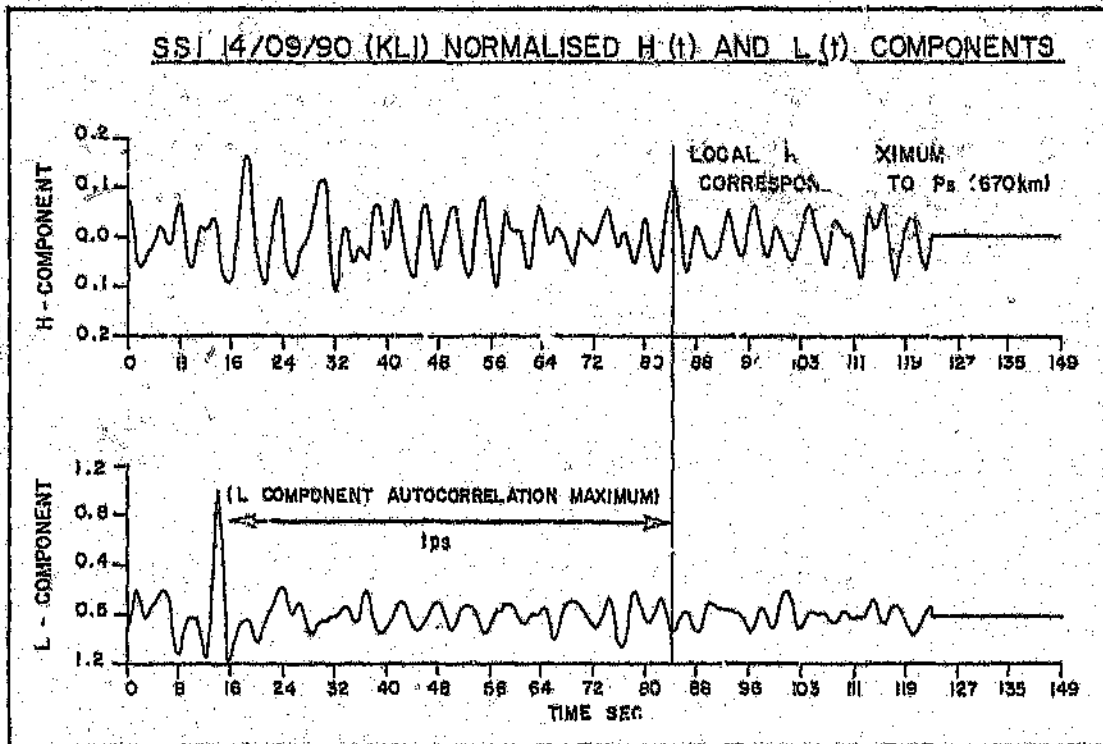


Figure 2.2.3 - Relationship between the normalised H(t) and L(t) components and  $t_{sa}$ .

The time interval,  $t_{Ps}$ , between the P and the Ps arrivals can be determined from equation 2.1.7 assuming that the ray parameter  $p$  is the same for both of these phases. This time interval is given by

$$t_{Ps} = \int_{r_p}^{r_o} \left( \frac{1}{V_s^2} - \frac{p^2}{r^2} \right)^{1/2} dr - \int_{r_p}^{r_o} \left( \frac{1}{V_p^2} - \frac{p^2}{r^2} \right)^{1/2} dr \quad 2.2.8$$

where  $r_p$  is the radius to the depth of conversion and  $r_o$  is the earth's radius. Velocities  $V_p$  and  $V_s$  can be taken from any reference earth model for example the IASPEI 1991 model (Kennett, 1991). For a fixed conversion depth  $t_{Ps}$  is strongly dependant on the ray parameter  $p$  or the epicentral distance of the event. The assumption that the ray parameter is the same for both the P and the Ps phases results in the exact values of  $t_{Ps}$  being slightly lower than the estimates. However, for upper mantle conversions the differences are of the order of a fraction of a second (Kind and Vinnik, 1988).

To enhance a wave converted at a depth  $r_p$  and to suppress waves converted at other depths the  $\hat{H}$  components for many seismic events covering a large range of epicentral distances are stacked for individual stations by a delay and sum technique (Fuchs et al, 1987). Stacking is another signal enhancement procedure which is permissible since the P-to-S converted phases are sensitive only to the discontinuity at depth near the receivers (Shearer, 1991). The delay  $\delta t_i(r_p)$  is given by:

$$\delta t_i(r_p) = t_i(r_p) - t_o(r_p) \quad 2.2.9$$

where  $t_i(r_p)$  is  $t_{Ps}$  calculated for the  $p$  value of the  $i$ th event and  $t_o(r_p)$  is  $t_{Ps}$  calculated for a reference value of  $p$  for an epicentral distance of  $67^\circ$ . This reference value is used in nearly all studies dealing with P-to-S converted phases quoted in the literature and is maintained in the current study. Stacking can be performed for a variety of trial conversion (phasing) depths while the true depth of conversion can be found with much higher accuracy using equation 2.2.8. Correspondence between results using the two methods would imply that the converted phase is a true phase

rather than a processing artifact.

These ideas will become clearer in section 3.3 when the data processing performed during the current study is discussed.



### 3) DATA ACQUISITION AND PROCESSING.

A detailed description of the data recording broad-band seismographs used during the Lithosphere Project are presented in Green(1992). This section will summarise some of the salient features of the acquisition system (after Green, (1992)) and describe how the data were extracted and converted to a form suitable for further processing.

#### 3.1) PC Based Field Recording System.

With the exception of station BPI situated at the University of the Witwatersrand in Johannesburg, all the broad-band seismographs were located in remote rural locations in South Africa away from sources of seismic noise. This was a problem in that these areas are also removed from mains power which would normally be required for personal computers (PCs), ideal for the handling and storage of large volumes of data. In order to overcome this problem and maintain the utility of PCs a field portable system was developed which operated using a practical number of photovoltaic cells for power.

The system consisted of five main components:

- A - Transducers;
- B - Compression amplifier and analog to digital (A to D) converter;
- C - System control and real time clock;
- D - Personal computer and
- E - Power source

The transducers (A) were Guralp CMG3 Force Balance Accelerometers the integrated output of which produced a flat velocity response from 0.05 Hz to 10 Hz. Analog to digital conversion (B) was performed using separate A to D cards for each channel with the seismic signal being filtered using a four pole Butterworth filter prior to conversion. Analog data compression was used to make efficient use of a PC hard

drive - quite simply each discrete seismic datum had to be stored in 8 bit format while yielding large dynamic range and maintaining data reliability to the 1 % error level. Using an 8th-order polynomial transfer function this was achieved while simultaneously increasing the dynamic range to approximately 84 Db. Details of the data compression are given in Green (1993).

The transducers and the A to D system were powered continuously while the PC was only powered up when the acquisition memory on the A to D cards was 90% full. The memory dump could store 28672 samples and the time interval between dumps was 2007 seconds (33m 27s). Thus, the sampling frequency was approximately 14.3 Hz yielding a Nyquist value of about 7.1 Hz. After the data were dumped from the acquisition card to the PC, the PC was switched off thus reducing power consumption. The triggering of the PC was monitored by the system control and real time clock (C).

PCs (D) for the project utilised XT (8086) motherboards and 42 Mb hard discs. When the disc contained 350 files (30.1 Mb) of data they were automatically dumped to a tape streamer. This procedure lasted approximately 25 minutes and occurred every 8 days. In terms of the 60 Mb capacity of the tapes used, each station had to be visited ever 24 days. Initially power (E) was supplied by two solar panels charging sealed lead acid batteries but this was changed to four solar panels to overcome problems associated with prolonged overcast periods.

[NOTE. The system described above was the system used to procure the data pertaining to this dissertation. The newer systems (Green, (1993) and personal communication) are different in many ways. The fundamental method of acquisition and storage has changed (for example, 16 bit data storage with no top compression applied) and all outdated electronics have been replaced (80386 technology, 200 Mb hard discs, 500 Mb cartridge tape dumps etc).]

In terms of the present study the following points concerning data acquisition are important -

1) No records suitable for analysis were found for stations KAM, KEN and WAR. The poor data quality at KEN and WAR is almost certainly as a result of these stations being operational only during the earliest phase of the project (table 1.1.1) when initial teething problems described by Green(1992) were examined and rectified. These problems included battery failure due to insufficient solar panels, mechanical and electrical failures in the transducers and, PC power, RAM and disc failures.

The transducers used at station KAM were not Guralp CMG3 force Balance Accelerometers as used at the other stations. This almost certainly resulted in the persistent failure of one of the channels at this station throughout its recording history - a problem which has rendered almost all data from KAM useless for further analysis.

2) At PIL the north/south and east/west transducer outputs were swapped over while at BPI the transducer polarities were reversed regularly (presumably whenever maintenance was performed on the station). There is also no consistency in polarities from station to station. This can easily be corrected for when individual records for each station are processed and should be kept in mind should the data base be used in the future. Polarities for the events processed in this study will be presented in section 3.4.

These polarities were established by comparing the P arrivals of all three components for the stations DOU, PIL, SAN and BPI for an event in the South Sandwich Islands on 09/05/1990. This event has a clear, simple P onset for all stations (figure 3.1.1) and a known source mechanism derived from the USGS Preliminary Determination of Epicentres bulletin. By comparing the P onset for each component at each station, a table of relative polarities was established. By comparing any one station with the expected polarity in terms of the source mechanism a table of absolute polarities for the four stations was established. By convention compressional motion to the south,

east and down has the polarity +1, +1, +1. (The result of this analysis was checked by performing a first motion weight drop test at BPI.)

The procedure was repeated for an event from the same region on 14/09/90 where the stations KLI, PIL, SAN and DOU were analyzed. Hence the absolute polarities for all five stations that produced suitable data were derived. During processing (section 3.3), data from each event used were checked against data from different stations for the same event to ensure that the polarities were consistent.

Only events with clear, simple P onsets indicative of good signal to noise (S/N) characteristics are suitable for consideration in terms of P-to-S analysis. Polarities for such events should be ascertainable from visual inspection of the decompressed records. For events where the onset is more uncertain in nature two component hodographs should assist in establishing the polarities (this is a more rigorous method of examining seismic velocity data in a Cartesian coordinate system).

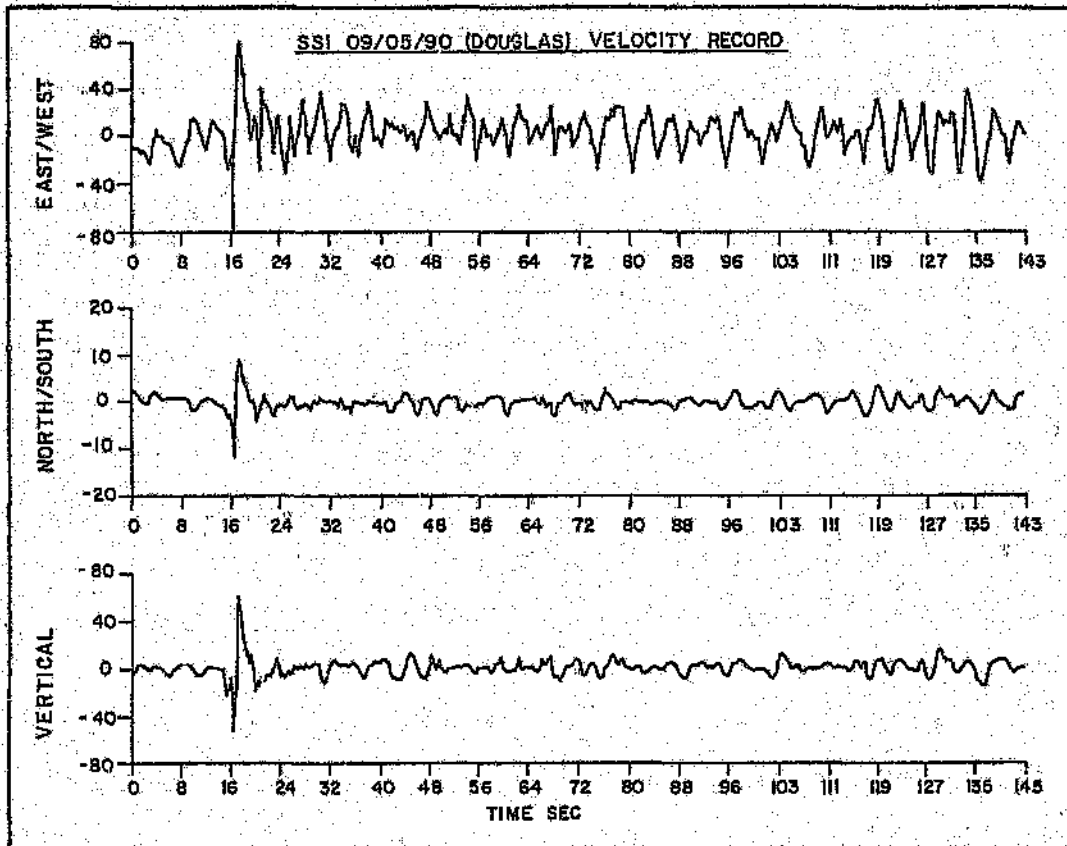


Figure 3.1.1 - Three components related to the correct polarities for an event at SSI on 09/05/90 recorded at Douglas. The clarity of the P arrivals for all three components is noted.

### 3.2) Preprocessing.

Using the USGS - Preliminary Determination of Epicentres bulletin, identifiable seismic events were extracted from the field tapes and placed on sets of consecutive floppy discs for each station. These data were later combined into a single data base on a 386 DX PC using software commissioned by the BPI. Lists which detailed the recorded events in terms of their geographic and depth locations, their magnitude and clarity of the onset of the arrival, were continually compiled and updated. This information was included in the data base.

When the current project commenced, data were extracted from the floppy discs, the top compression was removed and the data were converted from binary to Ascii format. With the current software, events are displayed on screen and are extracted simply by using the cursor to mark the beginning and end points of the file required. Decompression is performed automatically in the extraction software. In terms of the author's P-to-S analysis software the only prerequisite for the input files is that the arrival onset is approximately fourteen seconds after the starting time of the file and that at least 2048 data points are extracted (see section 3.3). The extracted binary files are converted to Ascii files containing data in a format suitable for the P-to-S analysis software using the program readfile.exe. The source code for this program (and all others used in this study) is included as an appendix to this dissertation.

The decompression of the data mentioned above and discussed by Green(1993) was one of the biggest problems associated with this study. Data processing performed during previous work completed during the Lithosphere Project was not sensitive to the decompression algorithm used. This algorithm, which deconvolves the response of the polynomial transfer function, initially neglected to account for the zero drift in the A to D conversion or the dc drift in the amplifier (see Green, 1993). Hence all the original data processing during this study was rendered redundant in that the decompression had not been performed correctly. Once it was established that the decompression was erroneous the problem was expediently resolved. A fundamental principal of signal and data processing was reiterated by this example -the reliability

of the  $n$ th data process is dependant on the reliability of the output from the  $(n - 1)$ th process.

### 3.3) Data Processing.

Data processing is synonymous with numerical processing in this study. Preprocessing produces, for each event to be analyzed, three files (one each for the vertical, north/south and east/west components) each containing a column vector of 2048 digital, time sequential data. Processing involves transforming and manipulating these data according to the theory of section 2.2. Hence, this section describes how each equation in section 2.2 was implemented as a numerical routine. All programs and subroutines discussed in this section were written in FORTRAN 77. They were compiled as 16 bit executables and run on 80386 PC. As was stated in section 3.2, all source code is listed in the appendix.

The main program unit for the P-to-S analysis software is called `filon`. This program allows the user to call all subsequent processing routines. These routines should be called in sequential order, the exception being the filtering routine `ffiltpc` which can be called at any point in the processing route. In order to simulate the acquisition of data over a limited pass band all filtering performed during this study was done immediately after reading the data into the program. The data are read in using subroutine `param`. The data file must contain a column of at least 2048 free format real numbers. The 2048 data points are needed because the Fourier filtering performed in `filter` operates on a 2048 point array. The onset of the P arrival should be approximately at array address 200 (14 s for a sampling interval of 0.07 s). Once the data are read in, an option is available to display them in graphical form, either on the screen or a printer. Velocity data read into `param` for an event in the South Sandwich Islands are displayed in figure 3.3.1. Hardcopy facilities are available for all data processing routines.

As mentioned above, filtering can be performed (simultaneously on all data components) in `ffiltpc` which calls routine `filter`. The seismic trace is transformed

discretely into the Fourier domain where it is band pass filtered. The transition between the pass and the reject bands is over one octave and takes the form of a cos squared roll-off. The filtered seismic trace is obtained by transforming the modified spectrum back to the time domain. Three pass bands were employed during the current study corresponding to:

- i) no filtering;
- ii) a pass band between 0.1 Hz and 0.4 Hz and
- iii) a pass band between 0.05 Hz and 0.2 Hz.

Pass bands ii) and iii) are over two octaves. Filtered versions of the velocity records shown in figure 3.3.1 are displayed in figure 3.3.2. A crucial point stated in the previous paragraph must be emphasised. Filtering was performed on the velocity records that were read into the program in order to simulate the acquisition of longer period data. Hence the filtered, stacked records displayed in section 4 are not the result of simply filtering the unfiltered, stacked records. The necessity and possible ramifications of filtering the data in this manner will be discussed in section 5.1.

Routine `veldis` and its subroutines convert the velocity records to displacement records using numerical integration and a linear trend removal. This option was not used during this study.

`Rotrt` performs Euler rotation on the north/south and east/west components to a radial/transverse coordinate system according to equation 2.2.3 and a corresponding equation for the transverse component. An example of this rotation is seen in figure 3.3.3. The noisy nature of the transverse component is indicative of the rotation having been performed correctly.

`Calce` calculates the emergent angle according to equations 2.2.4 and 2.2.5. These equations calculate an angle  $\epsilon$  for which the energy along the principal component  $L(t)$  is maximised. The rationale behind these equations is very similar to the method of principal component analysis.



Routine `rotlh` rotates the radial and vertical components to the  $H(t)$  and  $L(t)$  axes using the emergent angle calculated in `calce`. The result of this rotation is shown in figure 3.3.4.

Routine `cross` performs the following operations. It transforms the  $H(t)$  and  $L(t)$  components as for equations 2.2.6 and 2.2.7; it performs temporal shifting on the final arrays containing the normalised  $H(t)$  and  $L(t)$  components such that the autocorrelation maximum of the  $L(t)$  component resides at array address 200 and it allows for these final components to be written to a file. The final result of the single event processing is displayed in figure 3.3.5.

Program `tps` requires a little explanation. The program calculates the delay time between the  $P$  and the  $P_s$  phases according to equations 2.2.8. and 2.2.9. The code is divided into three parts:

- $P$  and  $S$  velocities are determined using the IASPEI 91 model (Kennet et al, 1991) at 10 km intervals from surface to a depth of 760 km;
- discrete numerical integration is used to calculate the time delay for an epicentral distance of  $67^\circ$  using the derived velocity function;
- the time delay for a specific event at a different epicentral distance is then calculated. The result for an epicentral distance of  $67^\circ$  is subtracted to give the final normalised time delay to be used in the stacking program `pcstack`.

The user entered parameter in `tps` is the theoretical angle of incidence of a  $P$  wave at the base of the crust for the epicentral distance of the event. This is used to calculate the ray parameter  $p$ . These theoretical angles are taken from Ben-Menahem and Singh(1981) and are included in table 3.3.1. The simplified IASPEI 91 velocity model used is shown in table 3.3.2. Table 3.3.3. shows the  $t_{p_s}$  delay of for an event at  $67^\circ$ , the  $t_{p_s}$  delay for an event at an epicentral distance of  $80^\circ$  and the final time delay  $\delta t$  used in the program `pcstack`.

Program `pcstack` delays and sums the final normalised components for each station. For each stack the user will enter a three character name of the station eg. `KLI` and

two filenames - one for the list of H components to stack and another for the corresponding time delay files. For each event, for each stacking depth the temporal delay is converted to an array address delay which is applied to the corresponding H component. The different H components are then summed for the particular phasing depth. Each H component's origin time must be at array address 200 when it is read into the program. This is performed automatically in routine `cross` in program `filon` as discussed previously. Twenty files are output from the program corresponding to twenty phasing depths from 0 km to 760 km at 40 km intervals. Zero time for the output files will be at 0 seconds.

`Seisgrf2` allows the final stacked H components to be displayed, either on screen or to a printer. Examples of output from `seisgrf2` abound in section 4. Program `stk467` allows output files from `pcstack` to be stacked. For example, in section 4, all stations' stacked results for a phasing depth of 400 km are added together to produce an additional stack.

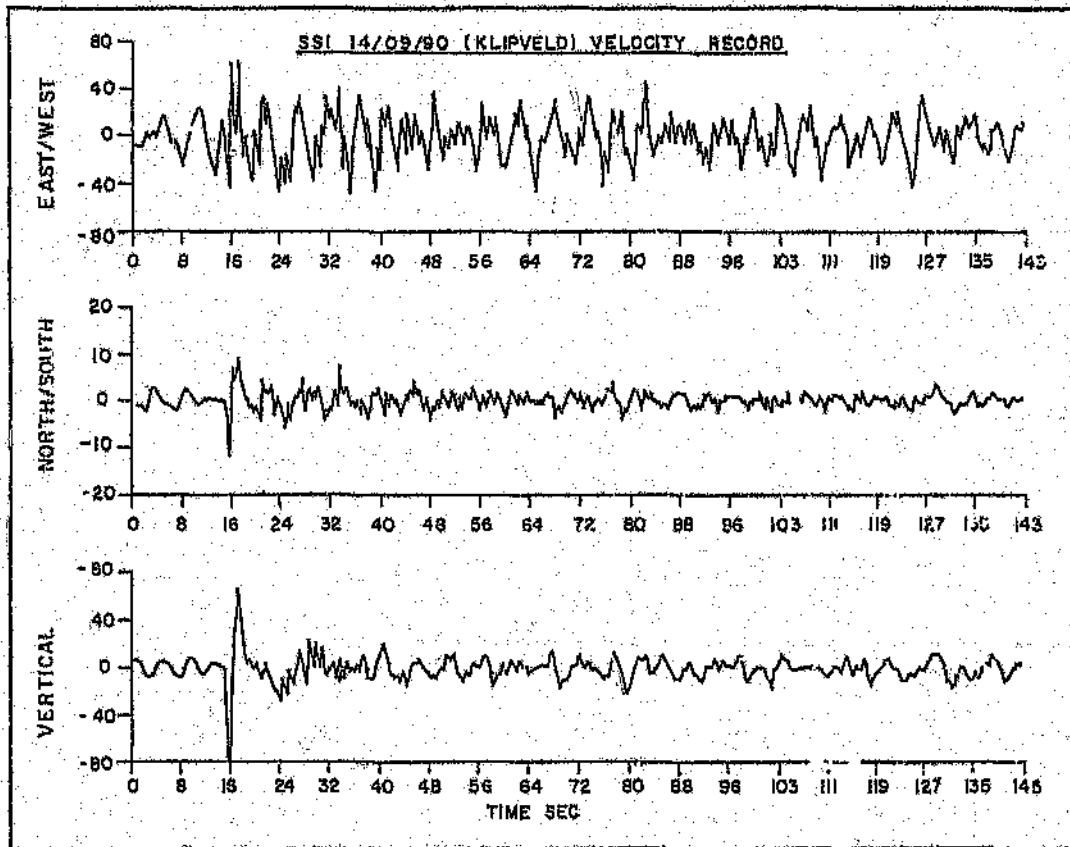


Figure 3.3.1 - Output from filter of velocity data for an event in the South Sandwich Islands

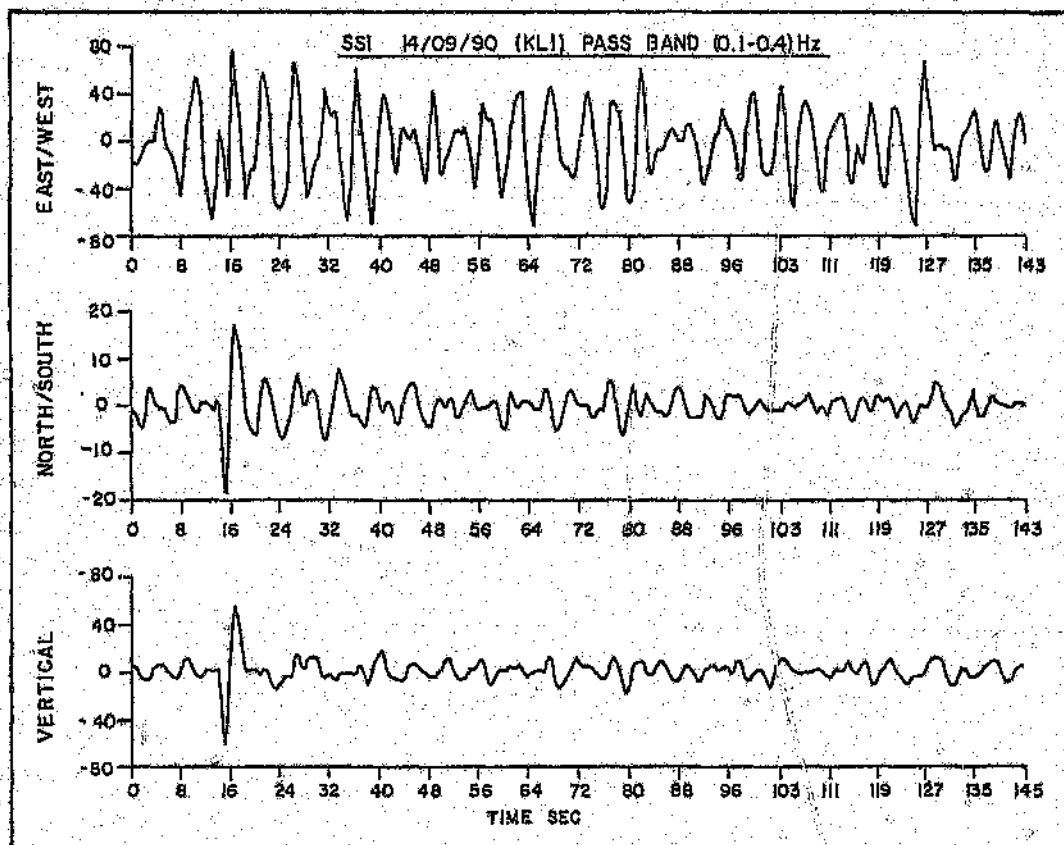
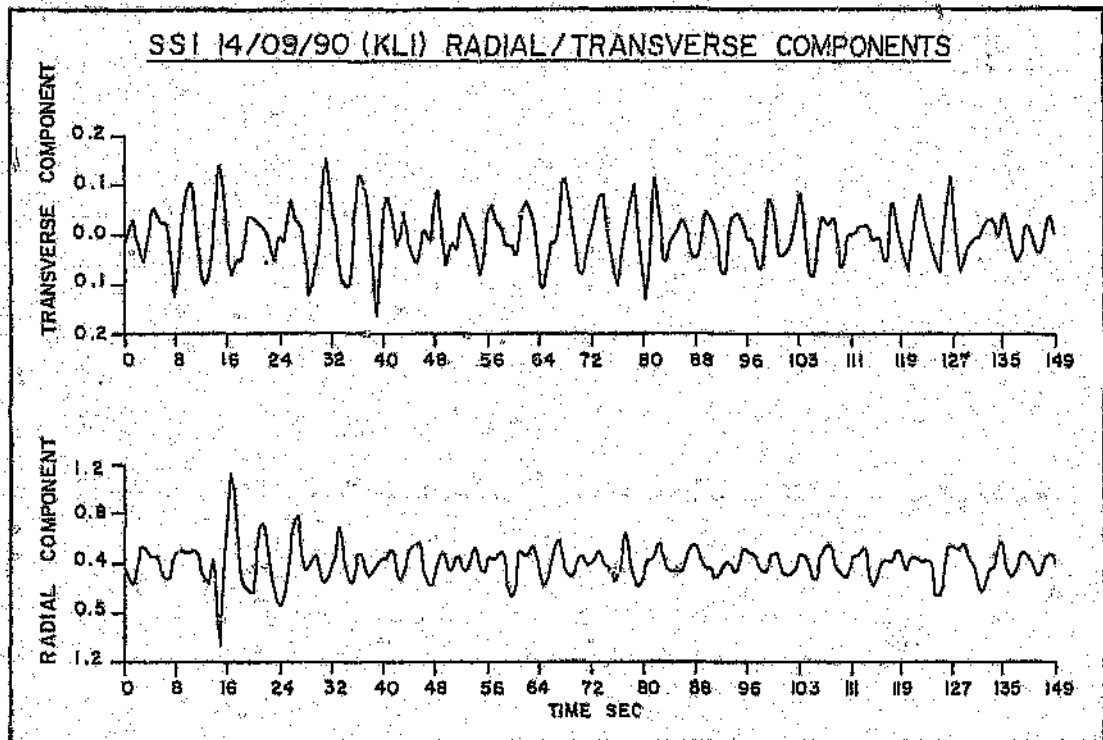


Figure 3.3.2 - Filtered versions of the velocity records shown in figure 3.3.1



**Figure 3.3.3 - Radial and transverse components of the velocity records shown in figure 3.3.1**

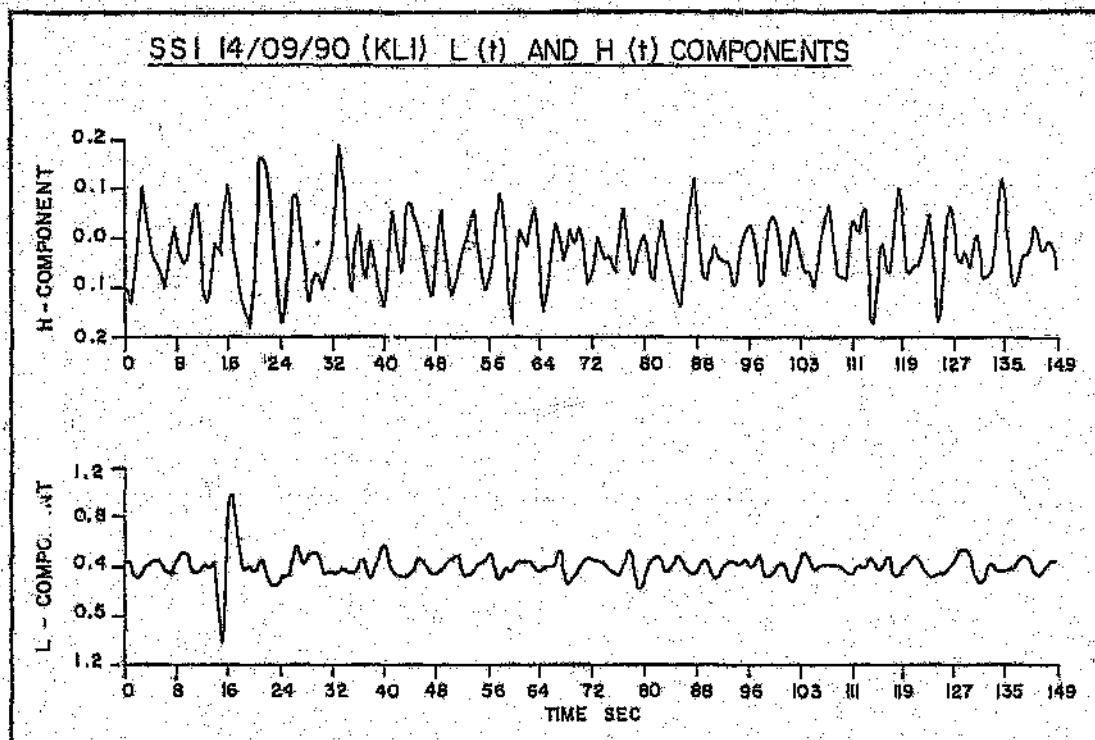


Figure 3.3.4 - H(t) and L(t) components calculated from the components displayed in figure 3.3.3 and the emergent angle  $\theta$  determined in calca.

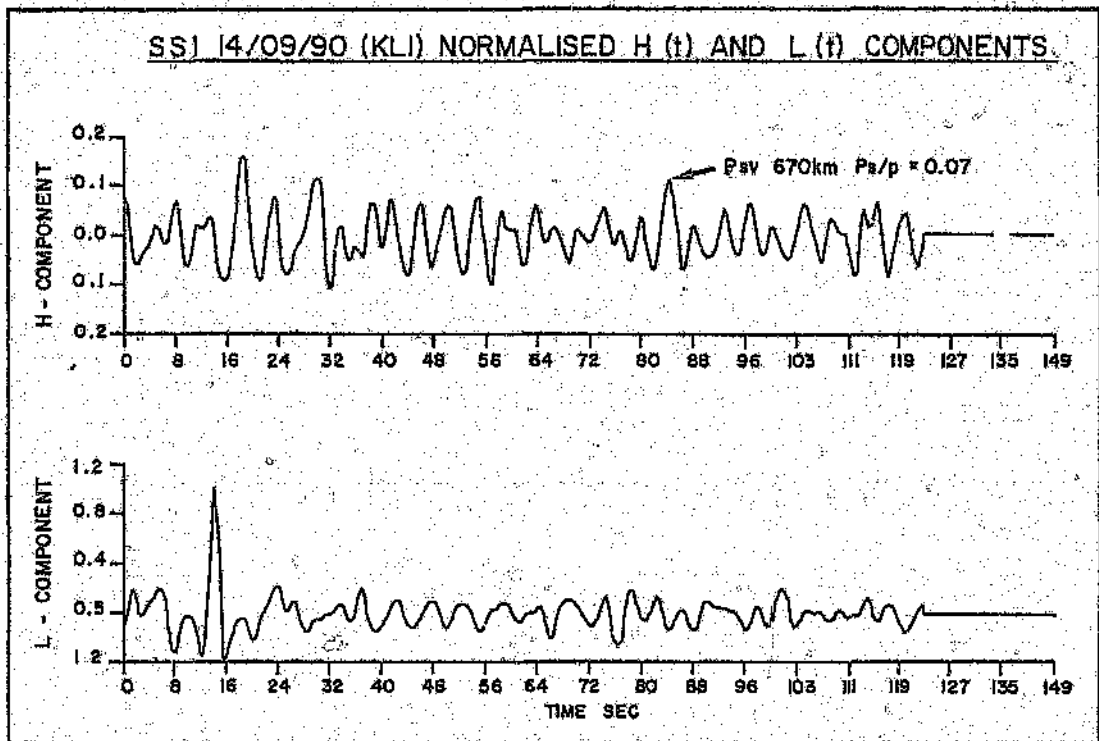


Figure 3.3.5 - Normalised, cross correlated components  $\hat{H}$  and  $\hat{L}$ .

$\Delta^\circ$										
<i>h</i>	21	24	27	30	33	36	39	42	45	48
Surface	45.5	42.3	39.9	38.3	37.3	36.3	35.5	34.8	34.0	32.9
800 km	37.3	36.7	35.9	35.3	34.8	34.1	33.2	32.4	31.5	30.6
$\Delta^\circ$										
<i>h</i>	51	54	57	60	63	66	69	72	75	78
Surface	32.0	30.9	29.7	28.6	27.5	26.5	25.5	24.5	23.5	22.6
800 km	29.5	28.5	27.6	26.7	25.8	24.9	24.0	23.1	22.2	21.3
$\Delta^\circ$										
<i>h</i>	81	84	87	90	93	96	99	102	105	
Surface	21.6	20.7	19.8	19.1	18.7	18.5	18.4	18.2	17.5	
800 km	20.4	19.6	19.0	18.6	18.5	18.4	18.1			

Table 3.3.1. - Theoretical angles of incidence for P waves at the base of the crust (after Ben-Menahem and Singh, 1981). Intermediate values obtained by linear interpolation.



DEPTH IN KM	P VELOCITY (km/s)	S VELOCITY (km/s)
40.0	8.04	4.47
80.0	8.05	4.49
120.0	8.05	4.50
160.0	8.16	4.51
200.0	8.27	4.52
240.0	8.41	4.57
280.0	8.56	4.64
320.0	8.70	4.71
360.0	8.85	4.78
400.0	8.99	4.85
440.0	9.46	5.13
480.0	9.60	5.22
520.0	9.73	5.30
560.0	9.86	5.39
600.0	10.00	5.47
640.0	10.13	5.56
680.0	10.84	6.00
720.0	10.95	6.11
760.0	11.06	6.21

Table 3.3.2. - Simplified IAPET 91 velocity model (after Kennett, 1991).

Phasing Depth (km)	Tps(67°) (s)	Tps(80°) (s)	$\delta T(80^\circ-67^\circ)$ (s)
40.0	4.80	4.63	-0.17
80.0	9.00	8.60	-0.40
120.0	13.17	12.54	-0.63
160.0	17.37	16.51	-0.86
200.0	21.63	20.52	-1.11
240.0	25.91	24.55	-1.37
280.0	30.15	28.52	-1.64
320.0	34.36	32.44	-1.91
360.0	38.52	36.32	-2.20
400.0	42.65	40.14	-2.51
440.0	46.62	43.79	-2.83
480.0	50.50	47.33	-3.17
520.0	54.32	50.80	-3.52
560.0	58.09	54.21	-3.88
600.0	61.81	57.56	-4.25
640.0	65.49	60.85	-4.64
680.0	69.04	63.98	-5.06
720.0	72.43	66.93	-5.50
760.0	75.76	69.80	-5.96

**Table 3.3.3.** - Table showing phasing depth, travel time delay and normalised travel time delay  $\delta t$ . Time delays corresponding to phasing depths of 400 km and 670 km are pertinent to this study.

### 3.4) Selection of Processed Events.

An event recorded at a station must have the following two properties for it to be suitable for stacking:

- a clearly identifiable, simple P onset;
- no peak H amplitudes greater than 10 % of that of the normalised L component for any phase other than the initial Ps crustal phase.

These properties are required to ensure that the individual events are characterised by propitious signal to noise characteristics. In addition, the focus of the event should preferably be either shallower than 100 km or deeper than 500 km to prevent other seismic phases being present at times corresponding to the Ps arrivals from the discontinuities of interest.

A list of events displaying the first property was drawn up by the author. This list was modified on the basis of the second property, by Vinnik, who worked independently with the data (Vinnik et al, 1993b) during the current study. The final list of events stacked at each station in this study - presented in table 3.4.1 - is almost identical to the final list used by Vinnik(1992). Table 3.4.1 lists the date, location, depth, epicentral distance and back azimuth of each event. As discussed in section 3.1, no suitable events were present in the records of stations KAM, KEN and WAR.

The polarities for stations DOU, SAN, PIL, and KLI were constant. These polarities were, for the vertical, north/south and east/west components respectively:

DOU - ( +1, -1, +1)

SAN - ( -1, +1, +1)

PIL - ( +1, +1, -1)

KLI - ( -1, -1, -1)

The polarities at BPI changed regularly, as mentioned in section 3.1. The polarities were ( +1, -1, -1) for the first two events listed in table 3.4.1 and ( +1, +1, +1) for the other four events.

The paucity of events suitable for stacking, as shown by the table, indicates that the stacked results discussed in section 4, must be viewed with a great deal of caution. Only six events suitable for stacking were found for stations BPI and DOU, five for SAN, seven for PIL and nine for KLI. This must be compared with the approximately fourteen events collected over a ten year period analyzed for each of the four stations studied by Vinnik et al(1983) in Europe and North America and the thirty six events recorded over the same period, used by Kind and Vinnik(1988) when examining the Gräfenburg records.

Stacking is a procedure performed to enhance true conversions and cancel out obfusatory random signal. Because suitable data were limited it cannot be said with any confidence that this was achieved with the stacking performed in this study.

	Date	Location		Depth	BPI	DOU	SAN	PIL	KLI
	d m y	Lat	Lon		Dlat Baz	Dlat Baz	Dlat Baz	Dlat Baz	Dlat Baz
MIR	080490	41.1S	80.8E	33					47.3 123
CHILE	210490	37.0S	73.3W	12			63.7 232		
SSI	090590	58.4S	87.1W	52	49.4 216	44.5 216	50.4 216	49.7 216	
C CHILE	140590	55.9S	71.4W	73	82.2 234	77.4 236	82.8 234	82.0 234	
SUDAN	240590	5.3N	31.8E	17					31.4 11
W.IRAN	200890	37.0N	49.4E	19	65.9 19		64.6 19		66.2 20
ASCEN.IS	140790	0.0N	17.4W	11	70.9 293			49.5 293	
SSI	140990	60.7S	22.8W	33		44.2 211	49.8 210	49.0 210	48.1 210
SUMATRA	151090	2.2S	92.2E	32					67.5 81
PERU/BRASIL	171090	11.0S	70.8W	599	93.0 256	88.7 258		92.4 257	91.5 257
IRAN	081190	28.3N	50.5E	11	60.2 28			59.7 29	60.7 30
MIR	281290	14.9S	66.8E	17		42.0 80			39.4 82
BURMA	050191	23.5N	96.0E	20		86.9 62		82.4 60	83.4 60

Table 3.4.1 - List of suitable events used for stacking at stations BPI, DOU, SAN, PIL and KLI.

#### 4) RESULTS.

The stacked results for the five stations where suitable data were available are presented in this section. As discussed in section 3.4, these results must be viewed in terms of having been derived from a limited data base. For each station three separate stacks are presented corresponding to the three frequency pass bands discussed in section 3.3:

- no filtering ( broad-band stack)
- 0.1 and 0.4 Hz ( intermediate period stack )
- and 0.05 to 0.2 Hz ( long period stack ).

Filtering is performed on the data in order to improve its signal to noise characteristics and if sufficient good data are available, to provide some insight into the order of any discontinuity observed. The RS values indicated on the stacks are the relative scales used to plot the records so that they appear similar to the reader.

In addition to describing the phases corresponding to possible upper mantle conversions, mention is also made of the near surface converted phases corresponding to a phasing depth of 0 km. Although these near surface phases relate to depths outside those of interest considered in this study, they are discussed to establish if there is any relationship between near surface and upper mantle features beneath a station. These phases also illustrate the utility of analysing converted phases when suitable data are available - near surface phases are much bigger in amplitude than mantle converted phases, hence, fewer events need to be stacked to obtain consistent results.

The near surface conversions are dominated by three phases (Vinnik, 1992):

- 1) a Ps phase converted at the crust mantle boundary;
- 2) a multiple of this phase reflected as a P wave at the earth's surface;
- 3) a multiple of (1) reflected as an S wave at the earth's surface.

These phases are illustrated as a sketch in figure 4.1. According to Vinnik(1992), for sharp crust-mantle transitions the three phases will be of approximately equal

amplitude (note the negative polarity of the Pps conversion) while for gradual or irregular transitions the amplitude of the phases corresponding to the multiples will be reduced.

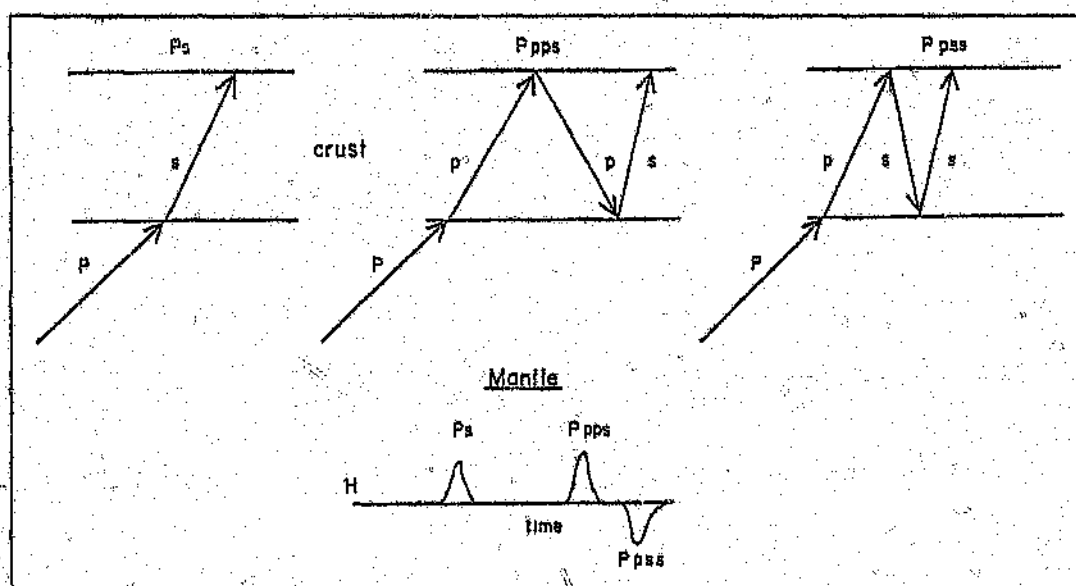


Figure 4.1 - Relationship between the near surface converted phases.

## 4.1) Results for Station BPI.

### Upper mantle conversions -

Figure 4.1.1. ( broad-band stack ): No evidence for any energy in this stack either at a delay time of 67.5s between phasing depths of 560 and 720 km or at a delay time of 40s for phasing depths between 400 and 500 km. These two areas on the stacked record correspond to the 400 km and 670 km discontinuities respectively.

Figure 4.1.2 ( intermediate period stack ): No energy above levels ascribable to seismic noise.

Figure 4.1.3 ( long period stack ): Evidence for some energy corresponding to the 400 km discontinuity. However, it is very difficult to distinguish this energy from noise present in other positions in the stacked record.

In summary, there are no clear upper mantle phases detectable in any pass band.

### Crustal conversions -

Figure 4.1.4 : A clear crust-mantle Ps converted phase is seen at 4.8s with an amplitude relative to the L onset of 9 % (figure 4.1.4). According to Vinnik (1992) a relative amplitude of 10 % corresponds to shear wave velocity contrast of approximately 1 km/s. The Ppps phase is evident with the same relative amplitude as that of the Ps phase at 16.5s. No Ppss phase is evident. A rogue conversion at 12s can only be ascribed to a processing artefact because of the high amplitude associated with it. Evidence from the Ps and Ppps phases indicates a simple one layer crust with a sharp crust-mantle transition.



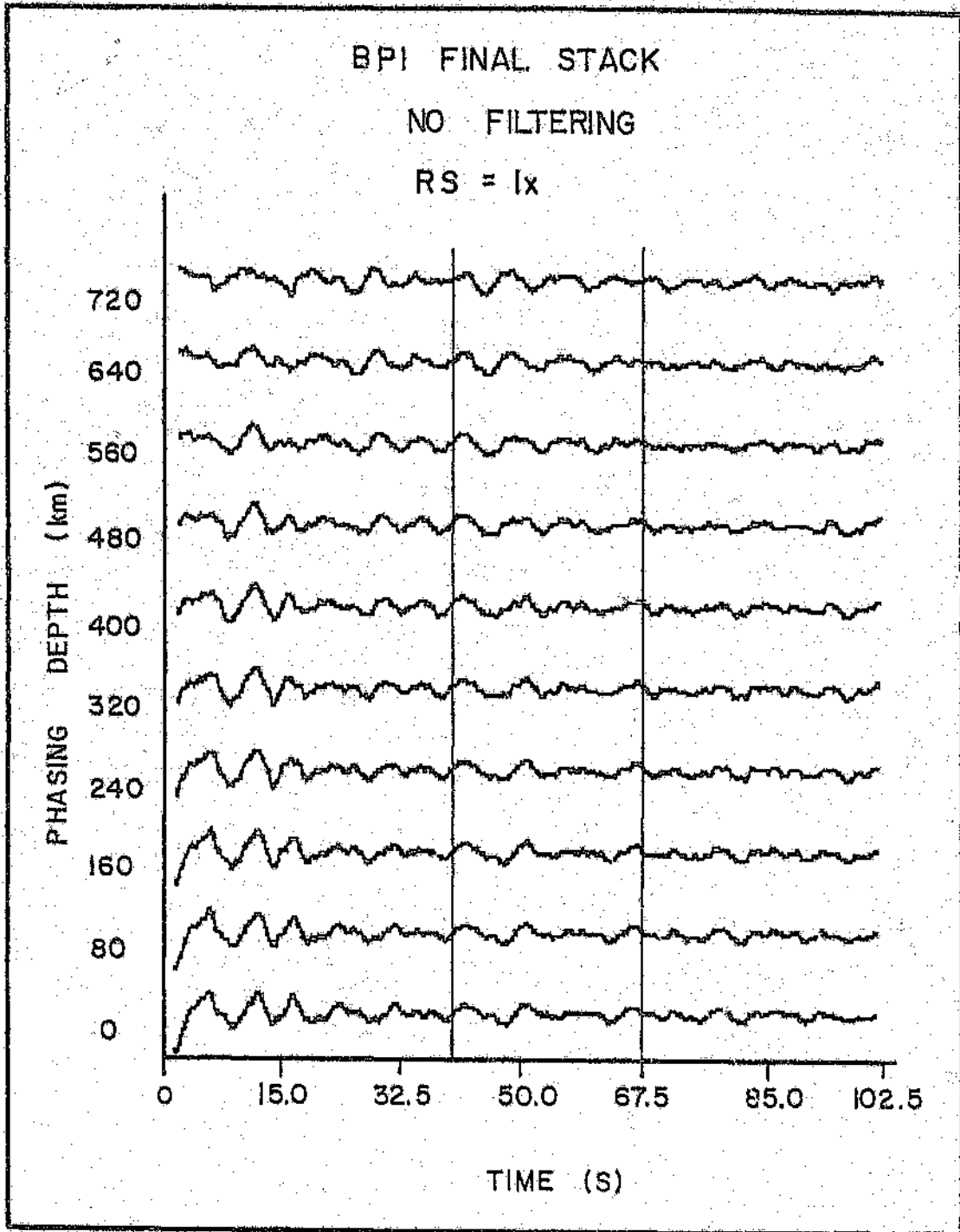


Figure 4.1.1 - Result of broad-band stack from station BPI.

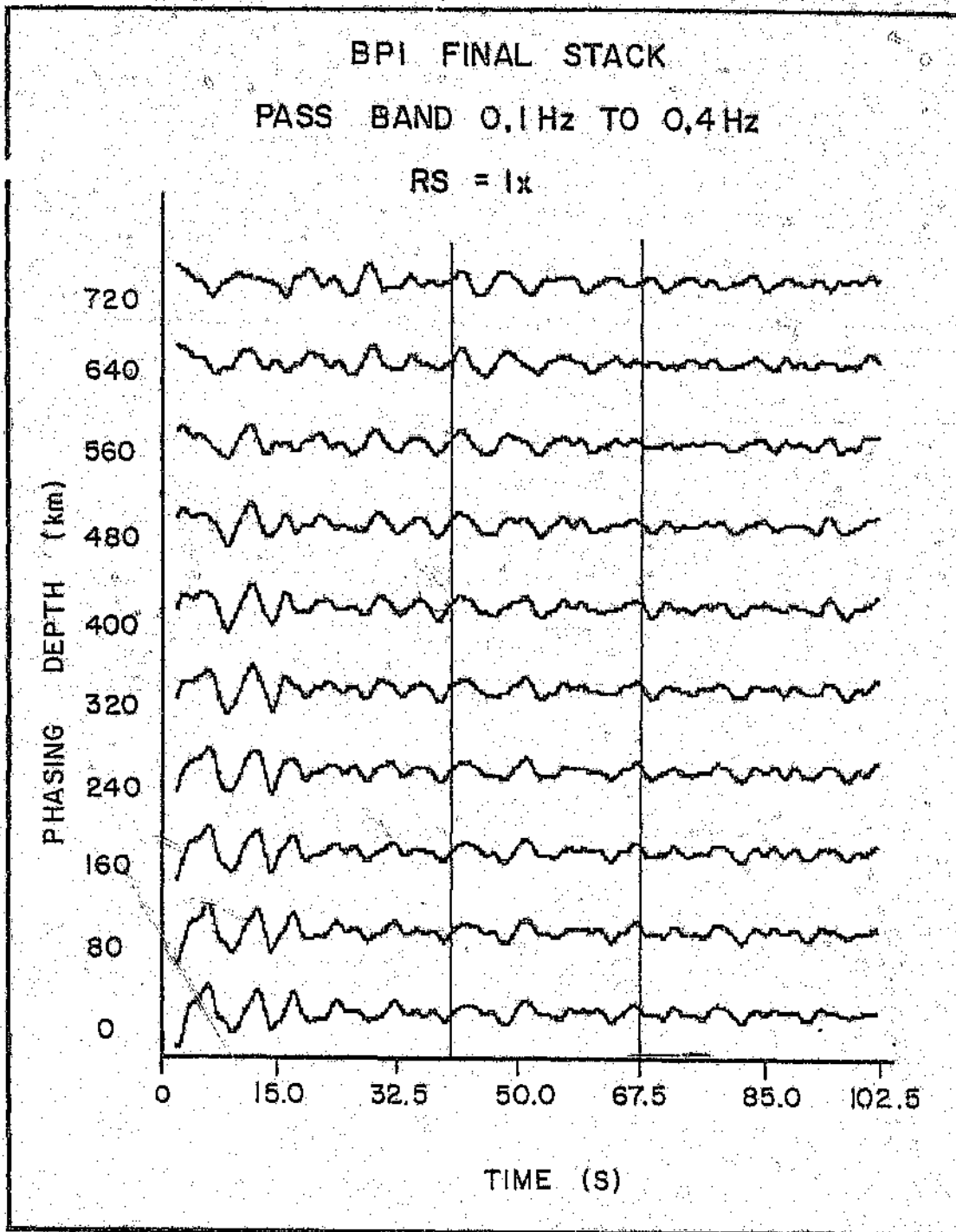


Figure 4.1.2 - Result of intermediate period stack from station BPI.

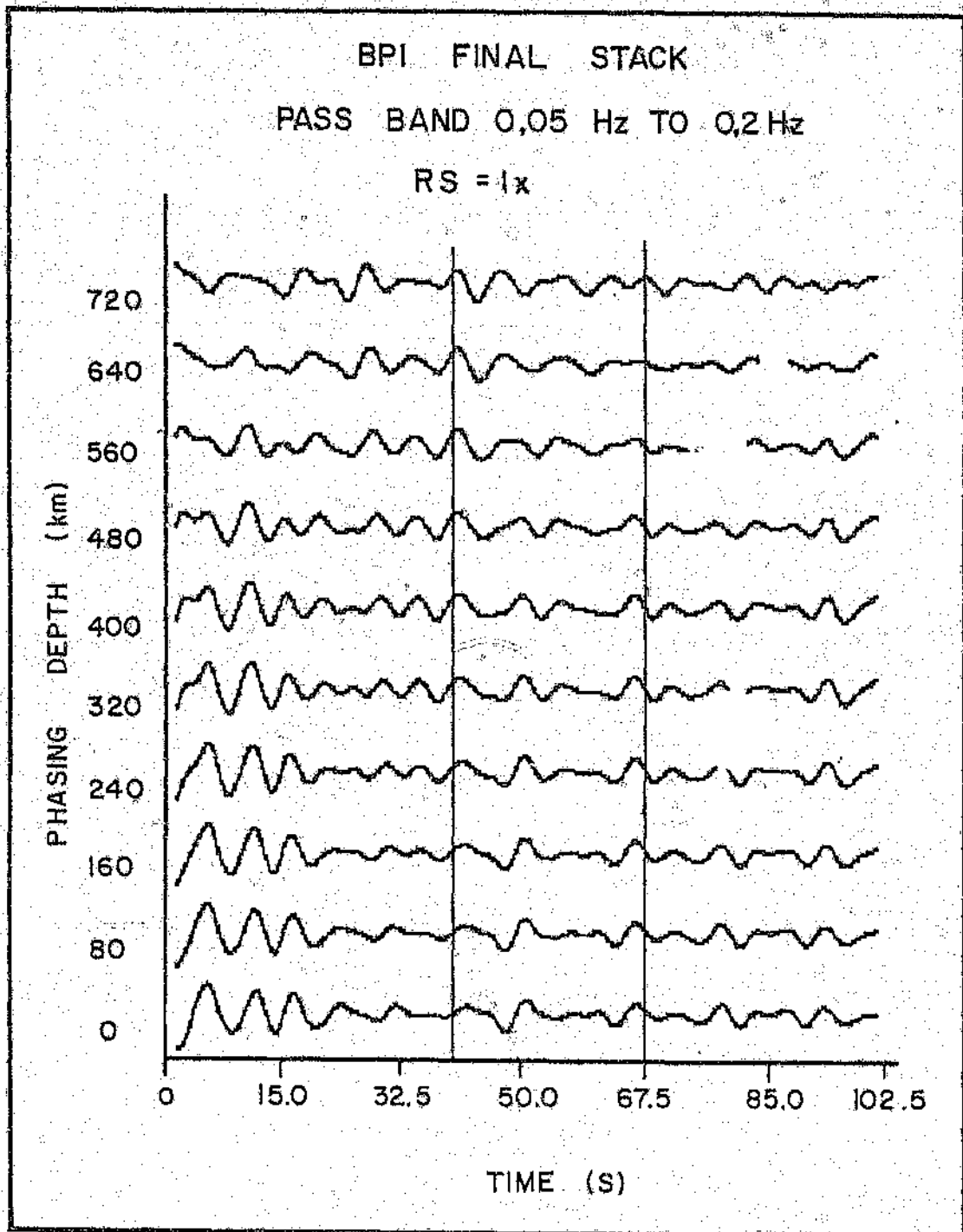
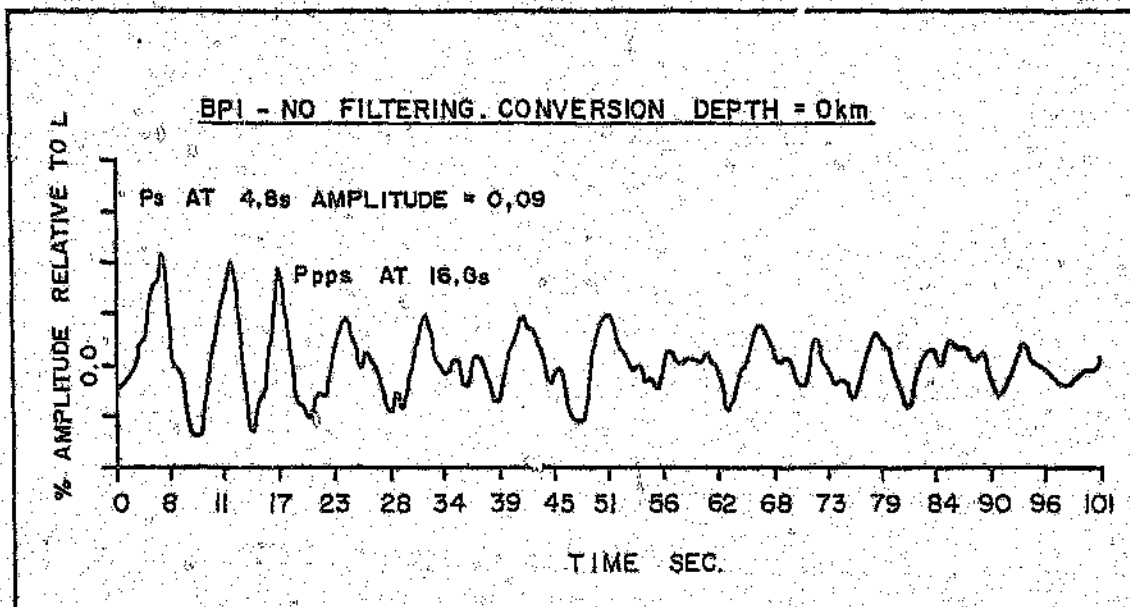


Figure 4.1.3 - Result of long period stack from station BPI.



**Figure 4.1.4** - Near surface conversions for station BPI. This stack corresponds to no filtering of the original records and a conversion depth of 0 km.

## 4.2) Results for Station DOU.

### Upper mantle conversions -

Figure 4.2.1 ( broad-band stack ): No energy corresponding to delay times of 40s and 67.5s. There is evidence for energy above seismic noise levels for phasing depths between 480 km and 640 km at a delay time of approximately 55s.

Figure 4.2.2 ( intermediate period stack ): Energy at 55s delay time is more evident. No other clear potential mantle phases visible.

Figure 4.2.3 ( long period stack ): Energy peak at 55.2s at a phasing depth of 560 km is clearly visible. The high noise levels associated with the rest of the long period record is disturbing as it indicates the presence of possible processing artifacts, probably introduced by the filtering procedure.

Table 3.3.3 indicates that the true delay time (relative to an epicentral distance of 67°) for a converted phase at 560 km should be approximately 58s. There is thus evidence for a discontinuity between 500 km and 560 km below DOU since a phase is present in all three pass bands at the correct phasing depth for the correct delay time.

### Crustal conversions -

Figure 4.2.4 : Clear Ps phase visible at 3.8s with a relative amplitude of 5 %. The Ppps and Ppss phases are also well defined. This implies a simple crustal model with the crust-mantle boundary being shallower than at BPI.

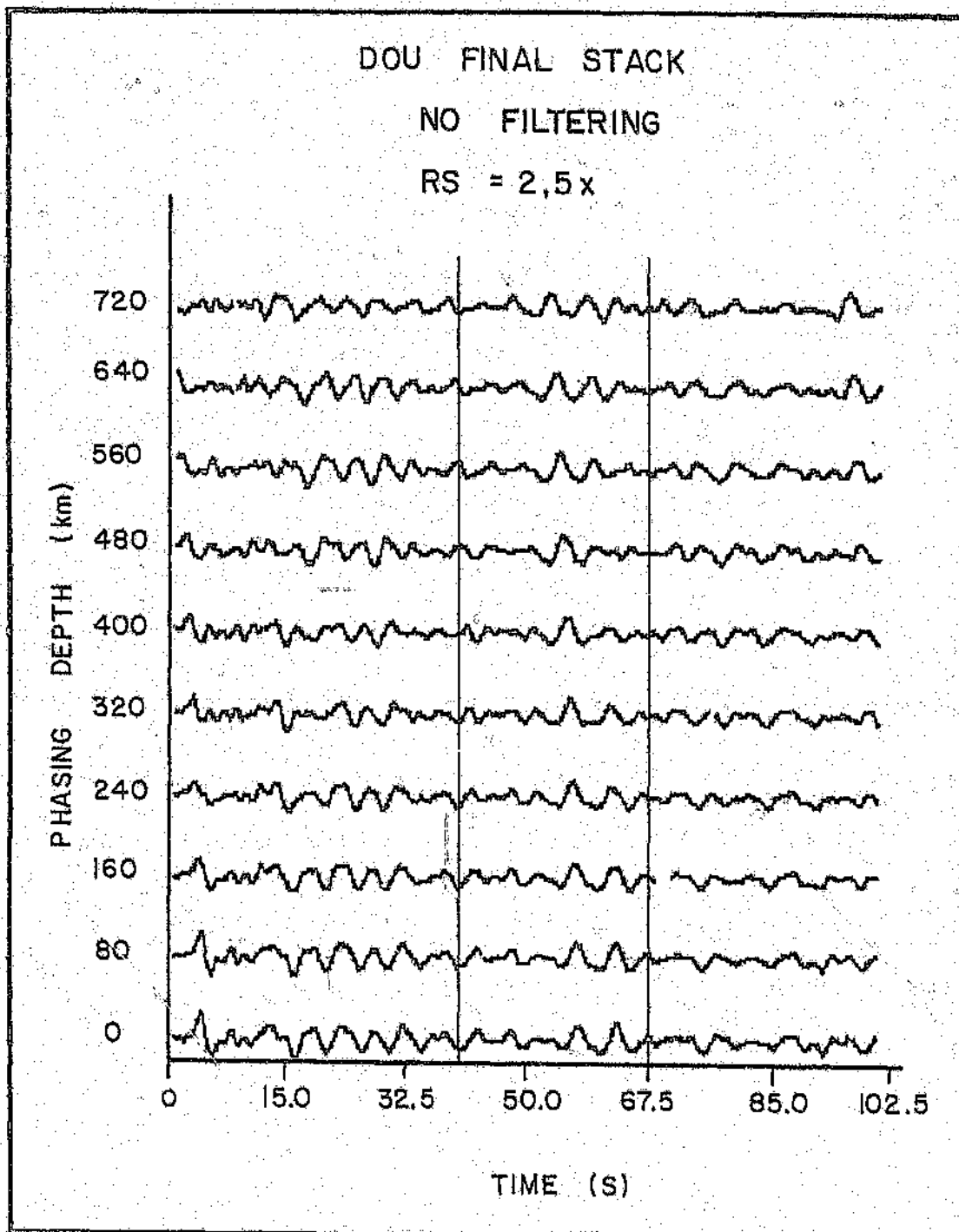


Figure 4.2.1 - Result of broad-band stack from station DOU.

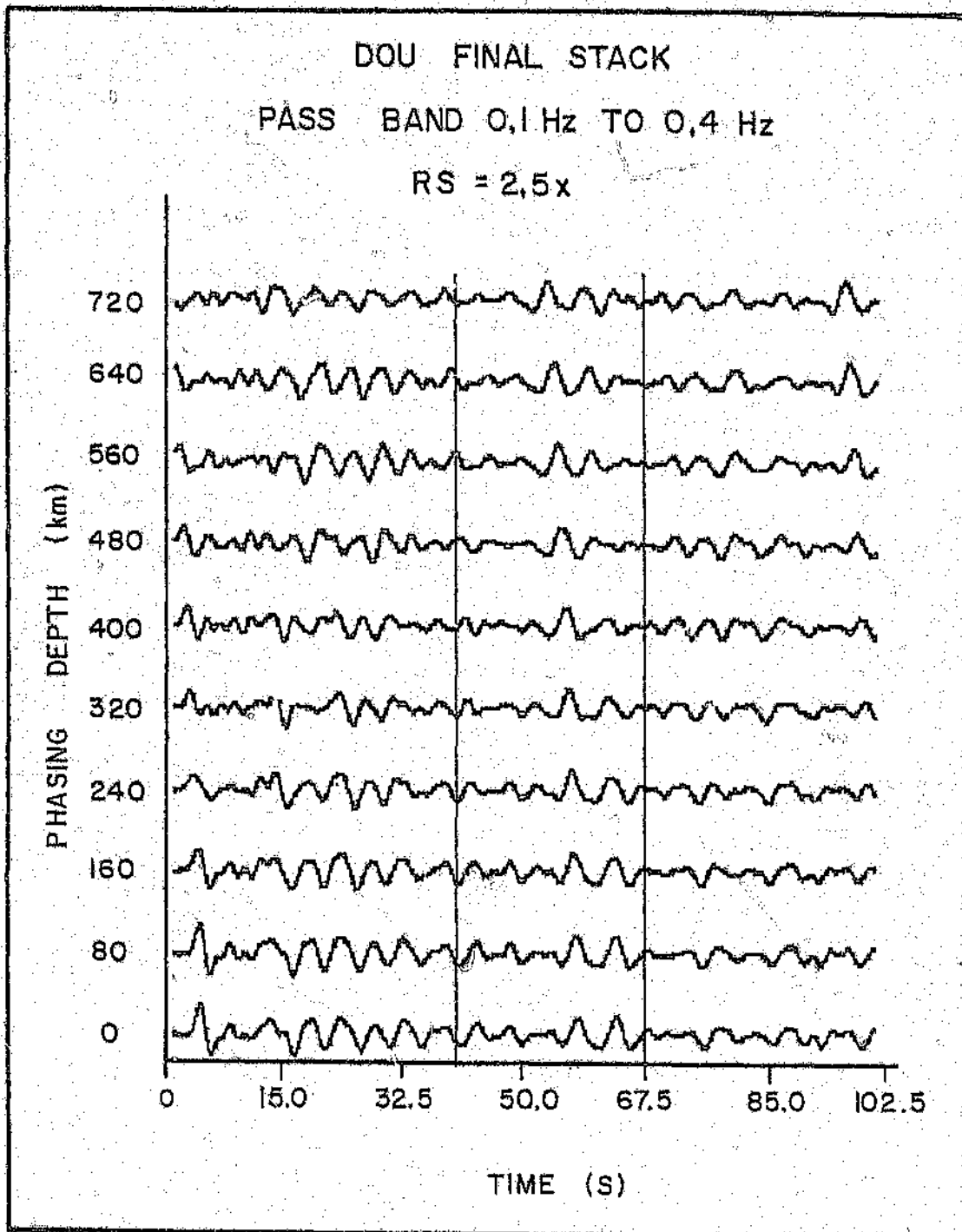


Figure 4.2.2 - Result of intermediate period stack from station DOU.

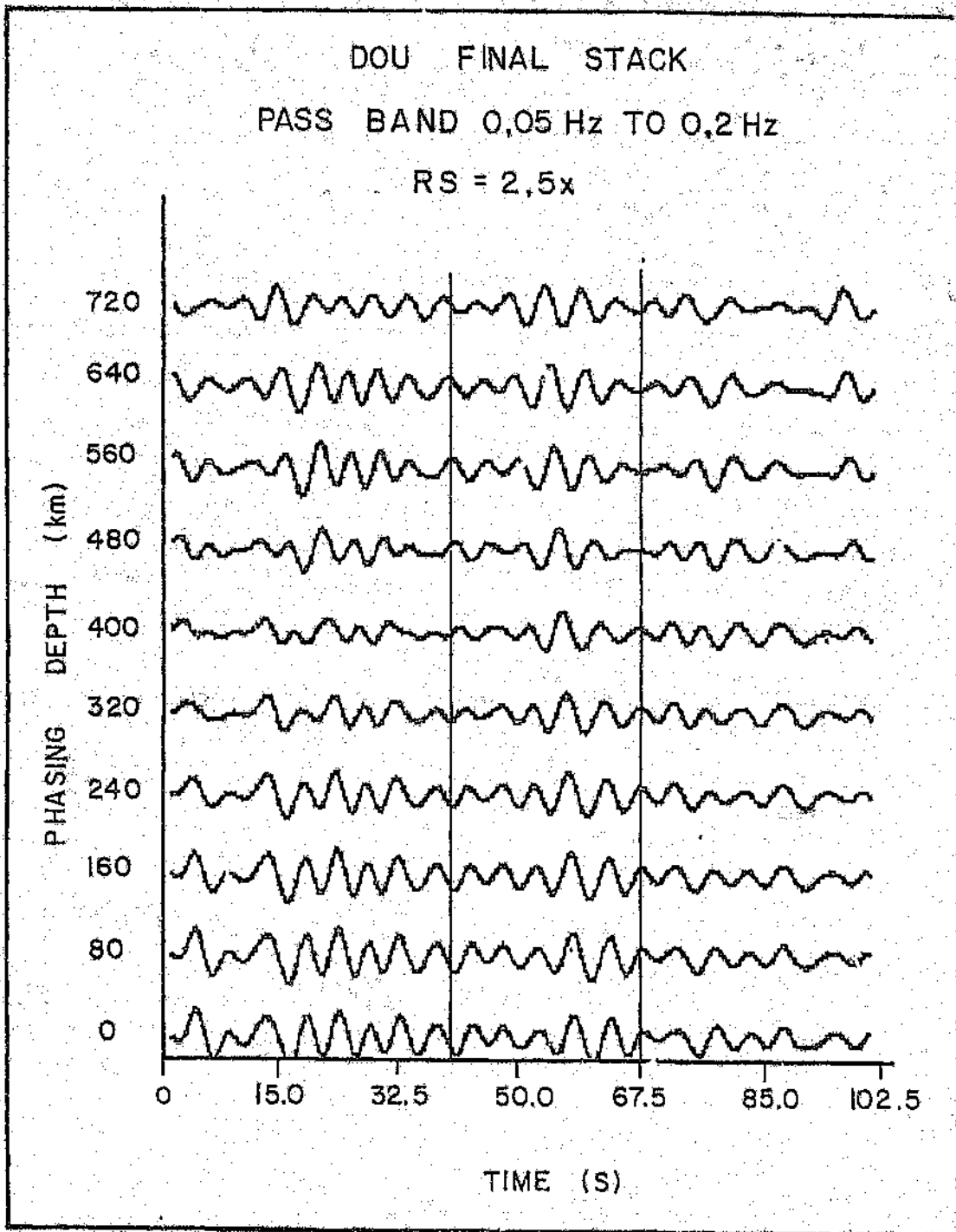
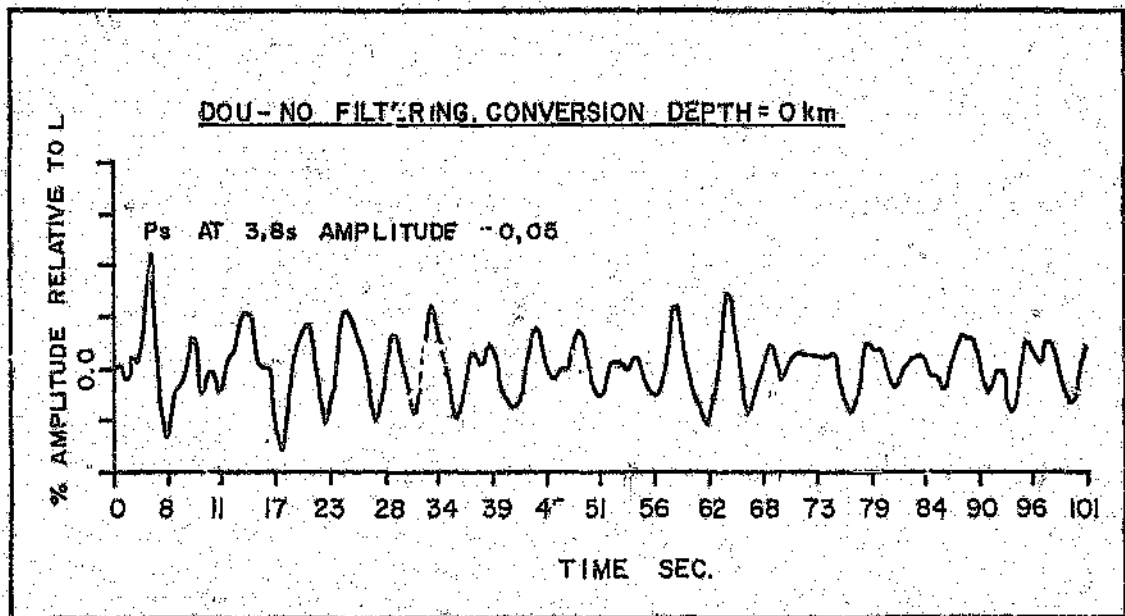


Figure 4.2.3 - Result of long period stack from station DOU.





**Figure 4.2.4** - Near surface conversions for station DOU. This stack corresponds to no filtering of the original records and a conversion depth of 0 km.

### 4.3) Results for Station SAN.

#### Upper mantle conversions -

Figure 4.3.1 (broad-band stack): No mantle transition phases distinguishable from seismic noise are visible in the stacked records.

Figure 4.3.2 (intermediate period stack): The records are very noisy. There is possible evidence for a converted phase corresponding to a depth of 560 km.

Figure 4.3.3 (long period stack): There is no evidence for any phase corresponding to a depth of 560 km, hence, the energy in this area of the stacked record in the previous figure is a processing artefact. However, there is an obvious phase at a delay time of 40s at a phasing depth of 400km. There is also energy at 67.5s between 400 km and 640 km, however peak energy is at a phasing depth shallower than 640 km, consequently this is probably another processing artefact.

The long period stack indicates the presence of a seismic discontinuity at a depth of approximately 400 km beneath SAN. There is no consistent evidence for any other mantle phases in the stacked records for this station.

#### Crustal conversions -

Figure 4.3.4 : The Ps conversion is clearly evident at 5.1s with a relative amplitude of 6 %. The Ppps and the Ppss phases are not seen in the near surface stack. The crust beneath SAN is probably complicated in nature.

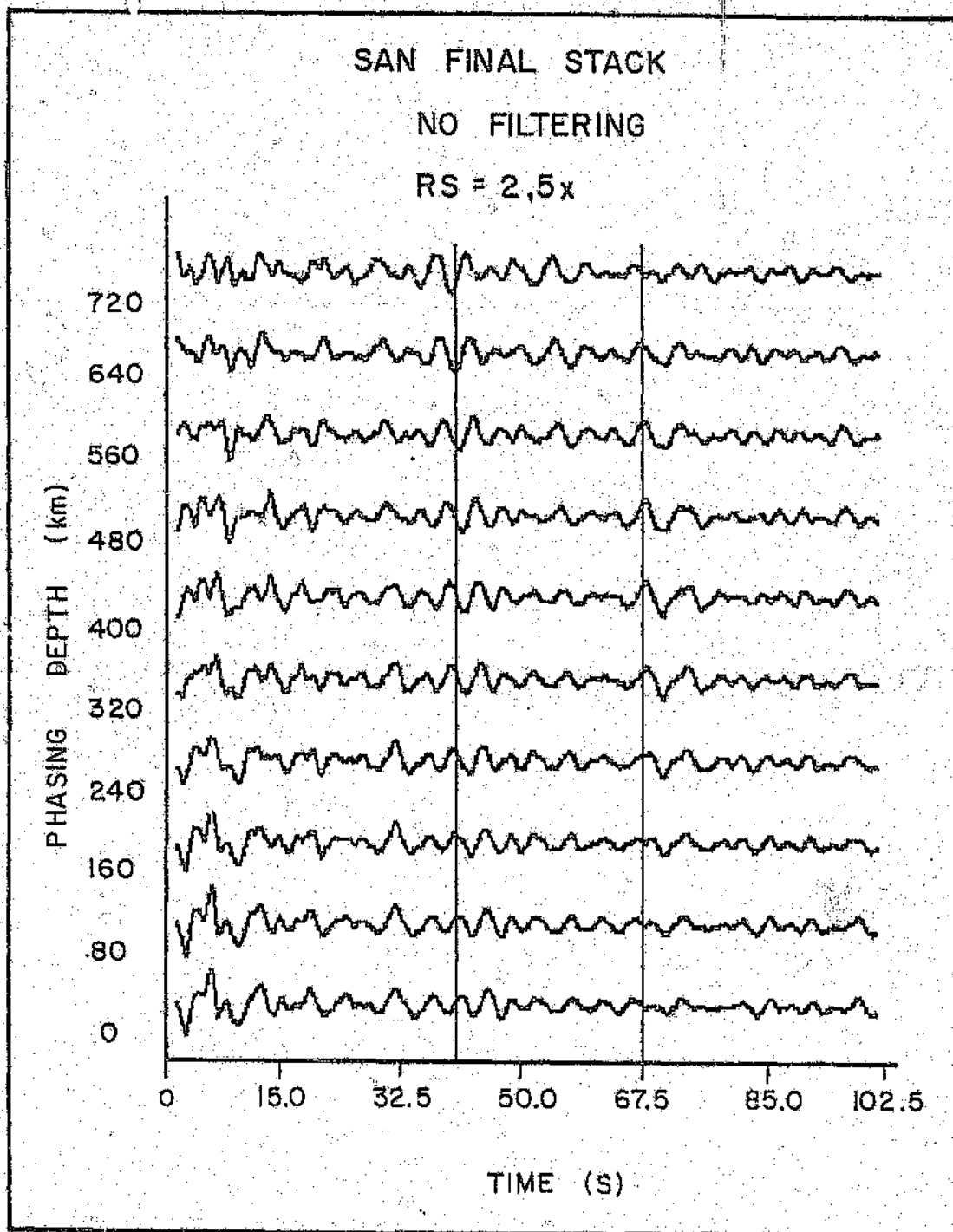


Figure 4.3.1 - Result of broad-band stack from station SAN.

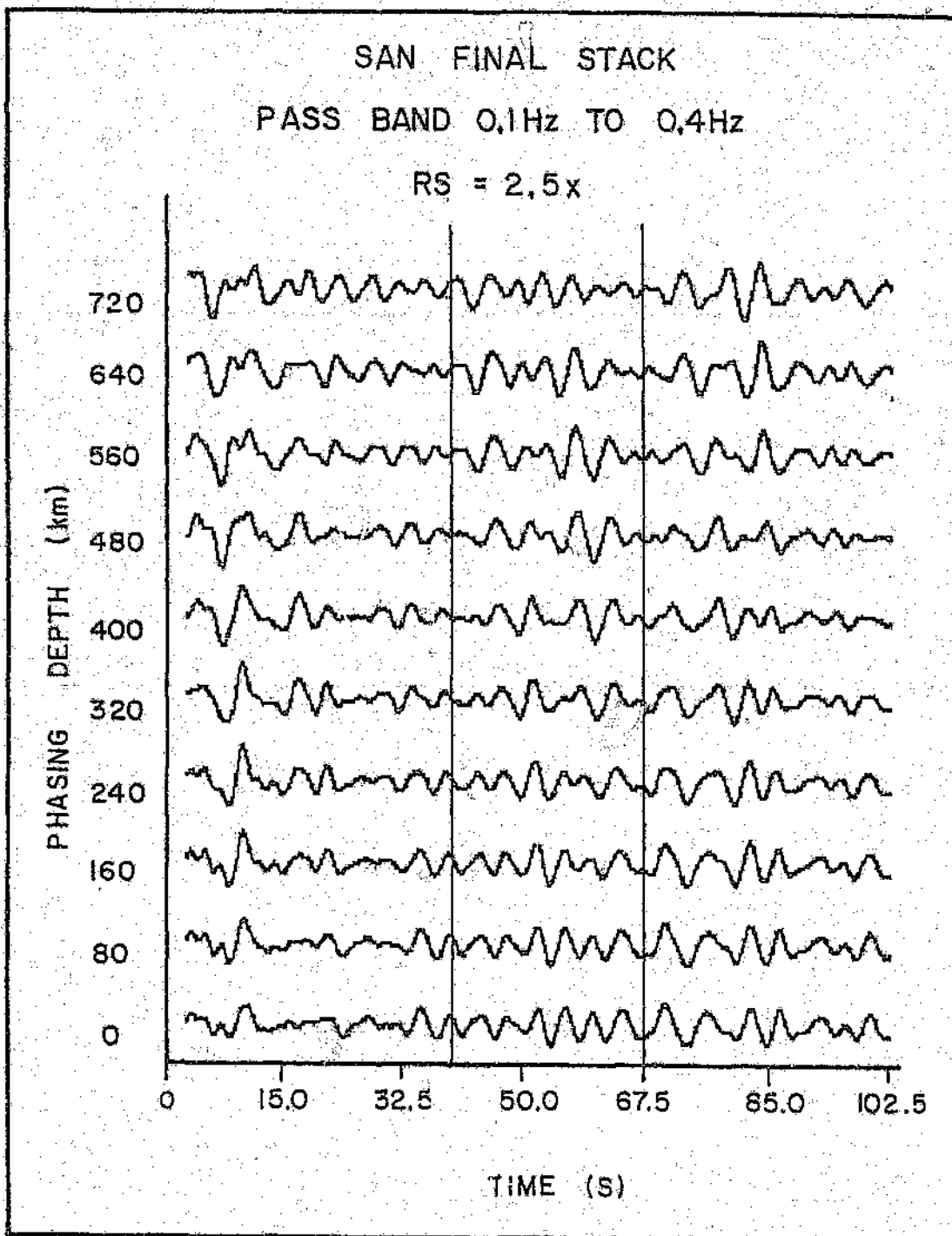


Figure 4.3.2 - Result of intermediate period stack from station SAN.

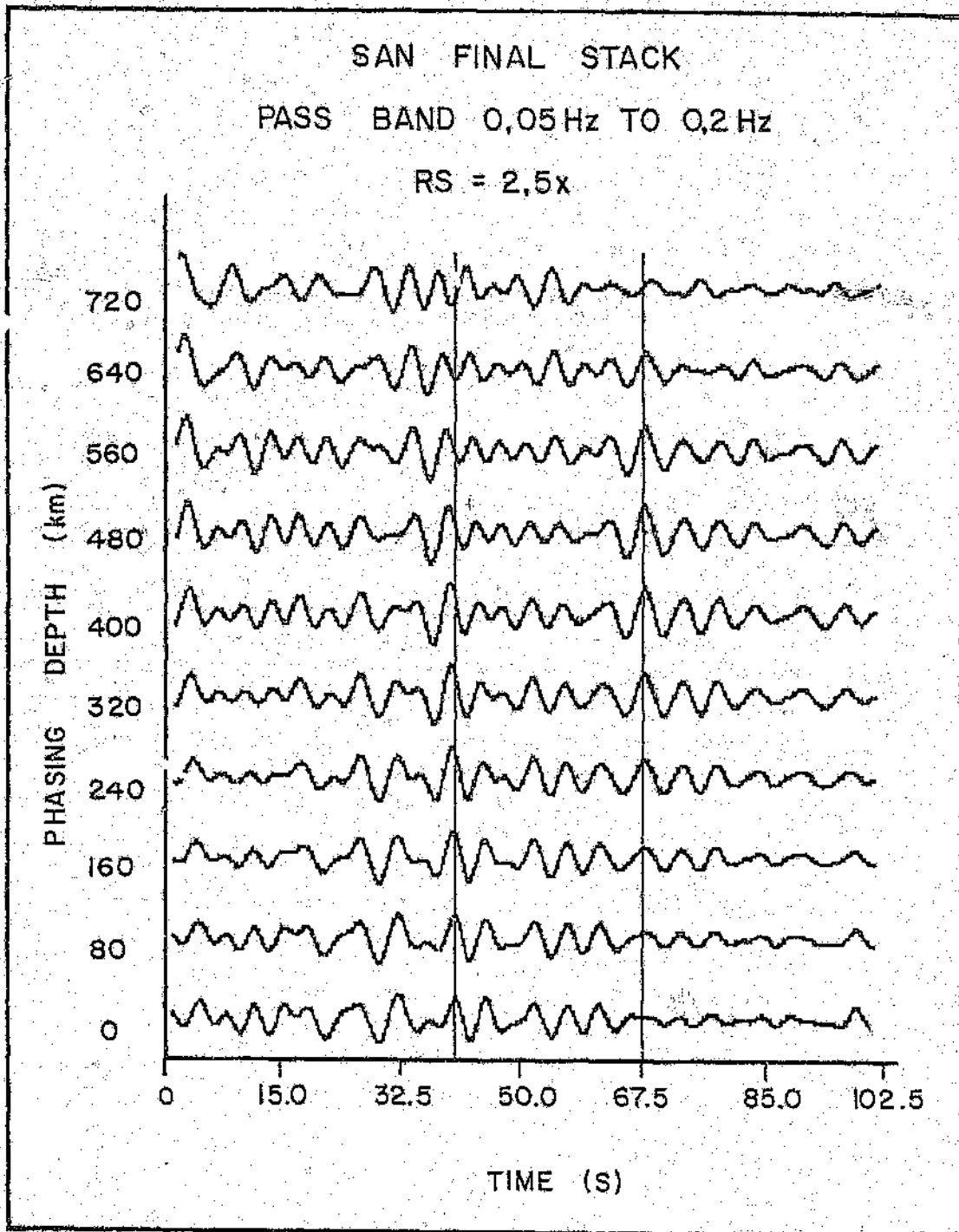
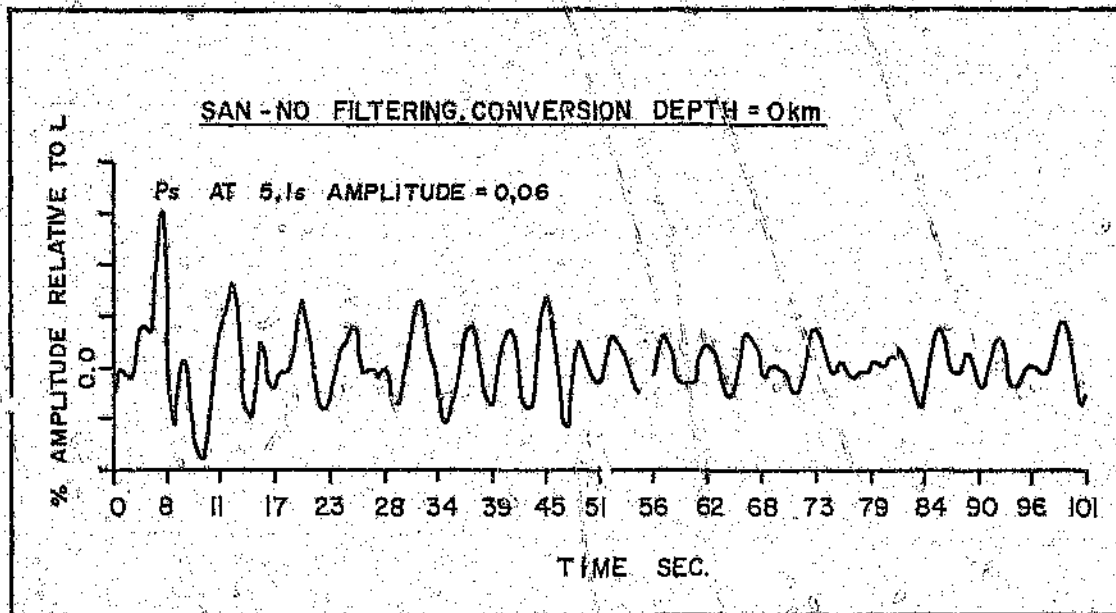


Figure 4.3.3 - Result of long period stack from station SAN.



**Figure 4.3.4** - Near surface conversions for station **SAN**. This stack corresponds to no filtering of the original records and a conversion depth of 0 km.

## 4.4) Results for Station PIL

### Upper mantle conversions -

Figure 4.4.1 ( **broad-band stack** ): There is a phase in the area of the stacked records corresponding to a discontinuity near 400 km. A well defined anomaly with reversed polarity is also visible at a delay time just before 40s at the same phasing depth. No other potential mantle phases are distinguishable from noise.

Figure 4.4.2 ( **intermediate period stack** ): The phase with normal polarity at 40s is still visible. The phase with reversed polarity is less well defined on this stack.

Figure 4.4.3 ( **long period stack** ): The long period records are very noisy. Both phases evident in the broad-band stack are evident in this stack. The complicated nature of the stack near 40s may be related to the nature of the 400 km discontinuity below PIL or to a processing artefact.

A seismic discontinuity at 400 km below PIL is indicated. This discontinuity may be complicated in nature with a reversed polarity phase providing evidence for a velocity inversion near this depth. There are similarities in the long period stacks of PIL and SAN at 40s delay time.

### Crustal conversions -

Figure 4.4.4 : The Ps crust-mantle conversion is at 5.4s with a relative energy of 7.5 %. A phase preceding this is also present in the records - this is probably related to an intra-crustal discontinuity. The Ppps and the Ppss phases are not seen in the near surface stack. A complicated, relatively deep crust-mantle transition is interpreted from this evidence.

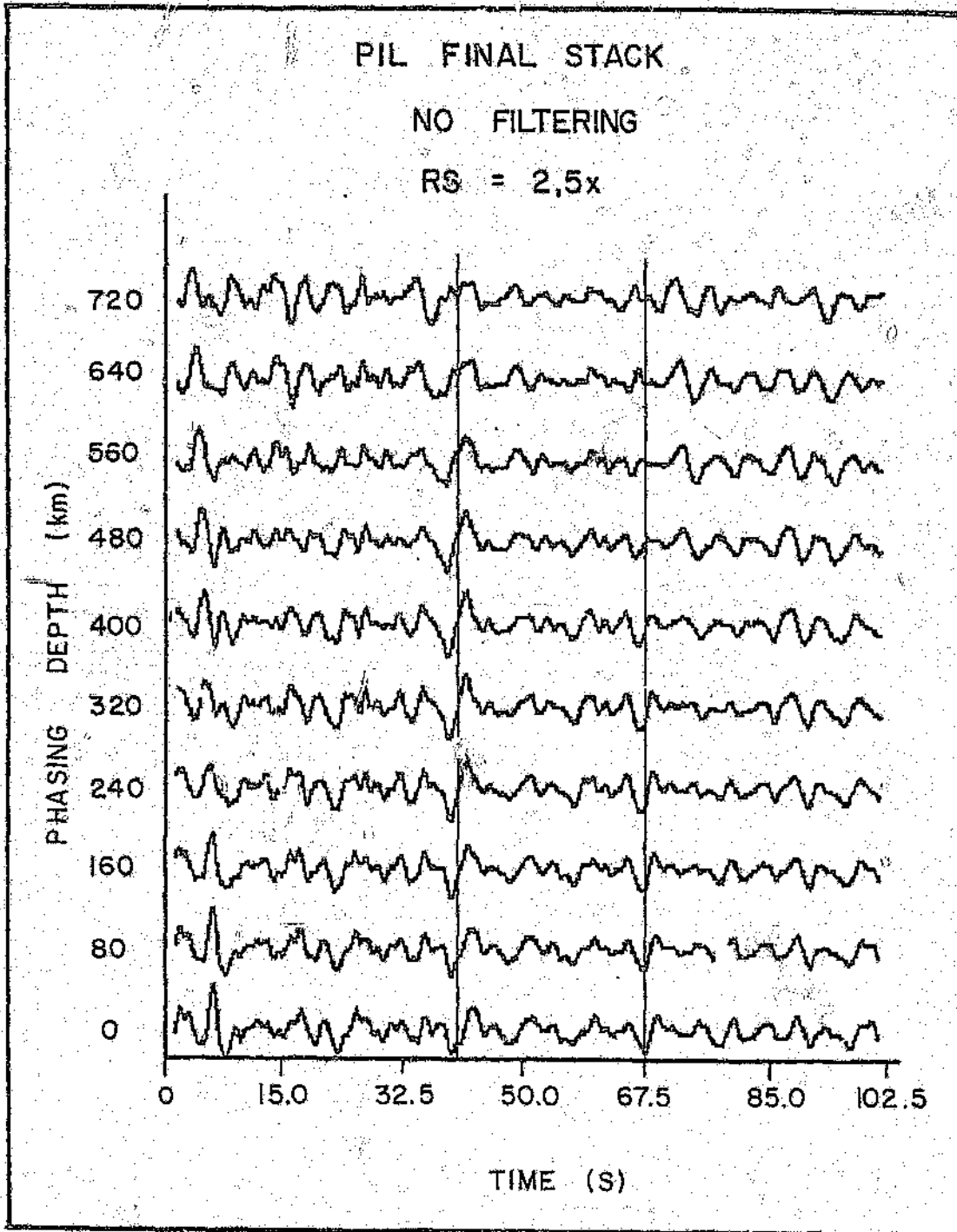


Figure 4.4.1 - Result of broad-band stack from station PIL.



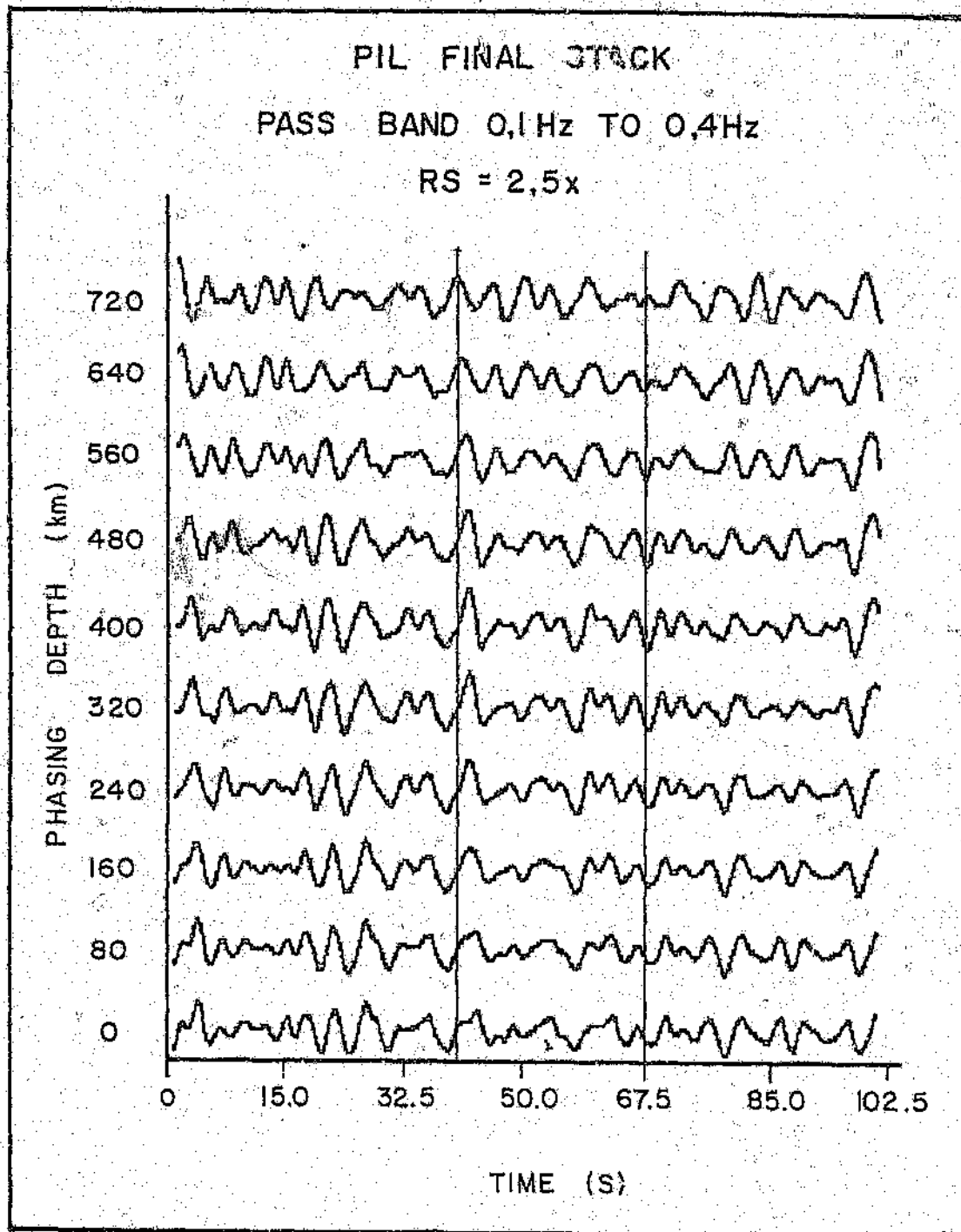


Figure 4.4.2 - Result of Intermediate period stack from station PIL.

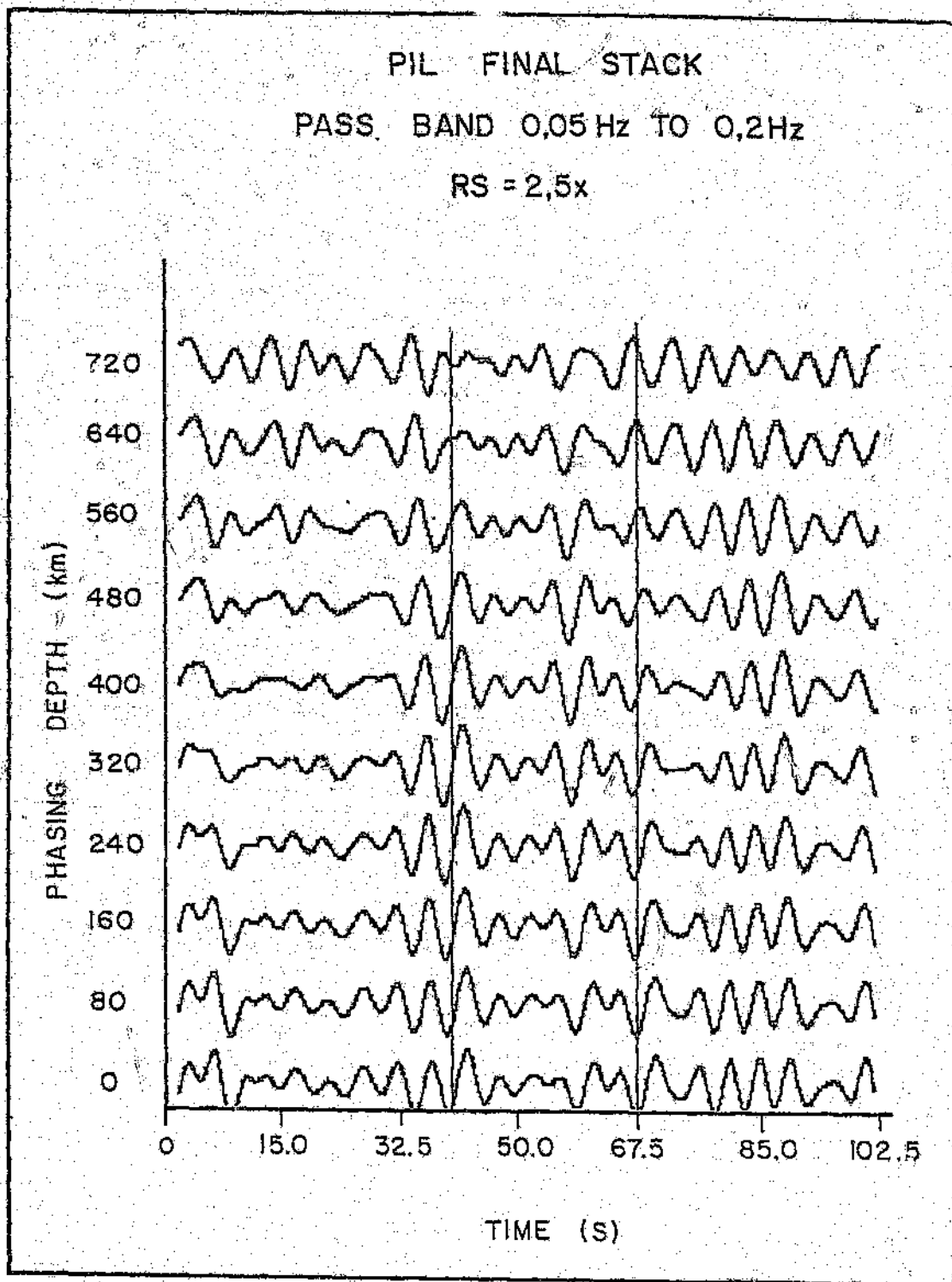


Figure 4.4.3 - Result of long period stack from station PIL.

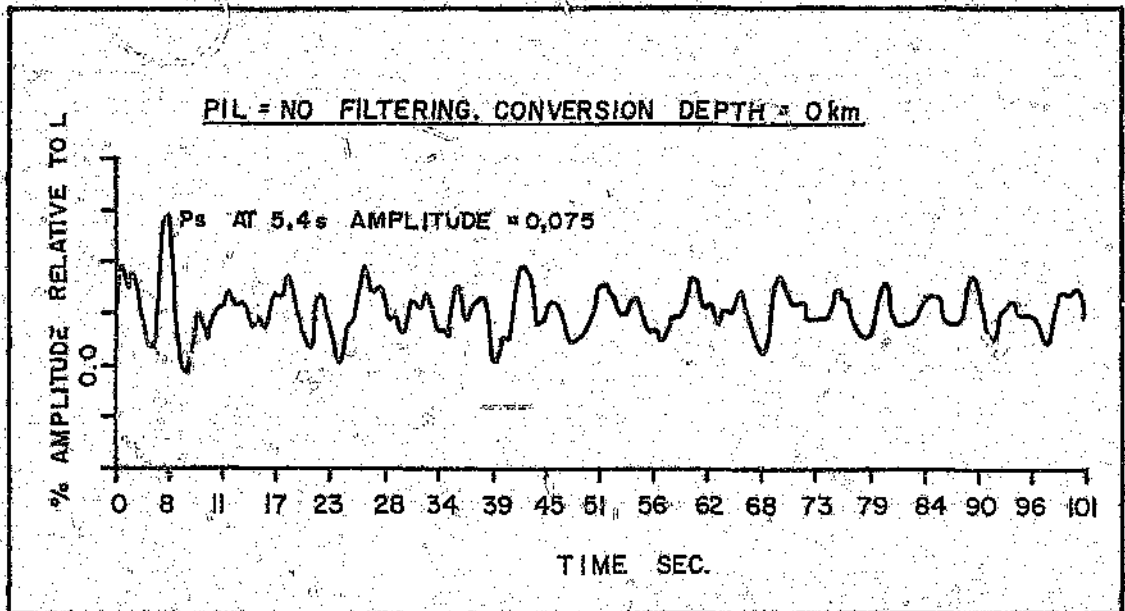


Figure 4.4.4 - Near surface conversions for station PIL. This stack corresponds to no filtering of the original records and a conversion depth of 0 km.

## 4.5) Results for Station KLI.

### Upper mantle conversions -

Figure 4.5.1 ( broad-band stack ): No phases corresponding to upper mantle discontinuities evident in the stacked records.

Figure 4.5.2 ( intermediate period stack ): No phases corresponding to upper mantle discontinuities evident in the stacked records.

Figure 4.5.3 ( long period stack ): There is some energy at 40s for phasing depths between 560 km and 720 km. The delay time and the phasing depth are discordant hence this phase does not represent an upper mantle conversion.

No evidence for upper mantle discontinuities is present in the stacked records of station KLI.

### Crustal conversions -

Figure 4.5.4 : The near surface conversions for KLI are very distinctive. The Ps phase at 4.8s with a relative amplitude of 7.2 %, the Ppps phase at 16.3s and the Ppss phase at 21.0s are well defined in the stacked record. The multiple phases have similar energy to the Ps phase. This information implies a simple crustal model with the crust-mantle transition at the same depth as station BPI.

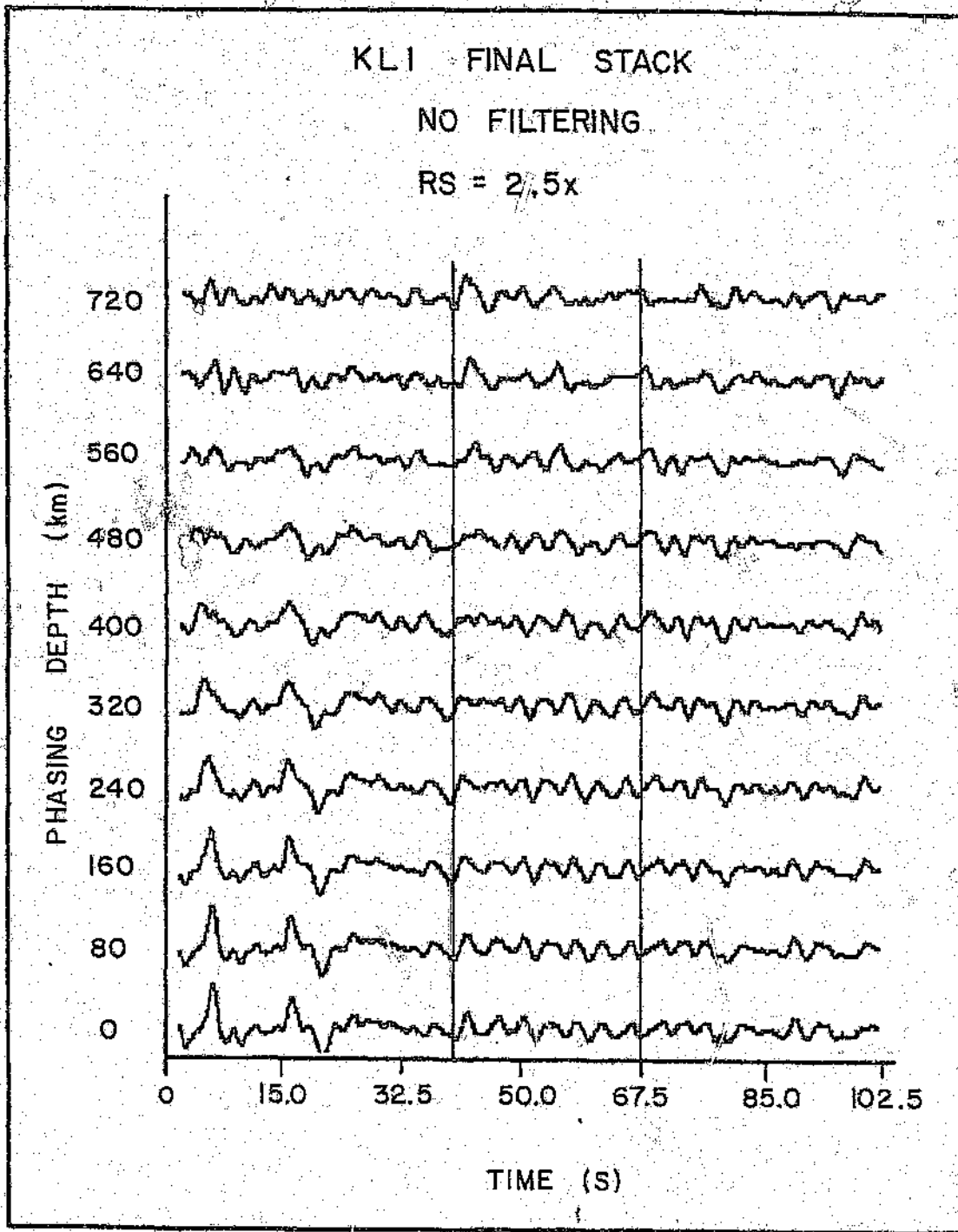


Figure 4.5.1 - Result of broad-band stack from station KLI.

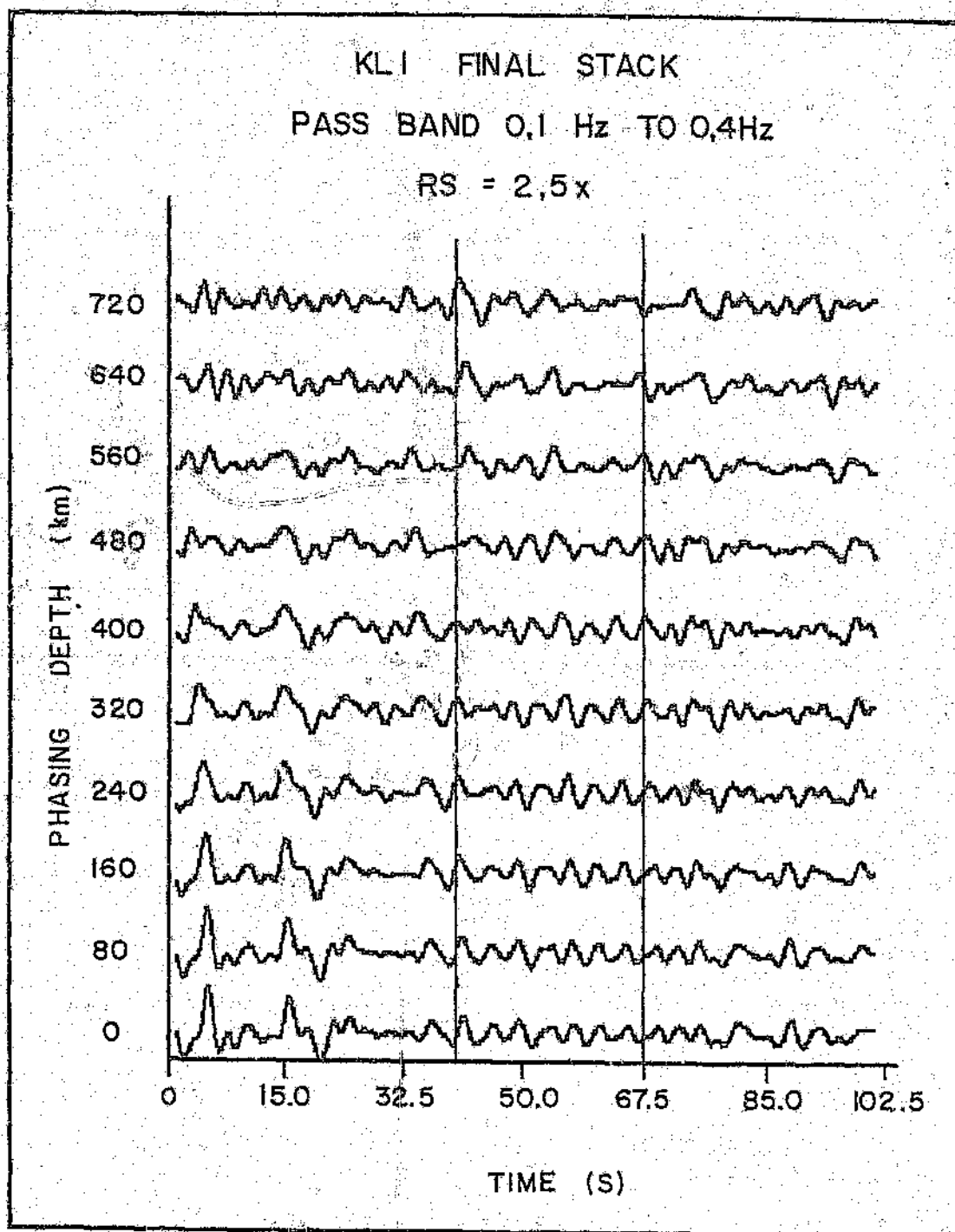


Figure 4.5.2 - Result of intermediate period stack from station KLI.

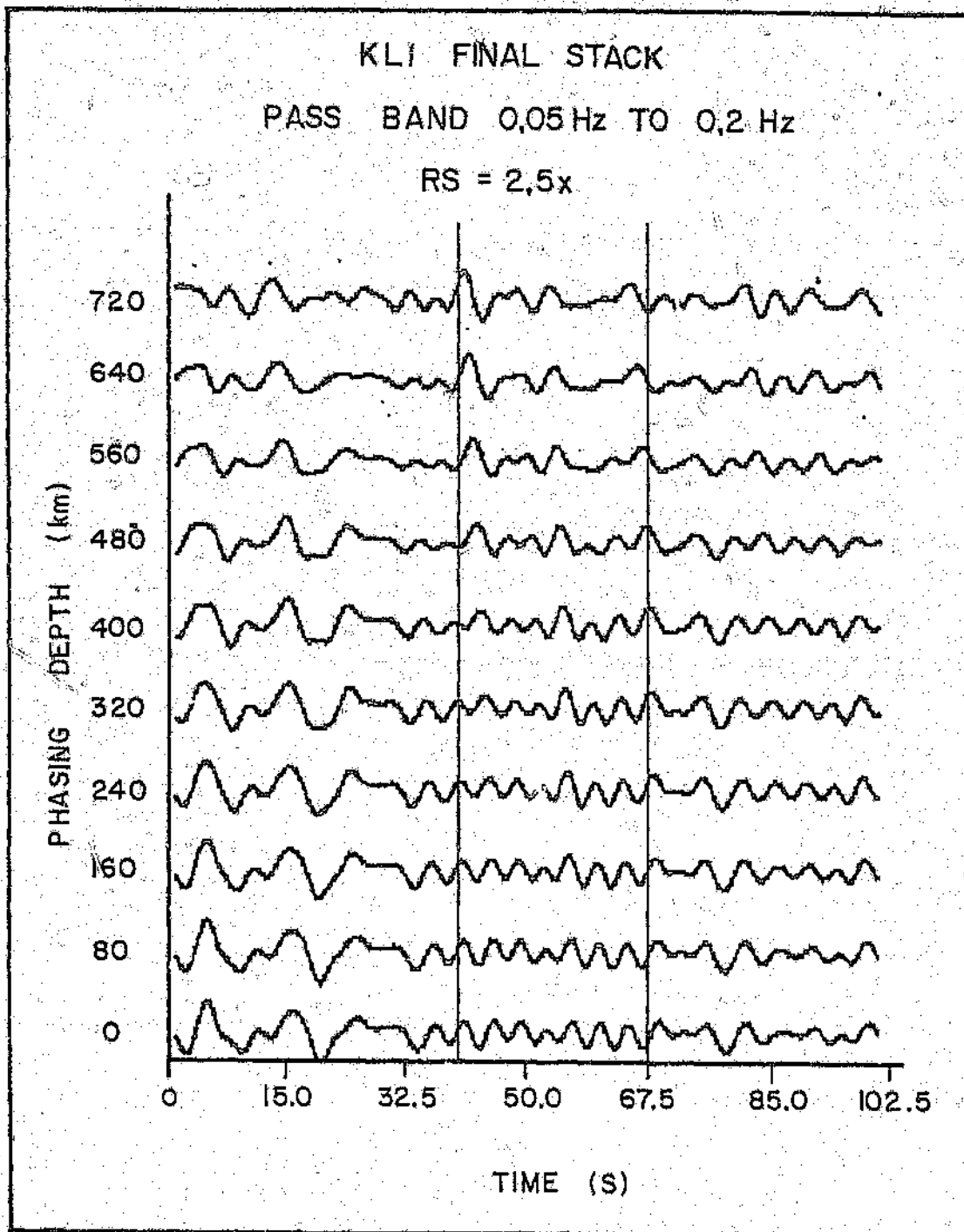
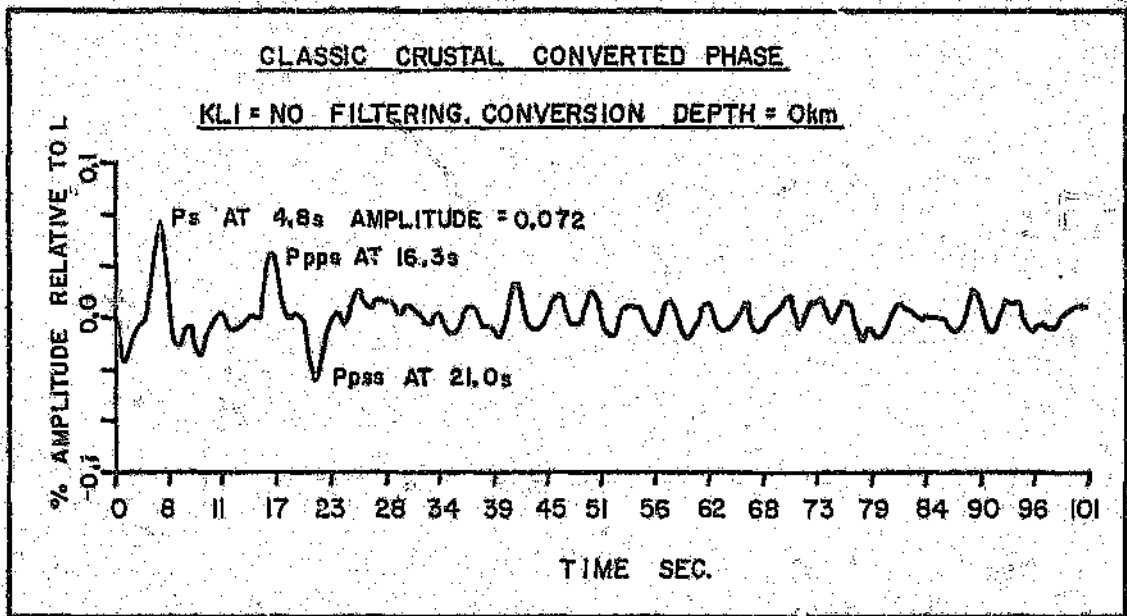


Figure 4.5.3 - Result of long period stack from station KLI.



**Figure 4.5.4** - Near surface conversions for station KLI. This stack corresponds to no filtering of the original records and a conversion depth of 0 km.



#### 4.6) The 400 km Discontinuity Revisited.

An additional type of stacking procedure was performed to investigate the 400 km discontinuity further. The broad-band stacked records for this discontinuity from different stations were stacked together, a procedure which has two effects:

- 1) It increases the fold of the stack dramatically.
- 2) It may, however, average out real differences existing in the stacks of the individual records.

Three individual composite stacks are shown in figure 4.6 - a stack of all five stations' records; a stack of the records of SAN, and PIL and a stack of the records for BPI, KLI and DOU. The division was on the basis of stations showing a clear phase at 400 km (SAN and PIL) as opposed to those showing no clear phase (BPI, KLI and DOU).

A double phase of normal polarity bounding a phase with reversed polarity in the vicinity of 40s is apparent on all three stacks. This feature has two possible origins:

- 1) The 400 km discontinuity is complicated in nature beneath all five stations.
- 2) An unusual processing artefact has been introduced into the five stacked records.

If the first origin is correct, two possible interpretations are the presence of a double discontinuity or a low velocity inversion layer at 400 km. The second interpretation is preferred since the two phases of normal polarity are most easily interpreted as sidelobes to an intercalated negative phase. The relatively short period of the observed phases (less than 5 seconds) implies a first order seismic boundary of whatever nature. If the second origin is correct it is unlikely that the original unfiltered records used to produce the five stacks would contain processing artifacts with such temporal consistency - hence the effect would have to be introduced in the delay time stacking procedure. This is also thought to be unlikely.

Similar additional stacking procedures applied to the 640 km records produced no

phases at the correct delay time.

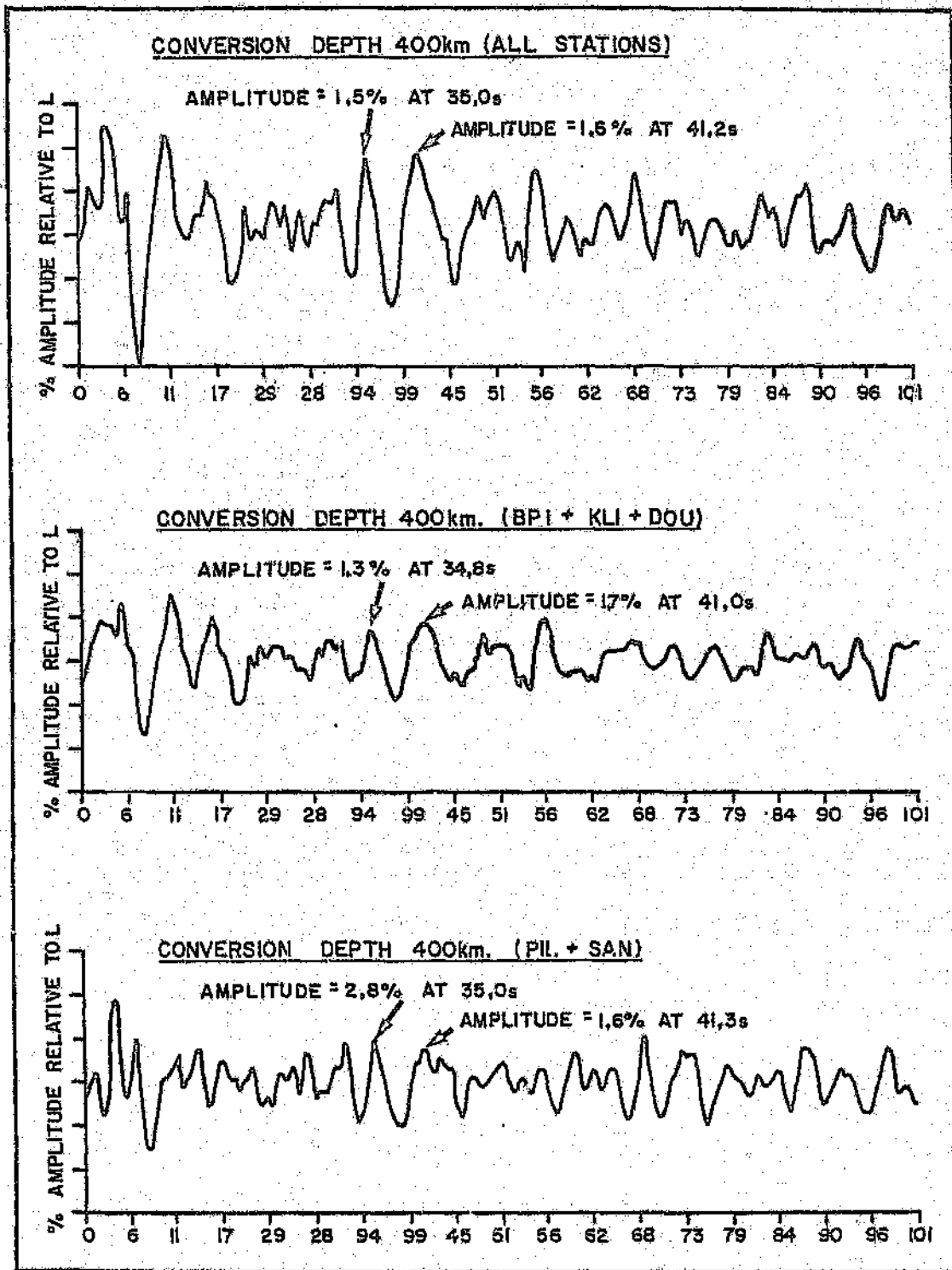


Figure 4.6 - Additional stacks produced for the 400 km discontinuity.

## 4.7) Summary of Results.

A brief summary of the observations of the stacked results for the five stations is presented.

### General observations -

The stacked records are generally noisy with the noise levels increasing as the pass band is narrowed. This indicates that the filters applied to the data may have introduced an unwanted signal to the final records used in the stack - this is disturbing since filtering should improve the signal to noise characteristics of the data. The problem is almost certainly exacerbated by the low fold of the stack caused by the lack of suitable records.

### Upper mantle phases -

Despite the problems mentioned above, the following potential upper mantle discontinuities were apparent in the stacked records:

- 1) A discontinuity between 500 km and 560 km beneath DOU.
- 2) A complicated discontinuity at 400 km beneath PIL.
- 3) A discontinuity at 400 km beneath SAN. There are similarities in the long period stacked records at SAN and PIL. It is interesting to note that these stations are associated with complicated crustal models.
- 4) There is no clear discontinuity at 400 km evident beneath the stations with simple crustal models - KLI, DOU and BPI. However, composite stacks indicate the presence of a complicated 400 km discontinuity beneath these stations as appears to occur beneath SAN and PIL. The period of the phases associated with this discontinuity indicate a relatively sharp seismic boundary.
- 5) No evidence for a discontinuity at approximately 670 km beneath any station was found.

## 5) DISCUSSION.

### 5.1) Methodology.

To facilitate critical assessment of the method employed in this study, comparison will be made with the results obtained by Vinnik(1992) who worked independently and contemporaneously with the same data. A selection of Vinnik's results are presented in figures 5.1.1 to 5.1.3. Figure 5.1.1 shows the broad-band stack for station KLI, figure 5.1.2 shows the long period (10s) stack for BPI and figure 5.1.3. shows the long period stack for PIL. A summary of the results from the current study and the results from Vinnik's study are presented in table 5.2.2 in section 5.2.3. - what is important at this stage is a visual comparison of Vinnik's results with those obtained in the current study.

The broad-band stacks for KLI are almost identical (figure 4.5.1 and figure 5.1.1). The pattern of the near surface conversions with increasing phasing depth and the lack of dominant mantle phases on both figures should be noted. The long period stacks for BPI and PIL (figures 4.1.3 and 5.1.2 and figures 4.4.3 and 5.1.3, respectively) are, however, in both cases radically different. Vinnik's long period results are virtually noise free. A dominant reversed polarity phase at PIL at 400 km and a normal polarity phase at BPI at 640 km are clearly visible. Similar differences in the quality of the long period stacks between the two analyses were observed at other stations as well. If it is assumed that Vinnik's results are correct within the known limitations of the data base, these differences can be accounted for in one of two ways:

- 1) The data of the current study have been processed incorrectly;
- 2) The methodology and processing software used by Vinnik is superior in its implementation.

With the exception of minor differences at BPI, the crustal conversions at all five stations were identical in both analyses. Figure 5.1.4 shows a broad-band stack for only two events at BPI, which contained energy in the cross correlated  $\hat{H}$  component

only two events at BPI, which contained energy in the cross correlated  $\hat{H}$  component records at times corresponding to a discontinuity at 670 km. The well pronounced energy peak at 67.5s between 640 km and 720 km indicates that the stacking procedure has been implemented correctly. The similarity of the crustal conversions with increasing phasing depth in both studies at KLI confirms this. These observations indicate that with the exception of the filtering, the processing of the individual records and stacking were implemented correctly in the current study.

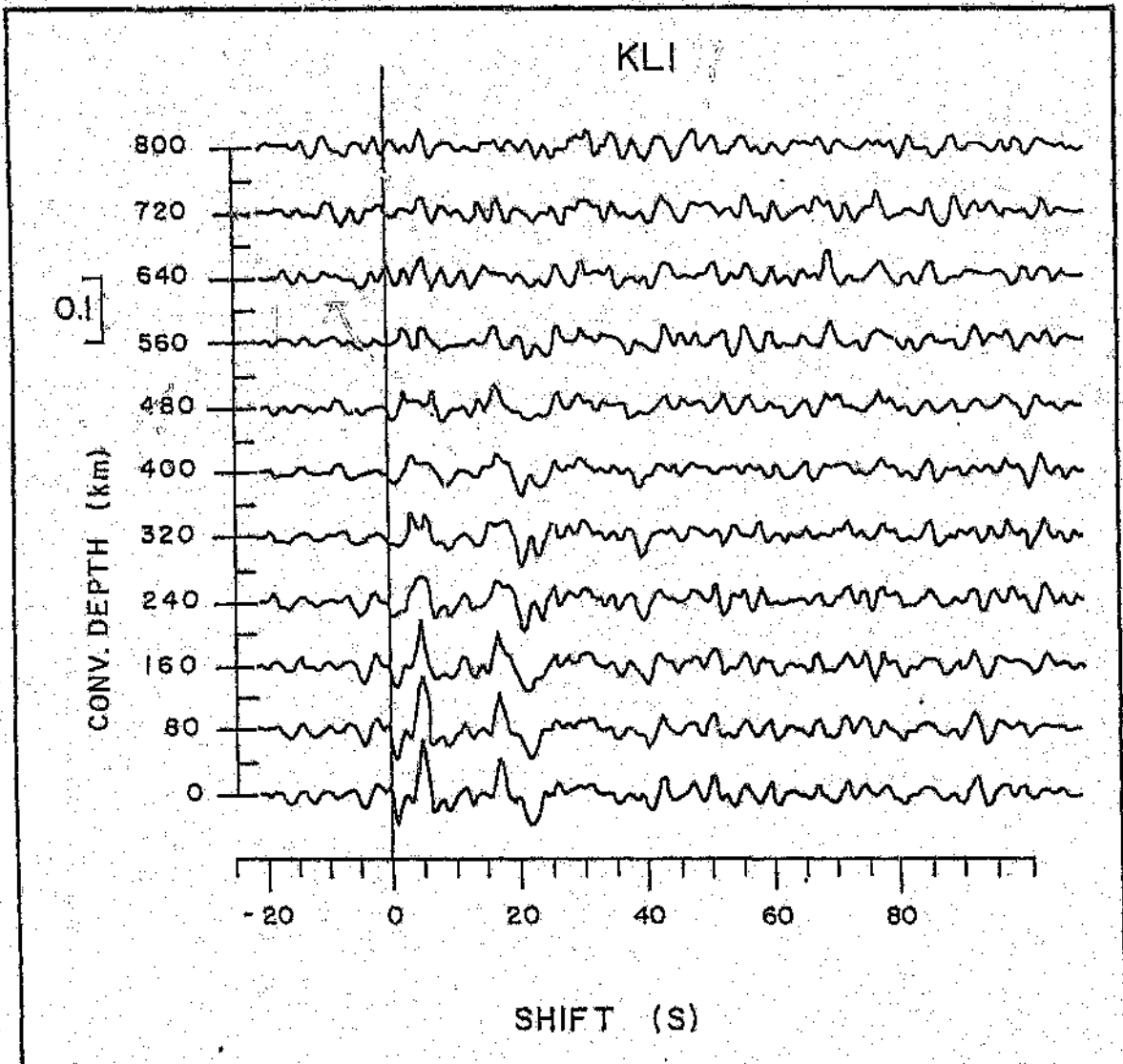


Figure 5.1.1 - Broad-band stack at station KLI after Vinnik(1992).

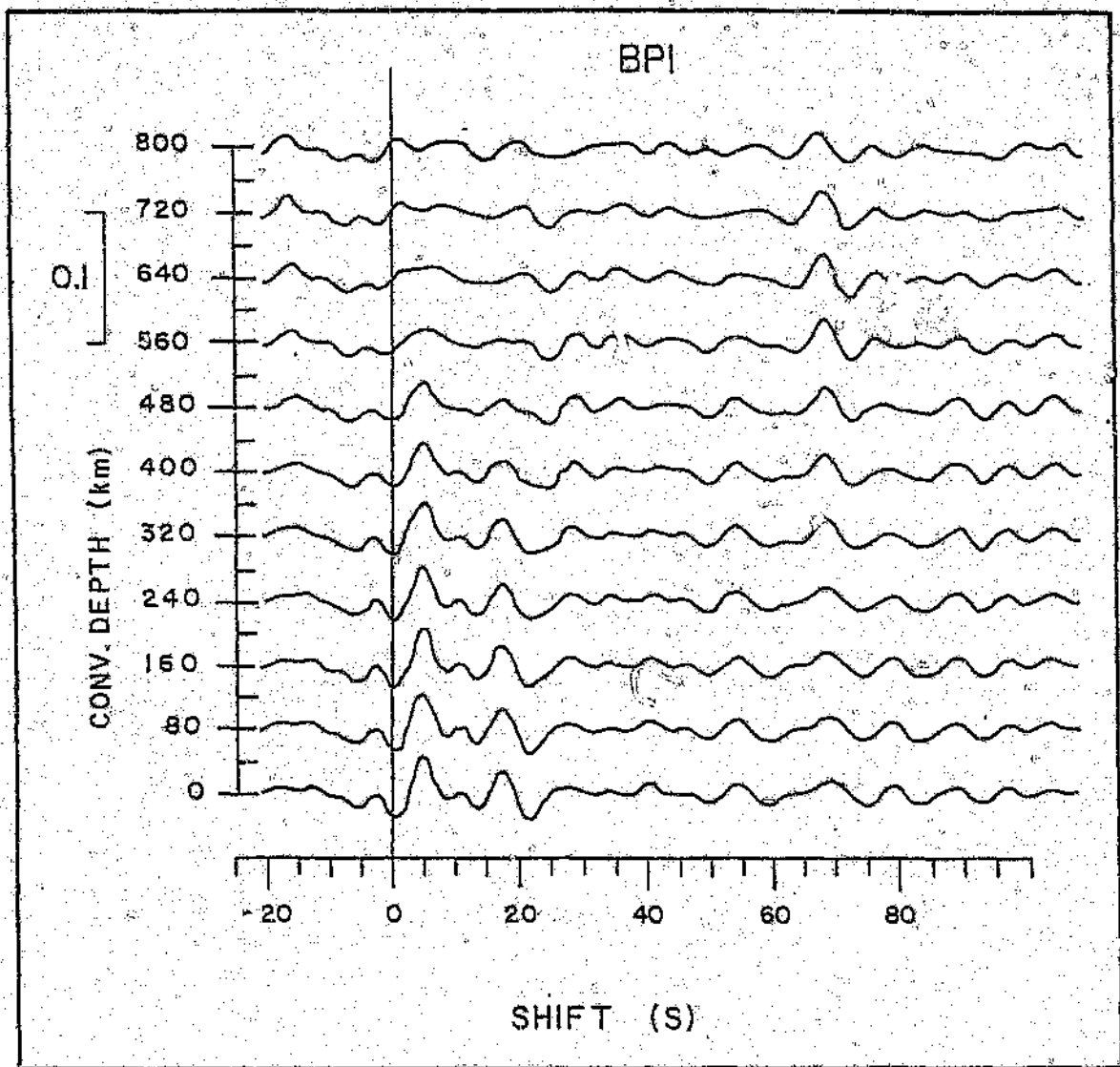


Figure 5.1.2 - Long period stack at station BPI after Vinnik(1992).

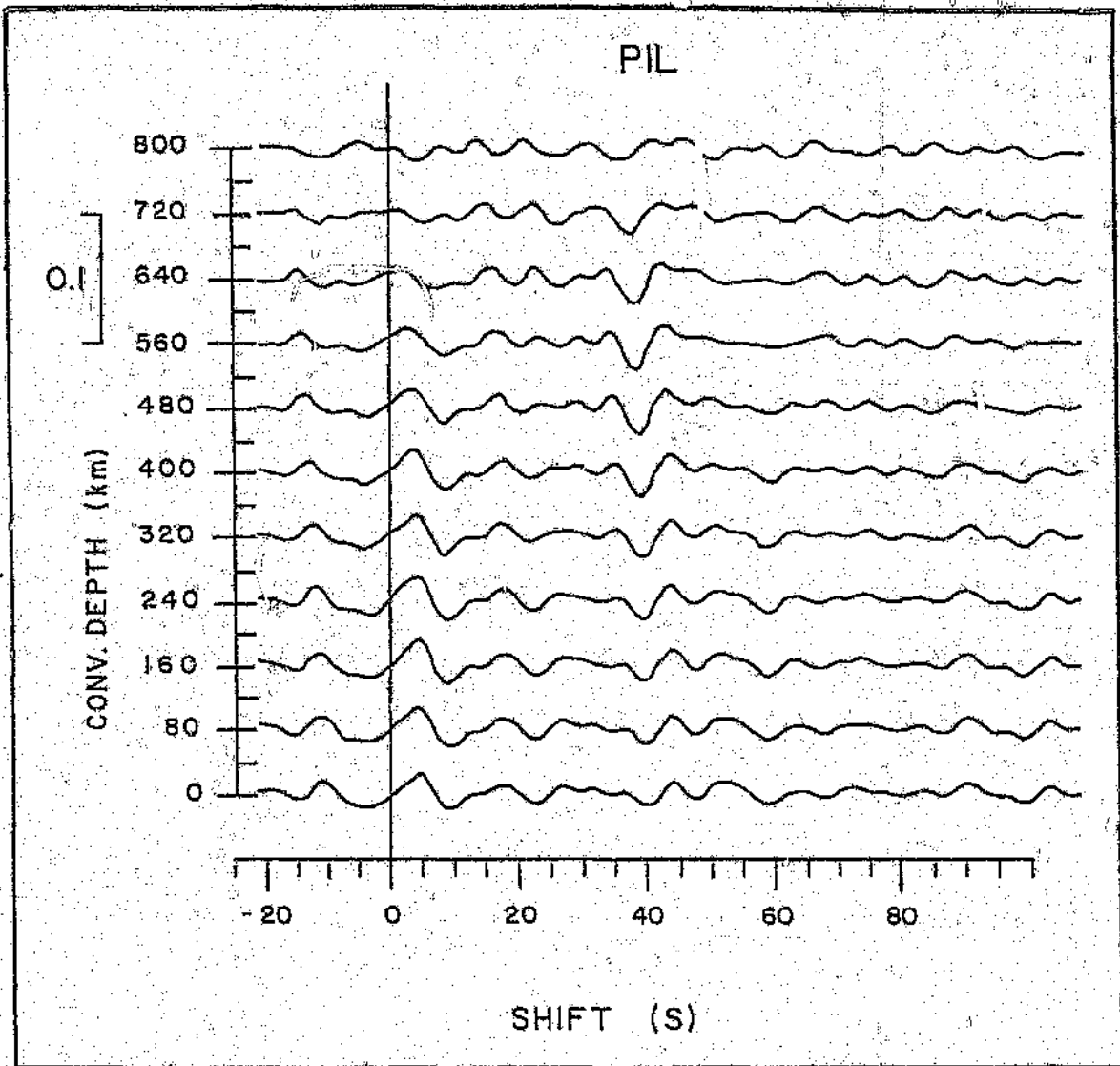


Figure 5.1.3 - Long period stack at station PIL after Vinnik(1992).

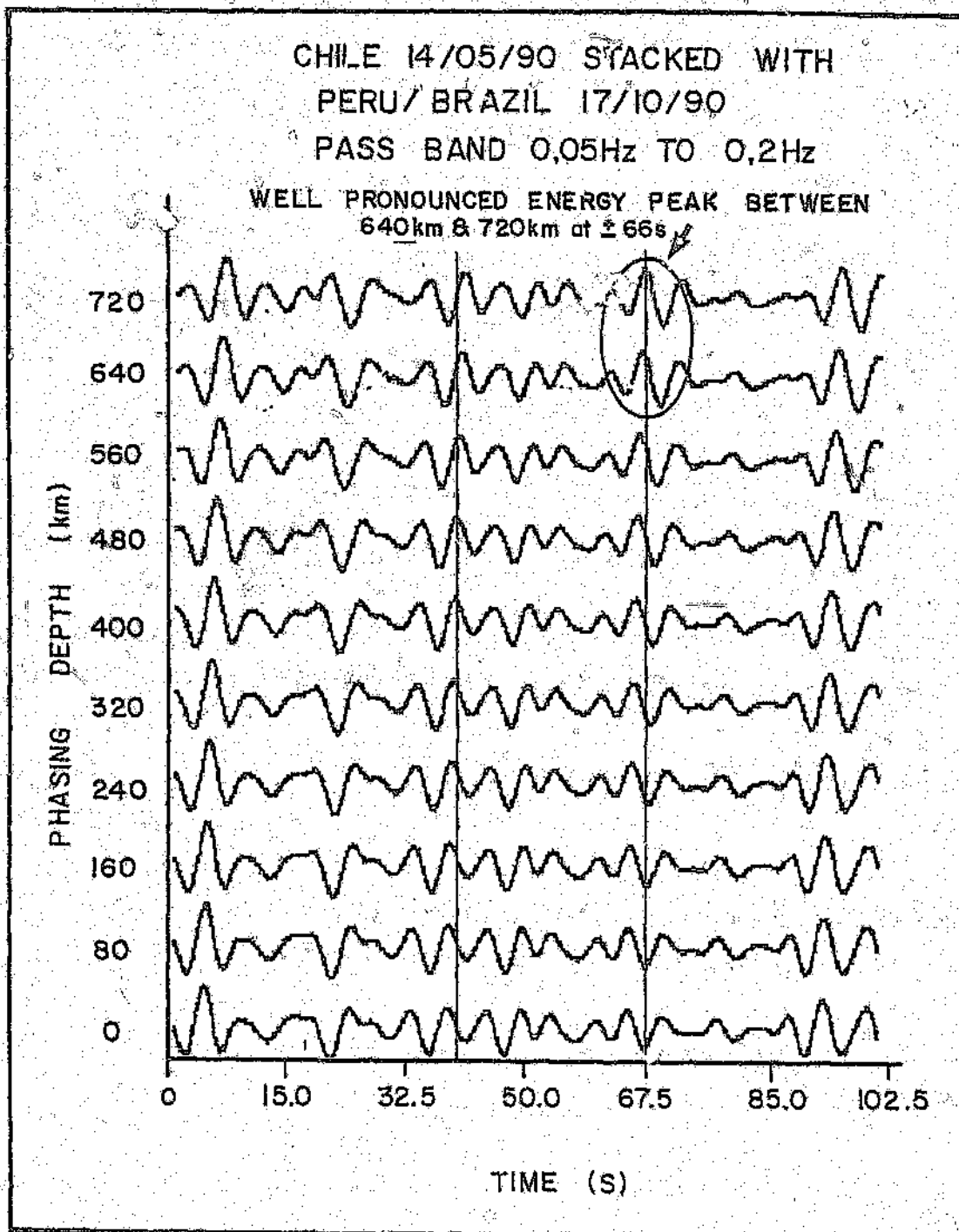


Figure 5.1.4 - Result of broad-band stack for two events recorded at BPI.



Therefore differences between the two sets of results can almost certainly be ascribed to the improved normalisation procedure implemented by Vinnik(1992). Instead of cross-correlating the H component with the onset of the L component, each  $\hat{H}$  component was generated in the time domain using a filter which minimised the damped least square difference between the L component of the P wave and a normalised delta function. Curiously, the details of this processing method with respect to P to S conversion analysis had not been published at the time of writing this dissertation. The method clearly represents a dramatic improvement over the previous cross-correlation technique in that clear phases from 400 km and 670 km can be observed in stacks derived from a very limited data base. The cross correlation technique clearly does not enhance these phases sufficiently in the individual records, hence, stacking data generated with this method can debilitate rather than enhance the final result.

No details of the filtering methodology employed by Vinnik (1992) are published except that the pass band was between 0.1 hz and 0.2 Hz (Vinnik et al, 1993b). The filtering performed in the present study could clearly be improved upon if the results are compared with those of Vinnik. The author filtered the raw velocity records in an attempt to simulate processing data acquired over a limited pass band. The danger with this is that any processing artifact introduced by the filter will be propagated (and possibly amplified) at each subsequent processing stage. With hindsight, it may have been better to filter the final  $\hat{H}$  and L' components just prior to stacking. Despite this, no artifacts should have been introduced by having too narrow a pass band (two octaves), however, a one octave intermediate band is possibly too narrow. The problem with increasing the width of the intermediate band is that more energy at unwanted frequencies will be present in the filtered records. This is especially relevant with the data under discussion where nearly all the energy is at frequencies below 1.0 Hz.

More experimentation could have been done with Butterworth filters which utilise poles and zeros in the Z-transform domain<sup>#</sup>. A Butterworth filter allows for much tighter ramps of the transfer function. The advantages of this would have to be offset

against phase problems related to these filters and the difficulties often encountered in implementing them as numerical routines. In addition, the author believes the effect of the filtering problems on the final results is probably small compared with the effect of processing a small data set with inferior numerical procedures.

The above discussion must be viewed in light of the work of Shearer(1991) who used data collected over a five year period from the Global Digital Seismograph Network to place constraints on the upper mantle discontinuities. The reference is a paragon of clarity in that all selection and processing procedures applied to the data are described in detail. The smoothing parameters discussed by Shearer, which are applied in addition to standard filters, could help explain the high noise levels in the long period stacks. The conclusions in this reference regarding the discontinuities of interest were also derived from results pertaining to P multiples, SH multiples and SS precursors in conjunction with P to S phases. Obviously, this lends confidence to the results obtained. Even without these additional constraints, the author believes that the results obtained in the current study could be greatly improved if the processing was performed using, for example, the rigorous method of Shearer(1991). The results of Vinnik(1992) and Vinnik et al(1993b) prove this - unfortunately, no detailed description of the methodology employed in these studies has been published.

# - No references are quoted with respect to data filtering. This topic is covered in most texts on numerical methods and digital signal processing, for example, Kanasewich(1975), Kuc(1990) and Press et al(1992).

## 5.2) Implications for the Upper Mantle Discontinuities.

### 5.2.1) The importance of the upper mantle discontinuities.

One of the most debated subjects in the last 30 years is whether the earth's mantle experiences whole-mantle or two layer convection (Silve, et al, 1988). Whole-mantle convection models are supported by seismological evidence of subducted oceanic lithosphere penetrating into the lower mantle and the absence of geophysical evidence for a large thermal boundary layer between the upper and lower mantle. Two layer convection is supported by observations of isotropic heterogeneity in the mantle. An understanding of the upper mantle discontinuities is of paramount importance in the understanding of upper mantle dynamics and its implications for many branches of earth science including the earth's origin, plate tectonics and geochemical reservoirs. If, for example, the discontinuity at approximately 670 km is characterised by an isochemical phase transition whole-mantle convection is implied, while a chemical boundary (with or without an associated phase change) implies two layer convection (Ringwood and Irifune, 1988).

Many arguments and counter-arguments have been proposed for the chemical and isochemical transition models over the years. Put simplistically, a model assuming isochemical boundaries requires a pyrolytic mantle consisting mainly of olivine and orthopyroxene with minor garnet and diopside, while a model involving a chemical transition requires a piclogitic mantle consisting of clinopyroxene and garnet with less olivine and orthopyroxene. Evidence, for and against each model, is derived from many sources including cosmochemistry, experimental petrology and seismology. Cosmochemistry is concerned with inferring mantle compositions from compositions observed in meteorites, experimental petrology is concerned with determining laboratory properties of assumed mantle minerals at temperatures and pressures experienced in the mantle while seismology attempts to establish the actual rheological properties at depth from seismic measurements. These techniques, succinctly described by Anderson(1992) and Wyllie(1992), are illustrated by the example in figure 5.2.1.

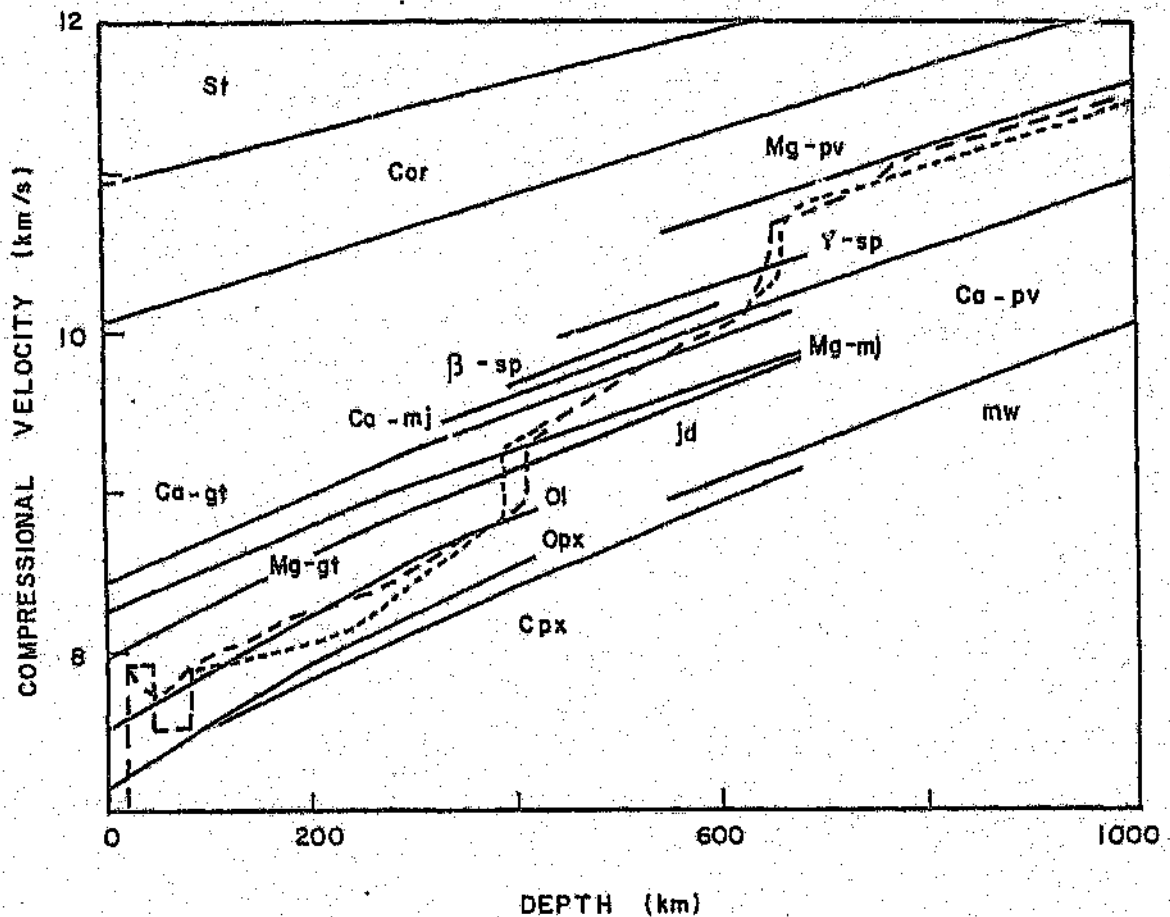


**Figure 5.2.1** - Calculated compressional velocities plotted against depth for a variety of mantle minerals. The dashed lines correspond to typical seismic velocity profiles. Calculations correspond to a 1400° C adiabat. The diagram reproduced from Anderson(1992) illustrates how laboratory observations of mineral properties can be combined with measured seismic velocities to constrain mantle mineralogy .

A simplified model of upper mantle rheology will be discussed in the next section (5.2.2) while the relevance of the data described in this study to the discontinuities beneath South Africa will be discussed in section 5.2.3. The historical progression of ideas and arguments relating to upper mantle models will not be discussed in this dissertation, however - the literature quoted in section 1.3 can be consulted in this regard. Quite simply, the limitations of experimental petrology and restricted resolution of limited seismic data mean that the issue cannot be resolved conclusively.

### 5.2.2) Current thinking on upper mantle rheology - a simplified model.

Anderson(1992) describes a current model of upper mantle mineralogy. The important upper mantle minerals (with estimated abundances in weight %) are olivine(37-51), orthopyroxene(26-34), clinopyroxene(12-17) and garnet(10-14). These minerals can be represented as solid solution series, for example, the forsterite  $Mg_2SiO_4$  + fayalite  $Fe_2SiO_4$  solid solution series of olivine. A phase diagram for this series with respect to pressure is presented in figure 5.2.2.

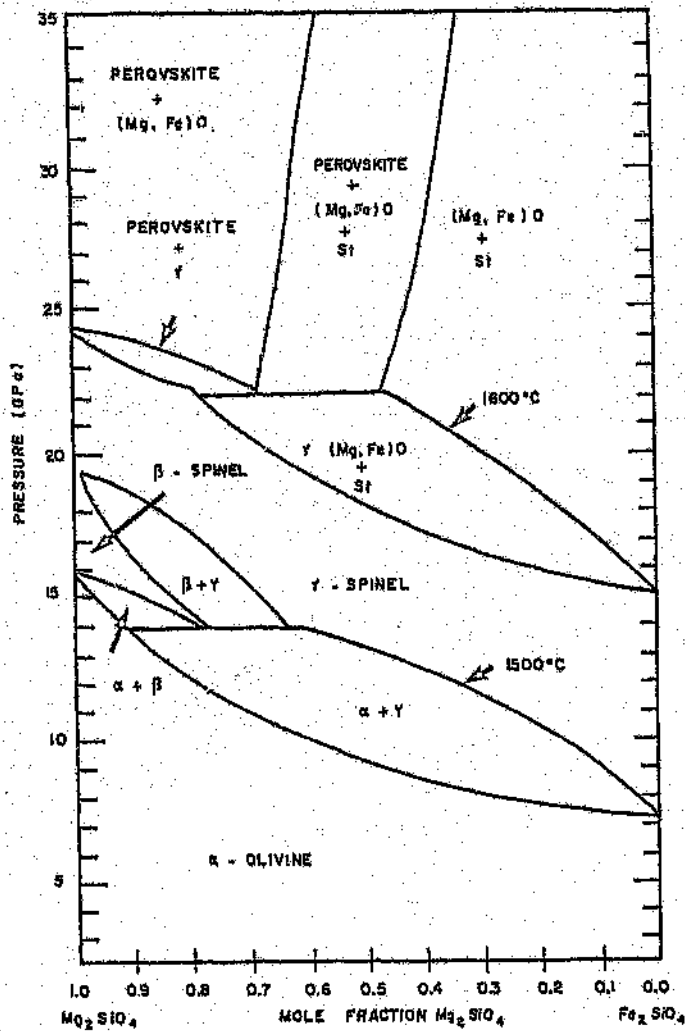


Figure 5.2.2. - Phase diagram of the olivine system showing the stability fields of various stable phases. The  $\alpha$  phase is olivine, the  $\beta$  and  $\gamma$  phases are forms of spinel. Both the olivine to spinel and spinel to perovskite phase changes occur at greater depths in Mg-rich than in Fe-rich rocks. These phase changes are important at the 400 and 670 km discontinuities, respectively. Diagram after Anderson(1992).

At high pressures, these minerals convert to denser forms with different crystal structures (solid-solid phase changes). For example at a depth of about 400 km (13-15 GPa, figure 5.2.2) olivine converts to a spinel structure - initially to the  $\beta$  phase which is approximately 7.5 % denser than olivine, while at greater depths the  $\beta$  phase converts to the  $\gamma$  phase which is approximately 10 % denser than olivine,

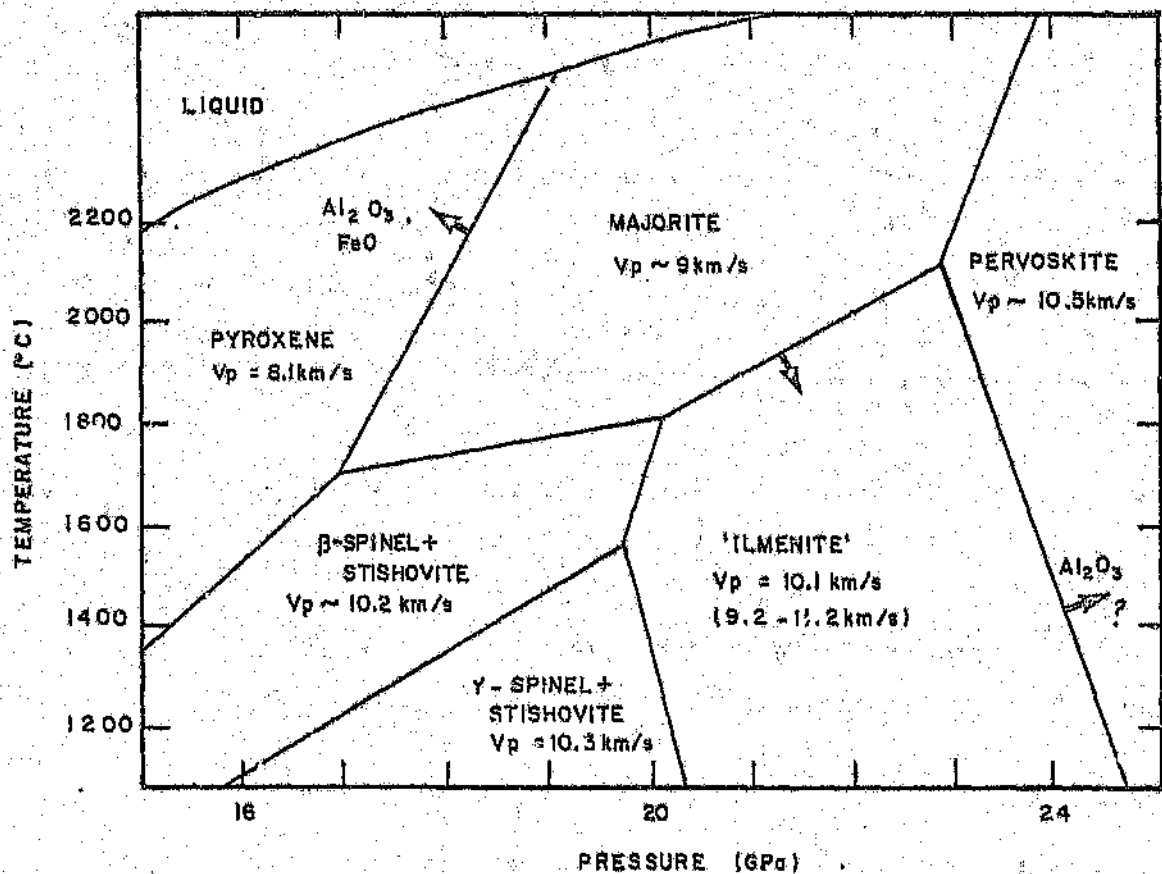


Figure 5.2.3. - Phase relations in pure  $MgSiO_3$ . The phase boundaries are for constant chemical composition and will move if impurities such as  $Al_2O_3$  or  $FeO$  are introduced (as illustrated). Diagram after Anderson(1992).

The effects of temperature and pressure on the crystal structure of  $MgSiO_3$  are shown in figure 5.2.3. Orthopyroxene, unstable below 400 km depth, transforms to a garnet form called majorite at high pressure.

At still higher pressures (corresponding to depths of approximately 670 km)  $\gamma$ -spinel collapses to ultradense perovskite and magnesio-wüstite structures. Garnet and majorite also collapse to perovskite structures at these pressures (Anderson, 1992).

A few modifications are necessary to this simple model. The jump in seismic velocity at 400 km is less than the jump predicted from a simple olivine to spinel and orthopyroxene to majorite phase change. The presence of additional minerals, for example garnet and clinopyroxene, is required (Anderson, 1992) to explain this velocity jump. Clinopyroxene is stable at the top of the transition region, but collapses - in a manner similar to orthopyroxene at 13 to 15 Gpa - to a garnet like phase at about 500 km. Indeed, Shearer (1991) describes evidence to support the presence of a weaker discontinuity at this depth.

Phase transitions in mantle materials generally occur over a large depth range (see figure 5.2.2). However, the 670 km discontinuity at 22-24 Gpa is a good reflector of seismic energy, implying a relatively abrupt transition (first order discontinuity). This evidence may once again imply that a chemical and phase transition occurs at this boundary. The depth to this discontinuity is also more variable than the depth to the 400 km discontinuity (Shearer, 1991). This result is in agreement with recent laboratory results which indicate that the Clapeyron slope<sup>6</sup> for the 670 km discontinuity is significantly larger in magnitude than the slope for the 400 km discontinuity (Akaogi et al, (1989). However, caution must be exercised in discriminating between real differences in depth to a discontinuity and apparent differences which result from heterogeneous velocities in the upper mantle (Shearer, 1991).

This model is summarised in table 5.2.1. In section 5.2.3 the model will be examined in terms of the results of the analyses of P to S converted phases described in this

study to establish (and hopefully explain) any discrepancies between the seismic observations for the five stations where suitable data were obtained and those implied by the simplified global model.

400 km	670 km
Olivine to spinel transition. Orthopyroxene to majorite and clinopyroxene to garnet transitions commence.	Spinel to ultradense perovskite and magnesio-wüstite transition. Garnet and majorite to perovskite transitions.
Increase in seismic velocity with depth.	Increase in seismic velocity with depth.
Probable first order discontinuity but not as sharp as at 670 km.	Definite sharp first order discontinuity.
Positive Clapeyron slope of lower magnitude than that at 670 km.	Clapeyron slope possibly negative with relatively large magnitude.

Table 5.2.1 - Simplified global model pertaining to the 400 km and 670 km discontinuities.

\$ - The Clapeyron slope is the slope  $dT/dP$  of the equilibrium boundary associated with a phase transition. For example, in figure 5.2.9, the majorite-perovskite boundary is characterised by a positive Clapeyron slope while the 'ilmenite'-perovskite boundary is characterised by a negative Clapeyron slope. Knowledge of the magnitude and sign of the Clapeyron slope is important in understanding upper mantle rheology.



### 5.2.3) Upper mantle discontinuities beneath South Africa.

The description of the geological setting of the Lithosphere Project (section 1.2) indicates that South Africa can be subdivided into various provinces (cratons and mobile belts) which exhibit different geophysical characteristics. Data from the project suitable for P to S analysis were only found beneath five stations situated on the Kaapvaal Craton (sections 3.1 and 3.4). Hence, conclusions regarding the upper mantle discontinuities beneath South Africa can only be made with regard to the Kaapvaal Craton.

There is no evidence for a discontinuity at 670 km beneath any station examined in this study. However, individual records and the results of Vinnik(1992) provide evidence for a phase corresponding to this discontinuity. Vinnik(1992) describes P to S conversions at approximately 66s beneath BPI, DOU, PIL and KLI. The delay time of 66s is lower than that observed in most stable platforms - this is indicative of anomalously high upper mantle velocities. The absence of a phase at SAN is probably not related to rheological conditions at 670 km beneath this station but to the paucity of suitable data acquired at this station. The complicated nature of the crust and the "unusual complexity of the earth's mantle underneath SAN"(Vinnik et al, 1992a), may be significant in this regard. The stacked results are not of suitable quality to make inferences about the order of the 670 km discontinuity beneath any station.

The discontinuity at about 560 km beneath DOU observed in the current study is problematic. Shearer(1991) stated, "Indeed, it would be hard to find a depth in the upper mantle for which a discontinuity has not at some time been proposed". Many of these proposals are probably based on processing artifacts and this may indeed be the case for this phase at DOU. However, i) this discontinuity is clear on all stacked records produced for this station, ii) the station has simple crustal and upper mantle models which should not complicate the upper mantle converted phases, and iii) the discontinuity at 670 km beneath DOU is only visible in the results of Vinnik(1992) on a composite stack of three stations whereas a more clearly defined

phase is present in the individual stack at approximately the same time and phasing depth as observed in the current study. This phase could represent an elevated 670 km discontinuity or the clinopyroxene-garnet transition at about 520 km. This station requires further analyses as current data lack sufficient temporal resolution for an unambiguous interpretation.

In summary, there are two possible models for the 670 km discontinuity beneath South Africa:

- 1) The discontinuity is continuous with no variations in depth;
- 2) The discontinuity shows lateral variation beneath DOU. This may be related to the magnitude of the Clapeyron slope at 670 km.

Neither model is discordant with the global model presented in the previous section or provides evidence for any relationship between the nature of this discontinuity and surface geology.

Two models are implied by stacked results for the 400 km discontinuity:

- 1) This study provides evidence for complicated first order type discontinuity without lateral variations beneath the stations studied. The discontinuity may be characterised by some kind of double boundary or a low shear velocity layer. The later interpretation is preferred (section 4.5).
- 2) Vinnik(1992) and Vinnik et al(1993b) provide evidence for an anomalous low shear velocity zone at approximately 400 km beneath DOU, PIL and KLI, and no anomalous structures at the same depth beneath BPI and SAN.

Both studies indicate that the 400 km discontinuity beneath the Craton cannot be explained in terms of the generalised global model presented in the previous section. Partial melts caused by the mantle solidus temperature being lowered by a dehydration of K-amphibole (Vinnik et al, 1993b) is one possible explanation of the observed phenomena. The studies differ with regard to the lateral variation of the discontinuity. Although the results of Vinnik(1992) are more reliable than those of the current study (section 5.1), the absence of an observed anomaly beneath SAN and BPI must be examined in terms of the following:

- 1) The stacks at these two stations had the lowest fold;
- 2) BPI was subject to high seismic noise levels as it is situated in an urban area;
- 3) The crust and upper mantle beneath SAN are complicated - this could easily obfuscate the upper mantle conversion pattern.

Additional data (both within and outside the boundaries of the Kaapvaal Craton) and additional analyses of the current data are required before it can be argued that the persistence of lateral heterogeneities at 400 km, in spite of the plate motion, imply the anomaly at this depth constitutes part of the plate (Vinnik et al, 1993b). Any relationship, inferred from P to S analyses, between the 400 km discontinuity and kimberlite magmatism is purely speculative at this stage.

The results observed and models obtained in the current study and the independent study of Vinnik (1992) are summarised in table 5.2.2.

	Current Study	Vinnik's Study
BPI	No phase for 670 km. Complicated phase for 400km inferred from composite stack.	Clear phase for 670 km. No phase for 400 km.
DOU	Phase for depths between 500 and 560 km. Complicated phase for 400 km inferred from composite stack.	Phase for 670 km Inferred from composite stack. Negative phase for 400 km.
SAN	No phase for 670 km. Complicated phase for 400 km visible.	No phases corresponding to upper mantle discontinuities.
PIL	No phase for 670 km. Complicated phase for 400 km visible.	Phase for 670 km inferred from composite stack. Clear negative phase for 400 km.
KLI	No phase for 670 km. Complicated phase for 400 km inferred from composite stack.	Phase for 670 km inferred from composite stack. Negative phase for 400km.
400 KM	Complicated first order discontinuity, probably characterised by a low shear velocity layer continuous beneath all stations.	Anomalous low shear velocity zone beneath DOU, PIL and KLI. No anomalous feature beneath BPI and SAN.
670 KM	Discontinuity elevated beneath DOU to approximately 560 km.	Continuous discontinuity with no variation in depth.

Table 5.2.2 - Summary of results and models related to the upper mantle discontinuities beneath South Africa. Neither model for the 400 km discontinuity accords with the global model presented in table 5.2.1.

## 6) CONCLUSIONS.

This research was undertaken to determine the depth, order and lateral variation of the 400km and 670 km discontinuities beneath South Africa by analysing P to S converted phases, and to examine whether these properties are related to surface geology. Unfortunately no data suitable for processing were found for station KEN situated in the Namaqua province or for stations WAR and KAM situated on the Kaapvaal Craton. Limited data suitable for processing were found for five stations - BPI, DOU, SAN, PIL and KLI.

Stacked data from the five stations analysed are noisy especially in the intermediate and long period bands where the data should be characterised by good signal to noise characteristics. This is ascribed to the application of sub-optimum filters and inferior numerical routines during processing. Despite this, by combining results from this study with those from an independent study (Vinnik, 1992) two possible models were derived for both the 670 km and 400 km discontinuities. Variations in neither discontinuity are directly related to surface geology.

Two alternative models proposed for the 670 km discontinuity are:

- 1) The discontinuity is laterally persistent at a depth of approximately 670 km beneath all stations;
- 2) The discontinuity is elevated beneath station DOU to a depth of about 560 km.

Data indicates that the first model may require the presence of an additional discontinuity between 500 km and 560 km beneath DOU. Both models are consistent with a global model for this transition and delay times imply anomalously high shear velocities in the upper mantle.

The two models proposed for the 400 km discontinuity are:

- 1) The discontinuity is complicated and probably characterised by a low shear velocity layer beneath all stations;

2) The discontinuity is characterised by a low shear velocity layer beneath DOU, PIL and KLI, only.

Both models for this discontinuity are anomalous when compared to a global model for this transition.

The way to resolve the discrepancy between the two models is to acquire more data both within and outside the boundaries of the Kaapvaal Craton - this will be discussed shortly. The existing data base should also be reassessed and analysed using a clearly documented methodology, for example that of Shearer(1991). The nature of the discontinuities could then be reinterpreted in conjunction with a consideration of other phases in a manner which is repeatable. Indeed, there is probably a plethora of information extractable from the current data base relating to many features within the earth. This information will only be realised if the data base is made available to the scientific community at large.

Apart from any insight gleaned into upper mantle rheology, the study was also valuable in that certain problems regarding the acquisition and storage of broad-band seismic data were revealed. The necessity for maintaining a record of accelerometer polarities and correct data decompression techniques are two examples in this regard.

It is hoped that this investigation of the upper mantle discontinuities and other studies resulting from the Lithosphere Project will stimulate interest in the establishment of a broad-band seismograph network covering not only the Kaapvaal Craton but also adjacent cratons and the surrounding mobile belts. Results from completed projects could be used to establish suitable station locations on the Kaapvaal Craton. For example, this study indicates that the localities DOU, PIL and SAN warrant further attention. Station localities in urban areas like Johannesburg (BPI) should be avoided. Because modern technology has allowed the time interval between visits to a station to be increased dramatically, many of the logistical problems associated with the Lithosphere Project can now be overcome. The following, however, must be borne in mind when establishing a broad-band network for southern Africa:

- 1) Studies such as this one require data suitable for analysis. The problem is that the southern African region is situated in an aseismic intraplate zone on the African plate - hence, suitable teleseismic events are recorded only rarely. In addition the azimuthal distribution of suitable events is very limited. Even local events suitable for crustal studies are rare.
- 2) It is difficult to state how long each station would need to record to establish a suitable data base as this time period is obviously dependant on what the data will be used for and global seismic activity. For studies such as the present one, a minimum of twelve suitable events are desirable for reliable results even if robust data processing techniques are employed. The criteria for a suitable event are much more relaxed for many other types of study, however, for example P and PKP travel time residuals.
- 3) Data must be monitored as they are acquired to ensure quality control. In this manner any problems related to the acquisition system can be established and resolved.
- 4) Provision must be made for sufficient analyses to be performed on the data.

This study has indicated that the structure at depth below the Kaapvaal Craton is anomalous when compared to a global model - it may also be heterogeneous within the boundary of the craton. To date, only limited seismic analyses have been done on the crucial depth interval between 150 km and 400 km. Data acquired in the manner described above would be invaluable in complementing existing data from many branches of the earth sciences, including the vast body of geochemical and isotope data from mantle peridotites and inclusions in kimberlites, to increase the understanding of the upper mantle. The Kaapvaal Craton is also heterogeneous in terms of its crustal and upper lithospheric structure (Muller, 1991) - this heterogeneity must be investigated further. Good broad-band seismic data are the only data which will provide insight into the various aspects of lithosphere and upper mantle structure currently perplexing various exploration and academic concerns in South Africa.

## 7) REFERENCES.

- Akaogi, M., Ito, E., and Navrotsky, A., Olivine-modified spinel-spinel transitions in the system  $Mg_2SiO_4$ - $Fe_2SiO_4$ : Calorimetric measurements, thermodynamic calculation, and geophysical application, *J. Geophys. Res.*, 94, 15671-15685, 1989.
- Anderson, D.L., Recent evidence concerning the structure and composition of the earth's mantle, *Phys.Chem.Earth*, 6, 1-131, 1965.
- Anderson, D.L., The 650 km mantle discontinuity, *Geophys. Res. Lett.*, 3, 347-349, 1976.
- Anderson, D.L., Global mapping of the upper mantle by surface wave tomography, Composition, Structure and Dynamics of the Lithosphere-Asthenosphere System, Geodynamics Series 13, Fuchs and Froidevaux (Eds.), *American Geophysical Union*, 89-97, 1987.
- Anderson, D.L., and Bass, J.D., Transition region of the earth's upper mantle, *Nature*, 320, 321-328, 1986.
- Anderson, D.L., The earth's interior, Understanding the Earth, Brown, Hawkesworth and Wilson (Eds.), *Cambridge University Press*, 44-66, 1992.
- Archaibeau, C.B., Flinn, E.A., and Lambert, D.G., Fine structure of the upper mantle, *J. Geophys. Res.*, 74, 5825-5865, 1969.
- Bass, J.D., and Anderson, D.L., Composition of the upper mantle: Geophysical tests of two petrological models, *Geophys. Res. Lett.*, 11, 237-240, 1984.
- Ben-Menahem, A., and Singh, S.J., Seismic Waves and Sources, *Springer-Verlag*, 1981.
- Bullen, K.E., and Bolt, B.A., An introduction to the theory of seismology, *Cambridge University Press*, 1985.
- Byerly, P., The Montana earthquake of June 28, 1925, *Bull. Seismol. Soc. Am.*, 16, 209-265, 1926.
- Byerly, P., The first preliminary waves of the Nevada earthquake of December 20, 1932, *Bull. Seismol. Soc. Am.*, 25, 62-80, 1935.
- Dziewonski, A.M., and Anderson, D.L., Preliminary reference earth model, *Phys. Earth planet. Inter.*, 25, 297-356, 1981.
- Dziewonski, A.M., and Anderson, D.L., Seismic tomography of the earth's interior, *American Scientist*, 72, 483-494, 1984.



- Fuchs, K., Vinnik, L.P., and Prodehl, C., Exploring heterogeneities of the continental mantle by high resolution seismic experiments, Composition, Structure and Dynamics of the Lithosphere-Asthenosphere System, Geodynamics Series 16, Fuchs and Froidevaux (Eds.), American Geophysical Union, 137-154, 1987.
- Green, R.W.E., Upper mantle studies using teleseismic events, Extended abstracts of the second technical meeting of the South African Geophysical Association, 97-99, 1991a
- Green, R.W.E., PC based continuous recording field seismic station, Bull. Seismol. Soc. Am., 82, 497-504, 1992.
- Green, R.W.E., Data compression of broad-band seismic data using a portable PC, Computers and Geosciences, 19, 259-262, 1993.
- Green, R.W.E., and Hales, A.L., The travel times of P waves to 30° in the Central United States and upper mantle structure, Bull. Seismol. Soc. Am., 58, 267-289, 1968.
- Hales, A.L., and Roberts, J.L., The Zoeppritz amplitude equations: more errors, Bull. Seismol. Soc. Am., 64, 285, 1976.
- Howell, B.F., Introduction to Geophysics, Mc Graw-Hill, 147-170 1959
- Husebye, E.S., Christoffersson, A., and Frasier, C.W., Orthogonal representations of array-recorded short period P-waves, Exploitation of Seismograph Networks, Beauchamp (Ed.), Nordhoff, 297-309, 1975.
- Jones, M.Q.W., Heat flow and heat production in the Namaqua Mobile Belt, South Africa, J. Geophys. Res., 92, 6273-6289, 1987.
- Jones, M.Q.W., Heat flow in the Witwatersrand basin and environs and its significance for the South African shield geotherm and lithosphere thickness, J. Geophys. Res., 93, 3243-3260, 1988.
- Jordan, T.H., The continental tectonosphere, Reviews of Geophysics and Space Physics, 13 - 3, 1-12, 1975.
- Julian, B.R., and Anderson, D.L., Travel times, apparent velocities and amplitudes of body waves, Bull. Seismol. Soc. Am., 58, 339-366, 1968.
- Kanasewich, E.R., Time sequence analysis in Geophysics, The University of Alberta Press, 1975.
- Kennett, B.L.N. (editor), IASPEI 1991 Seismological Tables, Research School of Earth Sciences, Australian National University, 1991.
- Kind, R., and Vinnik, L.P., The upper-mantle discontinuities underneath the GRF array

- from P-to-S converted phases, *J. Geophys.*, 62, 138-147, 1986.
- Kuc, R., An Introduction to digital signal processing, McGraw-Hill Book company, 1988.
- Lees, A.C., Bukowirski, M.S.T., and Jeanloz, R., Reflection properties of phase transition and compositional change models of the 670-km discontinuity, *J. Geophys. Res.*, 88, 8145-8159, 1983.
- McCamy, K., Meyer, R.P., and Smith, T.J., Generally applicable solutions of Zoeppritz amplitude equations, *Bull. Seismol. Soc. Am.*, 52, 923-955, 1962.
- Meade, C., and Jeanloz, R., The strength of mantle silicates at high pressures and room temperatures: implications for the viscosity of the mantle, *Nature*, 348, 533-535, 1990.
- Muller, M.R., Lithospheric structure for the Kaapvaal Craton and its margins from the analysis of long-period and broad-band teleseismic P-waves, MSc thesis, University of the Witwatersrand, 1991.
- Niazi, M., and Anderson, D.L., Upper mantle structure of Western North America from apparent velocities of P waves, *J. Geophys. Res.*, 70, 4633-4640, 1965.
- Paulssen, H., Upper mantle converted waves beneath the NARS array, *Geophys. Res. Lett.*, 12, 709-712, 1985.
- Press, W.H., Teukolsky, S.A., Vetterling, W.T., and Flannery, B.P., Numerical Recipes in Fortran, Cambridge University Press, 1992
- Qiyuan, L., and Kind, R., Lateral variations of the structure of the crust-mantle boundary from conversions of teleseismic P waves, *J. Geophys.*, 60, 149-156, 1986.
- Ringwood, A.E., and Irifune, T., Nature of the 650-km discontinuity: implications for mantle dynamics and differentiation, *Nature*, 331, 131-136, 1988.
- Romanowicz, B.A., and Dziewonski, A.M., Global digital seismographic network: Research opportunities and recent initiatives, Composition, Structure and Dynamics of the Lithosphere-Asthenosphere System, Geodynamics Series 16, Fuchs and Froidevaux (Eds.), American Geophysical Union, 99-110, 1987.
- Shearer, P.M., Constraints on upper mantle discontinuities from observations of long period reflected and converted phases, *J. Geophys. Res.*, 96, 18147-18182, 1991.
- Silver, P.G., Carlson, R.W., and Olson, P.O., Deep slabs, geochemical heterogeneity, and the large scale structure of mantle convection: Investigation of an enduring paradox, *Ann. Rev. Earth Planet. Sci.*, 16, 477-541, 1988.

- Souriau, A., First analyses of broadband records on the GEOSCOPE network: Potential for detailed studies of mantle discontinuities, *Geophys. Res. Lett.*, **13**, 1011-1014, 1986.
- Tankard, A.J., Jackson, M.P.A., Eriksson, K.A., Hobday, D.K., Hunter, D.R. and Minter, W.E.L., Crustal Evolution of Southern Africa - 3.8 Billion Years of Earth History, Springer-Verlag, 1982.
- Vinnik, L.P., Detection of waves converted from P to SV in the mantle, *Phys. Earth planet. Inter.*, **15**, 39-45, 1977.
- Vinnik, L.P., Avetisjan, R.A., and Mikhailova, N.G., Heterogeneities in the mantle transition zone from observations of P-to-SV converted waves, *Phys. Earth planet. Inter.*, **33**, 149-163, 1983.
- Vinnik, L.P., Preliminary results of processing the records of the DeBeers Lithosphere Project, Internal Document, University of the Witwatersrand, 1992.
- Vinnik, L.P., Green, R.W.E., and Nicolaysen, L.O., Recent deformations of the deep continental roots in Southern Africa, 1993a, IN PREPARATION.
- Vinnik, L.P., Green, R.W.E., and Nicolaysen, L.O., Deep seismic structure and kimberlites of the Kaapvaal craton, 1993b, IN PREPARATION.
- Wajeman, N., and Souriau, A., A possible local anomaly in the 670-km discontinuity beneath Kerguelen, *Phys. Earth planet. Inter.*, **49**, 294-303, 1987.
- Weidner, D.J., A mineral physics test of a pyrolytic mantle, *Geophys. Res. Lett.*, **12**, 417-420, 1985.
- Windley, B.F., The Evolving Continents, John Wiley, 1984.
- Woodhouse, J.H., and Dziewonski, A.M., Mapping the upper mantle: Three-dimensional modelling of earth structure by inversion of seismic waveforms, *J. Geophys. Res.*, **89**, 5953-5986, 1984.
- Wyllie, P.J., Experimental petrology: Earth materials science, Understanding the Earth, Brown, Hawkesworth and Wilson (Eds.), Cambridge University Press, 67-87, 1992.
- Young, G.B., and Bralle, L.W., A computer program for the application of Zoeppritz's amplitude equations and Knott's energy equations, *Bull. Seismol. Soc. Am.*, **66**, 1881-1885, 1976.

**APPENDIX**

This appendix contains a listing of all Fortran programs and subroutines used in this study. Many of these were written when the author had just started programming and in retrospect could be tidied up and the coding improved upon. They have, however, all been tested extensively and to the best of the author's knowledge work correctly. The routines are, in order of appearance:

readfile.for  
filon.for  
param.for  
filtpc.for  
filter.for  
fft.for  
bnd.for  
veldis.for  
integ.for  
trend.for  
roirt.for  
calce.for  
rotlh.for  
cross.for  
plsel.for  
tps.for  
pcstack.for  
seisgrf2.for  
stk467.for.

Routines `tps`, `stk467`, `pcstack`, `filter`, `bnd`, and `calce` were written by the author only. Many of the routines associated with the program `filon` were based on an earlier program by A Cichowicz<sup>‡</sup> but are now extensively modified. The following routines written by A Cichowicz<sup>‡</sup> are, however, virtually intact: `veldis`, `integ`, `trend` and `plsel`. The program `readfile` was written by W Theron<sup>#</sup> who also wrote the seismic data base package `BPI.EXE`. The framework for the program `seisgrf2` was written by G Cooper<sup>‡</sup> - the author simply modified it to render its utility compatible with the current study. The routine `fft` is taken from Numerical Recipes in Fortran (Press et al, 1992). The routine used here is, however, the one given in the first edition of the book published in 1986.

The functionality of all programs ( with the obvious exception of `seisgrf2` ) will be maintained if the graphic output facilities are commented out. The graphics drivers used in all programs are the `Plot88` and `Drive88` libraries marketed by Plotworks Inc<sup>‡</sup>. All programs were compiled using a Microsoft 5.0 Fortran compiler on a 386 DX personal computer.

<sup>‡</sup> Department of Geophysics, University of the Witwatersrand.

<sup>#</sup> Independent software writer, commissioned by the Bernard Price Institute.

& Plotworks Inc. La Jolla, California.

## DIRECTORY OF PROGRAMS AND SUBROUTINES.

Program Readfile .....	Appendix ii
Program Filon .....	Appendix iii
Subroutine Param .....	Appendix iv
Subroutine Ffiltpc .....	Appendix vii
Subroutine Filter .....	Appendix viii
Subroutine Fft .....	Appendix viii
Subroutine Bnd .....	Appendix x
Subroutine Veldis .....	Appendix xi
Subroutine Integ .....	Appendix xii
Subroutine Trend .....	Appendix xiii
Subroutine Rotrt .....	Appendix xiii
Subroutine Calce .....	Appendix xiv
Subroutine Rotlh .....	Appendix xv
Subroutine Cross .....	Appendix xvi
Subroutine Plsei .....	Appendix xix
Program Tps .....	Appendix xxii
Program Postack .....	Appendix xxiii
Program Seisgraf2 .....	Appendix xxvi
Subroutine DataRead .....	Appendix xxvi
Subroutine ScreenPlot .....	Appendix xxviii
Subroutine HardCopy .....	Appendix xxx
Program Stk467 .....	Appendix xxxii

```

Program Readfile
STORAGE:2
$NOFLOATCALLS
cA program to read binary data from the program BPI.EXE and convert
it to an Ascii file with each component having the correct polarity
cProgram by W Theron
character*20 filnam,nam2
integer*1 dummy1
integer*2 mode,dummy2
integer*4 size
real sign,value

write(*,'(A)') 'Enter required input filename: '
read(*,'(A)') filnam
open(unit=2,file = filnam,form='binary',status='old')
write(*,*) 'Enter the required output filename'
read(*,'(A)') nam2
open(4,file=nam2)
write(*,*) 'Enter the polarity +-1.0: '
read(*,*) sign

read(2) mode
write(*,'(A)') 'Mode (1=compressed,2=decompressed):'
write(*,'(I4)') mode
read(2) size
write(*,'(A)') 'Number of points in file:'
write(*,'(I4)') size
write(*,'(A)') 'Date(D:M:Y):'
do 100 i=1,3
  read(2) dummy2
  write(*,'(I3)') dummy2
100 continue
write(*,'(A)') ' '
write(*,'(A)') 'Time (H:M:S):'
do 110 i=1,3
  read(2) dummy2
  write(*,'(I3)') dummy2
110 continue
write(*,'(A)') ' '

do 200 i=1,size
  if (mode.eq.1) then
    read(2) dummy1
    dummy2=dummy1
  endif

  if (mode.eq.2) then
    read(2) dummy2
  endif
  value=sign*float(dummy2)

```

```

        write(4,'(f10.3)') value
200 continue
        close(4)
        end

c*****
      Program Filon
c
c PROGRAM FOR THE ANALYSIES OF P to S CONVERTED PHASES
c RECORDED BY THREE COMPONENT BROADBAND SEISMOMETERS
c Program by PA Cattermole, based on a program by A Cichowicz.
c-----
cThis program operates on NLAST-2 data points. Matrix size = NLAST
c for graphics purposes.

      parameter (nlast=2050)

      real V1(nlast),V2(nlast),V(nlast),WORK(nlast),WORK2(nlast),
      .MAT(2*nlast-4),auto(nlast)
      Common /temp/v1,v2,v,/temp1/work,work2/temp3/auto
      integer plomon,plopri,out,lparr
      character fn*20,ff*60

c Constants for plot88 library
c number of monitor =9, (VGA) number of printer =5
      DATA plomon/91/,plopri/5/,xmaxwi/22.0/,ymaxwi/12.0/
cTime and y axis lengths for monitor
      DATA tlengt/18.0/,ylengt/4.0/
cTime and y axis for printer is defined in subroutine PLSEI

c Three seismograms of a recorded event are read into three matrices
c in sub. PARAM. The seismograms can be band pass filtered in
c sub FFILT. Sub VELDISE converts the velocity record to a displacement
c record. Sub ROTRT calculates the radial and transverse components
c of the record while ROTLH calculates the component along the
c principal direction and transverse to it where the emergent angle
c is calculated in CALC2. The normalised cross correlated component
c HH is calculated in sub. CROSS. The rationale behind this is found
c in the reference of Vinnik (1977).
c
c V1 - Z - L
c V2 - N - R - H
c V - E - T - HH
c
c PARAM ROTRT ROTLH CROSS -- subroutine

      nr0 = 0
c number of the input file
      nf = 1

100 format(a)

```



```

120 format(5(/))
   write(nr0,120)

1  write(nr0,*) ' PROCESSING OPTIONS '
   write(nr0,*) ' '
   write(nr0,*) ' the time unit is sec '
   write(nr0,*) ' '
   write(nr0,*) ' 1 reading data and parameters of seismogram '
   write(nr0,*) ' 2 filtering in frequency domain'
   write(nr0,*) ' 3 conversion from velocity to displacement'
   write(nr0,*) ' 4 rotation from N, E to R, T'
   write(nr0,*) ' 5 calculate incident angle'
   write(nr0,*) ' 6 rotation from Z, R to L, H'
   write(nr0,*) ' 7 crosscorrelation of P-pulse (L-comp.) * H'
   write(nr0,*) '99 escape'
   write(nr0,*) ' previous option = 'KK
   read(nr0,*) KK
   if(KK.eq.1) call PARAM
     .(nr0,nf,v1,v2,v,nlast,dt,out,plomon,plopri
     .,tlengt,ylengt,xmaxwi,ymaxwi,work2,fn,
     .az,ff,iparr)
   if(KK.eq.2) call FFILTPC
     .(nr0,v1,v2,v,mat,work2,F1,F2,nlast,dt,out,
     .plomon,plopri,tlengt,ylengt,xmaxwi,ymaxwi,fn,ff)
   if(KK.eq.3) call VELDIS
     .(nr0,v1,v2,v,work,nlast,dt,plomon,plopri
     .,tlengt,ylengt,xmaxwi,ymaxwi,fn,ff)
   if(KK.eq.4) call ROTRT
     .(nr0,v2,v,work,nlast,dt,plomon,plopri,tlengt,ylengt,xmaxwi,
     .ymaxwi,fn,az,ff)
   if(KK.eq.5) call CALCE
     .(v1,v2,iparr,dt,aincde,nlast)
   if(KK.eq.6) call ROTLH
     .(nr0,v1,v2,work,nlast,dt,plomon,plopri,tlengt,ylengt,xmaxwi,
     .ymaxwi,fn,aincde,ff)
   if(KK.eq.7) call CROSS
     .(nr0,v1,v2,v,auto,work,nlast,dt,plomon,plopri,tlengt,ylengt,
     .xmaxwi,ymaxwi,fn,ff,iparr)
   if(KK.eq.99) stop
   goto 1
end

```

C\*\*\*\*\*

```

Subroutine Param(nr0,nf,v1,v2,v,nlast,dt
.,out,plomon,plopri,tlengt,ylengt,xmaxwi,ymaxwi,work2,fn,
.,az,ff,iparr)

```

oSubroutine reads in three components of the recorded event  
c and the event parameters

```

real v1(nlast),v2(nlast),v(nlast),work2(nlast)

```

## Appendix v

```

real dt,tlengt,ylengt,xmaxwf,ymaxwf,az
integer out,plomon,plopri,nr0,nf,iparr,nlast
character ch*20,fn*20,ff*60

```

```

cSampling period = dt
  dt = 0.07

```

```

100 format(a)
101 format(1x,a)
105 format(a60)

```

```

cNote - each component requires a separate filename

```

```

write(nr0,*) ' ENTER FILE NAME '
read(nr0,100) fn
write(nr0,101) fn
open(nf,file = fn)

```

```

cRead in back azimuth and time delay before start of
cP-wave

```

```

write(*,*) 'First file entry (y/n)'
read(nr0,100) ch
if (ch.eq.'n') goto 567
write(*,*) 'Enter back azimuth'
read(*,*) az
write(*,*) 'Enter p arrival time'
read(*,*) parriv
write(nr0,*) 'az = ',az
write(nr0,*) 'parriv = ',parriv,' sec'

```

```

cCalculate the number of samples before the P-arrival
c These parameters are used in other subroutines
  iparr = int(parriv/dt)

```

```

write(*,*) 'P arrival delay = ',iparr

```

```

cConvert az to radians
  az = 0.0174532*az
567 continue

```

```

cRead in three coordinates separately
cDATA ARE READ IN SIMPLY AS A SINGLE COLUMN OF REAL NUMBERS - ONE FILE
cFOR EACH COMPONENT.

```

```

write(*,*) 'Enter file coordinate'
write(*,*) 'Vertical = 1, N/S = 2, E/W = 3'
read(*,*) jjj
do 6 i = 1,nlast-2
  read(nf,*,end=6) v(i)

```

```

6 continue

```

```

cRemove any residual linear trend in the data. Subroutine redundant

```

cwith new top compression removal in BPI.EXE

call trend(v,nlast-2)

cPlace vertical component in matrix V1, NS component in V2, EW

c component in matrix V

if(jj.eq.1) then

do 7 i = 1,nlast-2

7 v1(i) = v(i)

endif

if(jj.eq.2) then

do 8 i = 1,nlast-2

8 v2(i) = v(i)

endif

333 continue

close(nf)

cCall plot functions

if(jj.eq.3) then

write(nr0,\*) 'Do you want to plot seismograms to check P arrival  
.time'

read(nr0,100) ch

if(ch.eq.'n') goto 999

write(\*,\*) 'Enter the title for the graph 60 char. max'

write(\*,\*) 'Eg.: Costa Rica 12/04/90 (KLI) Velocity'

read(\*,105) ff

998 continue

cinitialise Plot88

write(nr0,\*) 'Define the output device'

write(nr0,\*) 'monitor=1, printer=2'

read(nr0,\*) out

if(out.ne.1.and.out.ne.2) goto 998

if(out.eq.1) call plots(0,plomon,plomon)

if(out.eq.2) call plots(0,0,plopri)

fn = 'Vertical'

call plsel(out,work2,v1,nlast,dt,tlengt,ylengt,xmaxwi,ymaxwi

.,fn,ff,1,0.0,'n')

fn = 'North/South'

call plsel(out,work2,v2,nlast,dt,tlengt,ylengt,xmaxwi,ymaxwi

.,fn,ff,2,0.0,'n')

fn = 'East/West'

call plsel(out,work2,v,nlast,dt,tlengt,ylengt,xmaxwi,ymaxwi

.,fn,ff,3,0.0,'n')

call plot(0.0,0.0,999)

cEnd of plotting

write(\*,\*) 'Do you wish to change P arrival time ?'

read(\*,100) ch

if(ch.eq.'y') then

```

        write(*,*) 'Enter new arrival time'
        read(*,*) parriv
        iparr = int(parriv/dt)
    endif

    endif
999  continue
    return
    end

c*****
c Subroutine Ffiltpc(nr0,v1,v2,v,mat,work2,F1,F2,nlast,dt
c ,out,plomon,plopri,tlengt,ylengt,xmaxwl,ymaxwl,fn,ff)

    real v1(nlast),v2(nlast),v(nlast),work2(nlast),mat(2*nlast)
    integer out,plomon,plopri
    real F1,F2
    character ch*20 ,fn*20 ,ff*60

c This subroutine reads in the low and high pass parameters
c of the band to be passed. Filtering, in the frequency domain
c is done in sub. FILTER

        write(nr0,*) 'Parameters of the band pass filter'
        write(nr0,*) ' F1 < f < F2 '
        write(nr0,*) 'ENTER F1 low frequency cutoff'
        read(nr0,*) F1
        write(nr0,*) 'ENTER F2 high frequency cutoff'
        read(nr0,*) F2

        write(nr0,101) F1,F2
101  format(3x,'Parameters of a band pass filter',1(/),
c .3x,' F1=',f7.3,5x,' F2=',f7.3)

        call filter(v1,mat,nlast,F1,F2,dt)
        call filter(v2,mat,nlast,F1,F2,dt)
        call filter(v,mat,nlast,F1,F2,dt)
cNote - MAT is a 2*nlast-4 matrix needed for the FFT subroutine.

100 format(a)
105 format(a60)
        write(nr0,*) 'Do you want to plot seismograms'
        read(nr0,100) ch
        if(ch.eq.'n') goto 414
        write(*,*) 'Enter the title of the graph'
        write(*,*) 'Eg.: South Sand.Is. 14/09/89 (SAN) 0.065-0.13 Hz'
        read(*,105) ff

c Initialise Plot88
998  write(nr0,*) 'Define the output device'
        write(nr0,*) 'monitor ', printer=2'

```

```

read(nr0,*) out
if(out.ne.1.and.out.ne.2) goto 998
if(out.eq.1) call plots(0,plomon,plomon)
if(out.eq.2) call plots(0,0,plopri)

fn = 'Vertical'
call plsel(out,work2,v1,nlast,dt,tlengt,ylengt,xmaxwi,ymaxwi)
.,fn,ff,1,0.0,'n')
fn = 'North/South'
call plsel(out,work2,v2,nlast,dt,tlengt,ylengt,xmaxwi,ymaxwi)
.,fn,ff,2,0.0,'n')
fn = 'East/West'
call plsel(out,work2,v,nlast,dt,tlengt,ylengt,xmaxwi,ymaxwi)
.,fn,ff,3,0.0,'n')
call plot(0.0,0.0,999)

414 continue
return
end

```

C\*\*\*\*\*

\*\*\*

```

Subroutine Filter(y,spec,nlast,F1,F2,dt)
real spec(2*nlast-4),y(nlast)
real F1,F2
integer i,s

```

c Each matrix is FFT'd in sub. FFT. Band pass filtering  
c of the spectrum is then performed in sub. BND. The filtered  
c time series is then calculated by the inverse transform in FFT.  
c The time series is read into a 2\*nlast-4 matrix SPEC with the  
c imaginary component initialised to zero.

```

do 8 i=1,nlast-2
      spec((2*i)-1) = y(i)
8      spec(2*i) = 0.0

```

cCalculate the forward transform

```

s = 1
call fft(spec,nlast-2,s)

```

cFilter the spectrum using BND

```

call bnd(y,spec,nlast-2,f1,f2,dt)

```

cCalculate the filtered time series by inverse transforming

```

s = -1
call fft(spec,nlast-2,s)

```

cPlace filtered signal back into the original matrix

```

do 10 i = 1,nlast-2
10      y(i) = spec((2*i)-1)
return
end

```

```

Subroutine Fft(DATA,NN,ISIGN)
REAL*8 WR,WI,WPR,WPI,WTEMP,THETA

```

- \* This FFT subroutine is taken from page 394 of the book
- \* Numerical Recipes
- \* The Art of Scientific Computing
- \* Press et al
- \* Cambridge University Press
- \* 1986

```

      N=2*NN
      DO 3 I=1,N
3     DATA(I) = (1/SQRT(NN))*DATA(I)
      J=1
      DO 11 I=1,N,2
      IF(J.GT.I)THEN
        TEMPR=DATA(J)
        TEMPI=DATA(J+1)
        DATA(J)=DATA(I)
        DATA(J+1)=DATA(I+1)
        DATA(I)=TEMPR
        DATA(I+1)=TEMPI
      ENDIF
      M=N/2
1     IF ((M.GE.2).AND.(J.GT.M)) THEN
        J=J-M
        M=M/2
        GO TO 1
      ENDIF
      J=J+M
11    CONTINUE
      MMAX=2
2     IF (N.GT.MMAX) THEN
        ISTEP=2*MMAX
        THETA=6.28318530717959D0/(ISIGN*MMAX)
        WPR=-2.D0*DSIN(0.5D0*THETA)**2
        WPI=DSIN(THETA)
        WR=1.D0
        WI=0.D0
        DO 13 M=1,MMAX,2
          DO 12 I=M,N,ISTEP
            J=I+MMAX
            TEMPR=SNGL(WR)*DATA(J)-SNGL(WI)*DATA(J+1)
            TEMPI=SNGL(WR)*DATA(J+1)+SNGL(WI)*DATA(J)
            DATA(J)=DATA(I)-TEMPR
            DATA(J+1)=DATA(I+1)-TEMPI
            DATA(I)=DATA(I)+TEMPR
            DATA(I+1)=DATA(I+1)+TEMPI
12         CONTINUE
            WTEMP=WR
            WR=WR*WPR-WI*WPI+WR
            WI=WI*WPR+WTEMP*WPI+WI
13        CONTINUE
          MMAX=ISTEP
        GO TO 2

```

```

ENDIF
RETURN
END

```

```

Subroutine Bnd(x,spec,n,f1,f2,dt)
real x(n),spec(2*n)
Integer f1pos,f2pos,i,j,taper1,taper2,temp1,temp2
data pibytwo/1.5708/

```

- \* This subroutine filters the spectrum of the seismogram
- \* The edges of the window take the form of a sin squared function.
- \* The falloff is over one octave.
- \* The sampling frequency of the data is 14.28 Hz

```

    sampfreq = 1.0/dt

```

- \* The position of the high and low frequency cut-off positions
- \* is calculated here

```

    f1pos = int((f1/sampfreq*n)+1)

```

```

    f2pos = int((f2/sampfreq*n)+1)

```

- \* The position of the zero amplitude end points is established here
- \* Note - falloff is over one octave

```

    temp2 = int(((f2*2.0)/sampfreq*n)+1)

```

```

    temp1 = int(((f1/2.0)/sampfreq*n)+1)

```

- \* The number of data points over which the falloff occurs
- \* is calculated here. These values are used to normalise
- \* the falloff of the sin curve.

```

    taper2 = temp2-f2pos

```

```

    taper1 = f1pos-temp1

```

- \* Check to ensure a falloff of 1 octave can be maintained
- \* on both sides of the window

```

    if(temp2.ge.n/2+1) then

```

```

        write(*,*) 'High frequency cutoff is too high'

```

```

        goto 155

```

```

    endif

```

```

    if(taper1.le.1) then

```

```

        write(*,*) 'Low frequency cutoff is too low'

```

```

        goto 113

```

```

    endif

```

- \* Place real components into a matrix

- \* Note to conserve memory the original matrix (say V1) is destroyed
- \* by this operation

```

    do 93 i=1,n

```

```

    93      x(i) = spec((2*i)-1)

```

- \* Filter the real components by setting the stop band amplitudes to
- \* zero

```

    do 106 i = 2,temp1

```

```

    106      x(i) = 0.0

```

- \* Each discreet entry in the amplitude spectrum within the
- \* window is now scaled by a factor of  $\sin^2(j/\text{taper})$

```

    j = 1

```

```

    do 112 i=temp1+1,f1pos

```

```

        x(i) = sin(j*pibytwo/taper1)*sin(j*pibytwo/taper1)*x(i)

```

```

112     j = j-1
113     j = taper2
        do 116 i=f2pos,temp2
            x(i) = sin(j*pi/2/taper2)*sin(j*pi/2/taper2)*x(i)
116     j=j-1
        do 120 i=temp2+1,n/2+1
120     x(i) = 0.0
*Calculate mirror image for reals
        do 122 i = n/2+2,n
122     x(i) = x(n-i+2)
*Place real comp of filtered spectrum into original matrix
        do 123 i = 1,n
123     spec((2*i)-1) = x(i)
*Place imag comps into matrix
        do 133 i = 1,n
133     x(i) = spec(2*i)
*Filter the imag components (Same logic as for the reals)
        if(taper1.le.1) goto 148
        do 142 i = 2,temp1
142     x(i) = 0.0
            j = 1
            do 145 j=temp1+1,f1pos
                x(i) = sin(j*pi/2/taper1)*sin(j*pi/2/taper1)*x(i)
145     j = j+1
148     j = taper2
            do 149 i=f2pos,temp2
                x(i) = sin(j*pi/2/taper2)*sin(j*pi/2/taper2)*x(i)
149     j=j-1
            do 152 i=temp2+1,n/2+1
152     x(i) = 0.0
            do 153 i = n/2+2,n
153     x(i) = -x(n-i+2)
*Place imag comp of filtered spectrum into original matrix
        do 154 i = 1,n
154     spec(2*i) = x(i)
155     continue
        return
        end

```

C\*\*\*\*\*

```

Subroutine Veldis(nr0,v1,v2,v,work,nlast,dt
,plomon,plopri,tlengt,ylengt,xmaxwi,ymaxwi,fn,ff)

```

```

real v1(nlast),v2(nlast),v(nlast),work(nlast)
real dt,tlengt,ylengt,xmaxwi,ymaxwi
integer out,plomon,plopri,nr0,nlast
character ch*20,fn*20,ff*60

```

c This subroutine converts the velocity record to a displacement  
c record by performing numerical integration followed by least  
c squares linear trend removal on each component. This option was never



```

o used in the current study.
  call integ(v1,work,nlast-2,dt)
  call trend(v1,nlast-2)
  call integ(v2,work,nlast-2,dt)
  call trend(v2,nlast-2)
  call integ(v,work,nlast-2,dt)
  call trend(v,nlast-2)
o Call plot software.
100 format(a)
105 format(a60)
  write(nr0,*) 'Do you want to plot 3-comp d'splacement? (y,n)'
  read(nr0,100) ch
  if(ch.eq.'n') go to 11
  write(*,*) 'Enter the title of the graph'
  write(*,*) 'Eg.: Rumania 13/07/89 (BPI) Displacement'
  read(*,105) ff

o Initialize Plot 88
9  write(nr0,*) 'Define the output device for plot'
  write(nr0,*) 'monitor out =1 ; printer out =2 '
  write(nr0,*) 'ENTER out '
  read(nr0,*) out
  if(out.ne.1.and.out.ne.2) goto 9
  if(out.eq.1) call plots(0,plomon,plomon)
  if(out.eq.2) call plots(0,0,plopri)

  fn = 'Vertical '
  call plsel(out,work,v1,r1last,dt,tlengt,ylengt,xmaxwi,ymaxwi
  ,fn,ff,1,0,0,'n')
  fn = 'North/South '
  call plsel(out,work,v2,r1last,dt,tlengt,ylengt,xmaxwi,ymaxwi
  ,fn,ff,2,0,0,'n')
  fn = 'East/West '
  call plsel(out,work,v,nlast,dt,tlengt,ylengt,xmaxwi,ymaxwi
  ,fn,ff,3,0,0,'n')
  call plot(0,0,0,0,999)
11 continue
  return
  end

```

C\*\*\*\*\*

```

Subroutine Integ(X,Y,N,DT)
REAL X(N),Y(N)

```

c This is a simple numerical integration subroutine to convert  
c the velocity record to a displacement record

```

  Y(1)=0.
  DO 1 I=1,N
  II=I+1
1  Y(II)=Y(I)+X(I)*DT+0.5*(X(II)-X(I))*DT
  DO 2 I=1,N
2  X(I)=Y(I)

```

```

RETURN
END
C*****
Subroutine Trend(X,N)
C Least squares linear trend removal subroutine
DIMENSION X(N)
FN=FLOAT(N)
S=0.
DO 1 I=1,N
1 S=S+X(I)
SK=0.
DO 2 I=1,N
2 SK=SK+X(I)*FLOAT(I)
RNN1=FN*(FN-1.)
RNN21=FN*(FN*FN-1.)
C0=(2.*(2.*FN+1.)*S-6.*SK)/RNN1
C1=(12.*SK-6.*(FN+1.)*S)/RNN21
DO 3 I=1,N
3 X(I)=X(I)-C0-C1*(FLOAT(I)-1.)
RETURN
END
C*****
Subroutine Rotr
.(nr0,v2,v,work,nlast,dt,plomon,plopri,tlengt,ylengt,xmaxwi,
.ymaxwi,fn,az,ff)
real v2(nlast),v(nlast),work(nlast)
character ch*20,fn*20,ff*60,ch1*1
integer out,plomon,plopri

cThis subroutine operates on the NS (V2) and EW (V) components.
c The user entered value of the BA' azimuth is used to convert
c these components to radial and t ransverse components. V2 becomes
c the radial component while V becomes the transverse component.
do 1 I=1, nlast-2
RR = -(v2(I)*cos(az)+v(I)*sin(az))
TT = -v(I)*cos(az)+v2(I)*sin(az)
v2(I) = RR
1 v(I) = TT

cPlot software called here
100 format(a)
105 format(a60)
write(nr0,*)
.' Do you want to plot R-radial and T-transverse component? (y,n)'
read(nr0,100) ch
if(ch.eq.'n') go to 11
write(*,*) 'Is a new title required for the graph'
write(*,*) 'Enter (y) if graphics were not called in FILTER'
read(*,100) ch1
if(ch1.ne.'y') goto 9

```

```

write(*,*) 'Enter the title of the graph'
read(*,105) ff

c Initialise Plot88 software
9 write(nr0,*) 'Define the output device for plot'
write(nr0,*) 'monitor out =1 ; printer out =2 '
write(nr0,*) 'ENTER out '
read(nr0,*) out
if(out.ne.1.and.out.ne.2) goto 9
if(out.eq.1) call plots(0,plomon,plomon)
if(out.eq.2) call plots(0,0,plopri)

fn = 'Radial '
call p1sel(out,work,v2,nlast,dt,tlengt,ylengt,xmaxwi,ymaxwi
,fn,ff,1,0.0,'n')
fn = 'Transverse '
call p1sel(out,work,v,nlast,dt,tlengt,ylengt,xmaxwi,ymaxwi
,fn,ff,2,0.0,'n')
call plot(0.0,0.0,999)

11 continue
return
end

C*****
Subroutine Calce(v1,v2,iparr,dt,ainode,np)
real v1(np),v2(np)
integer time,j,loop
real q,r,z,zr,a,b,c,z2,r2,rz,disc,root1,root2,l
character ch1*1

cThis subroutine calculates the angle of emergence between L
c and the radial direction R after the method of Vinnik et al
c (1983) which is in fact the method of Husebye et al (1975).
c Reference to this paper will have to be made to follow logic
c of this subroutine.
100 format(a)

cCalculate the number of data points representative of the main
c P wave arrival.
10 write(*,*) 'Enter the duration time of the main P'
write(*,*) 'arrival'
read(*,*) q
time = int(q/dt)
loop = iparr+time

c Note- the parameter IPARR was determined in the PARAM subroutine
c initialise loop variables to zero
z2=0
r2=0
rz=0

cCalculate the averages

```

```

do 12 j=iparr,loop
  z2 = z2 + v1(j)*v1(j)
  r2 = r2 + v2(j)*v2(j)
  rz = rz + v1(j)*v2(j)
12 continue
z=float(z2/time)
r=float(r2/time)
zr=(float(rz/time))*(float(rz/time))
c Establish u, b and c for the quadratic formula
a=1.0
b= -(z+r)
c = (z*r-zr)
cCalculate the appropriate roots
disc = b*b - 4*a*c
if (disc.le.0) then
  write(*,*) 'Discriminant less than zero'
  goto 999
endif
disc = sqrt(disc)
root1 = (-b+disc)/2*a
root2 = (-b-disc)/2*a
cCalculate the larger root
l = jmax(root1, root2)
cUse the larger root to calculate the emergent angle
zr = sqrt(zr)
l = l - z
aincde = atan(zr/l)

write(*,*) 'The angle of emergence is ',aincde
write(*,*) 'Would you like to change the P wave duration'
read(*,100) ch1
if(ch1.eq.'y') goto 10
write(*,*) 'Enter aincde'
read(*,*) aincde

999 continue
end

c*****
Subroutine Rotlh
.(nr0,v1,v2,work,nlast,dt,plomon,plopri,tlengt,ylengt,xmaxwi,
.ymaxwi,fn,aincde,ff)
real v1(nlast),v2(nlast),work(nlast)
character ch*20,fn*20,ff*60,ch1*1,na:ne1*12
integer out,plomon,plopri

cThis subroutine operates on the vertical (V1) and radial components
c (V2) and converts them to a component in the principal direction L
c and to a component transverse to this HH. In theory the HH component
c should only contain Sv energy. The L component is stored in V1 while the
c HH component is stored in V2. The emergent angle 'e' is calculated

```

```

c in subroutine CALCE.
  e = aincde
  do 1 l=1,niast-2
    HH = v2(l)*sin(e)-v1(l)*cos(e)
    BAL = v1(l)*sin(e)+v2(l)*cos(e)
    v1(l)=BAL
  1  v2(l)=HH

cProvision is now made to plot the graphs on the screen

100 format(a)
105 format(a60)

write(nr0,*)
' do you want to plot L-radial and H comp? (y,n)'
read(nr0,100) ch
if(ch.eq.'n') go to 11

write(*,*) 'Is a new title required for the graph'
write(*,*) 'Enter (y) if graphics where not called in FILTER'
read(*,100) ch1
if(ch1.ne.'y') goto 9
write(*,*) 'Enter the title of the graph'
read(*,105) ff

cinitialise the plot88 software
9 write(nr0,*) 'Define the output device for plot'
write(nr0,*) 'monitor out =1 ; printer out =2 '
write(nr0,*) 'ENTER out '
read(nr0,*) out
if(out.ne.1.and.out.ne.2) goto 9
if(out.eq.1) call plots(0,plomon,plomon)
if(out.eq.2) call plots(0,0,plopri)

fn = 'L-Component '
call plsei(out,work,v1,niast,dt,tlengt,ylengt,xmaxwi,ymaxwi
,fn,ff,1,0.0,'n')
fn = 'H-Component '
call plsei(out,work,v2,niast,dt,tlengt,ylengt,xmaxwi,ymaxwi
,fn,ff,2,0.0,'n')
call plot(0.0,0.0,999)
11 continue

return
end
c*****
Subroutine Cross
.(nr0,v1,v2,v,auto,work,niast,dt,plomon,plopri,tlengt,ylengt,
.xmaxwi,ymaxwi,fn,ff,iparr)
real v1(niast),v2(niast),v(niast),L:uto(niast),work(niast)
character ch*20,fn*20,ff*60,fsta*20,ch1*1,ch2*1,name1*20

```

Integer out,plomon,plopri

cThis subroutine calculates the standardized H component. It  
c effectively calculates the cross correlation of the H and L  
c components, normalised with respect to the energy of the L  
c component

```
write(nr0,*) 'ENTER length of P-pulse sec'
read(nr0,*) pleng
ipleng = int(pleng/dt) + 1
write(nr0,*) 'ipleng=',ipleng,'iparr=', iparr
```

cCalculate the energy of the L component

```
snorm = 0.0
do 1 i = iparr, iparr + ipleng - 1
1 snorm = v1(i) * v1(i) + snorm
```

cCalculate the normalised cross correlation of the L and H components.

```
do 2 j=1,nlast-2-ipleng+1
s = 0.0
s2=0.0
do 3 i=iparr,iparr+ipleng-1
s = v2(i+j-iparr)*v1(i) + s
3 s2 = v1(i+j-iparr)*v1(i) + s2
work(j)=s2/snorm
2 v(j) = s/snorm

do 4 j =nlast-2-ipleng+2,nlast-2
work(j)=0.0
4 v(j) = 0.0
```

cWrite L's autocorrelation back into the matrix V1 noting the auto-  
ccorrelation peak position

```
do 10 i=1,nlast-2
10 v1(i)=work(i)
Lmax=v1(1)
mmm=1
do 5 l=iparr-50,iparr+ipleng
if(v1(l).ge.Lmax) then
Lmax=v1(l)
mmm=l
5 endif
write(*,*) 'L - component maximum at ', mmm
```

cCall plot software

```
100 format(a)
105 format(a60)
```

```
write(nr0,*)
```

```

.' Do you want to plot a HH- component ? (y,n)'
read(nr0,100) ch
if(ch.eq.'n') go to 11

write(*,*) 'Is a new title required for the graph'
write(*,*) 'Enter (y) if graphics were not called in FILTER'
read(*,100) ch1
if(ch1.ne.'y') goto 9
write(*,*) 'Enter the title of the graph'
read(*,105) ff

```

c Initialize Plot88

```

9 write(nr0,*) 'Define the output device for plot'
write(nr0,*) 'monitor out =1 ; printer out =2 '
write(nr0,*) 'ENTER out '
read(nr0,*) out
if(out.ne.1.and.out.ne.2) goto 9
if(out.eq.1) call plots(0,plomon,plomon)
if(out.eq.2) call plots(0,0,plopr1)

fn = 'H'-Component '
call p1sel(out,work,v,nlast,dt,tlengt,ylengt,xmaxwi,ymaxwi
,fn,ff,2,ymax,ch2)
fn = 'L'-Component '
call p1sel(out,work,v1,nlast,dt,tlengt,ylengt,xmaxwi,ymaxwi
,fn,ff,1,ymax,ch2)
call plot(0,0,0,0,999)

```

cProvision is made at this stage to write out the required H and L  
c components.

cThe auto-correlation maximum of the L component will be at a time  
c given by mmm. The following algorithm shifts the H-component  
c matrix so that all arrivals relative to this time will be relative  
c to a matrix address of 200 or 14 seconds (ie. L(mmm) is shifted to  
c L(200) with a corresponding shift in H()

```

11 write(nr0,*)
.' Do you want to save the HH-component ? (y,n)'
read(nr0,100) ch
if(ch.eq.'n') go to 12

```

```

      ill=200-mmm
      do 400 i=1,nlast
        work(i)=v1(i)
400      auto(i)=v(i)

      if (ill.ge.0) then
        do 401 i=1,nlast-ill
          v1(i+ill)=work(i)
401      v(i+ill)=auto(i)
      do 402 i=1,ill
        v1(i)=0.0

```

```

402          v(i) = 0.0
do 403 i=nlast-iii+1,nlast-2
          v1(i)=0.0
403          v(i) = 0.0
endif

if (iii.lt.0) then
  jjj=-1*iii
do 404 i=jjj+1,nlast-2
          v1(i+iii)=work(i)
404          v(i+iii)=auto(i)
do 405 i=1,|jjj|
          v1(i)=0.0
405          v(i)=0.0
do 406 i=nlast-2+iii,nlast-2
          v1(i)=0.0
406          v(i)=0.0
endif

140 format(f8.3,5x,f10.3)
v1(nlast-1)=mmm

write(nr0,*) ' ENTER FILE NAME - H seismogram'
read(nr0,100) fsta
open(2,file = fsta)
write(2,140) (i*0.07,v(i),i=1,nlast-2)
close(2)

write(nr0,*) ' ENTER FILE NAME - L seismogram'
read(nr0,100) fsta
open(2,file = fsta)
write(2,140) (i*0.07,v1(i),i=1,nlast-1)
close(2)
12 continue
return
end

```

c\*\*\*\*\*

```

Subroutine Plsel(out,x,y,n,dt,tlengt,ylengt,xmaxwi,ymaxwi
,fn,ff,|jj|,delta,chdelt)
  real dt,tlengt,ylengt,xmaxwi,ymaxwi,delta
  real x(n),y(n)
  Integer out,|jj|,n
  character tekst*13,fn*20,ff*60,chdelt*1

```

cThis subroutine initialises and plots the graphs required at  
c various places in the main program. Use is made of the PLOT88  
c and DRIVE88 libraries which must be declared at compile time.  
c Obviously the program can be run without an on screen graph ever  
c being called. Thus this subroutine is separate from the main program  
c and no attempt will be made to comment on it in any detail here.



c Hard copy routines were written for original 'ancient' IBM type  
c printers. They should work provided initialization is performed  
c correctly in FILON.FOR.

```

inc = 1
if(out.eq.2) tiengt=6
if(out.eq.2) ylengt=2
do 1 i = 1, n-2
1      x(i) = dt*(i-1)
      x(n-1) = x(1)
      x(n) = (x(n-2)-x(1))/tiengt

if(jj.eq.1) then
      tekst='T I M E sec'
else tekst='
endif

kt=0
dts=dt
st=10,
3  dts = dts * st
   kt = kt + 1
   if(dts.gt.1.) go to 4
   go to 3
4  kt=kt-2
   if(kt.gt.2) then
       kt=kt-2
       tekst='T I M E msec'
   endif
if(out.eq.1) ymaxwi = 1.2 * ymaxwi
call window(0.,0.,xmaxwi,ymaxwi)
cRedefine a new origin
plone1 = 1.4*ylengt*(jj-1) + 1.5
if(out.eq.1) call plot(2.5,plone1,-3)
plone2 = 3.3/2.*ylengt*(jj-1) + 1.4
if(out.eq.2) call plot(plone2,0.7,-3)
      qwert=3.E
      call symbol(0.4,ylengt-0.1,0.3,ff,0.,50)
cPlot the graphs
if(out.eq.1) call staxis(0.25,0.3,0.2,0.2,kt)
if(out.eq.2) call staxis(0.11,0.2,0.2,0.25,kt)
call scale(y,ylengt,n-2,inc)
if(chdelt.eq.'y') y(n) = delta
if(chdelt.eq.'y') y(n-1) = -y(n)
if(out.eq.1)
.call axis(0.0,0.0,tekst,-13,tiengt,0.,x(n-1),x(n))
if(out.eq.2)
.call axis(ylengt,0.0,tekst,-13,tiengt,90.,x(n-1),x(n))
      ndeca = 1
      if(abs(y(n-1)).le.0.01) ndeca=2
if(out.eq.1) call staxis(0.22,0.3,0.3,0.25,ndeca)
if(out.eq.2) call staxis(0.11,0.2,0.2,0.25,ndeca)

```

```

tekst='
if(out.eq.1)
.call axis(0.0,0.0,fn,13,ylengt,90.,y(n-1),y(n))
if(out.eq.2)
.call axis(ylengt,0.0,fn,13,ylengt,180.,y(n-1),y(n))

if(out.eq.1) call line(x,y,n-2,inc,0,0)
if(out.eq.2) then
do 41 i=1,n-2
41  y(i) = - y(i)
    call line(y,x,n-2,inc,0,0)
do 42 i=1,n-2
42  y(i) = - y(i)
endif
return
end

c*****
      Program Tps
* A program to calculate the time interval between p and psv arrivals
* with the angle of emergence at the base of the crust a user entered
* parameter. Velocities are based on the lasp91 model from the 1991
* IASPEI Seismological Tables. The depth corresponding to
* matrix element i is i*10.0 km.
      real x,a,rayp,deltar,newang,origang,dum1,dum2
      real pve(100),svel(100),vpint(100),vsint(100),time(100),temp(100)
      integer r,
      character name*20
100  format(a)
* Read in incident angle at the base of the crust
13  write(*,*) 'Enter the incident angle at the base of the crust in
      .degrees. Enter 0. to exit program.'
      read(*,*) newang
      newang=newang+.0174533
      if (newang.eq.0.) stop
      write(*,*) 'Enter the output filename'
      read(*,100) name
      open(20,file = name)
* Earth's radius (a) = 6371km
* Radial distance (from the earth's surface) = r*10.0
* Calculate the velocity model
      a = 6371.0
      do 9 r = 1,2
          pvel(r) = 5.8
          svel(r) = 3.36
9
      pvel(3) = 6.8
      svel(3) = 3.75
      do 15 r = 4,12
          x = (a-r*10.0)/a
          pvel(r) = 8.7854 - 0.7495*x
15          svel(r) = 6.7062 - 2.2486*x

```

```

do 16 r = 13,21
  x=(a-r*10.0)/a
  pvel(r) = 25.4139-17.6972*x
  svel(r) = 5.7502 - 1.2742*x
16 do 17 r = 22,41
  x=(a-r*10.0)/a
  pvel(r) = 30.7876 - 23.2541*x
  svel(r) = 15.2421 - 11.0855*x
17 do 20 r = 42,66
  x=(a-r*10.0)/a
  pvel(r) = 29.3889 - 21.4066*x
  svel(r) = 17.7073 - 13.5065*x
20 do 21 r = 67,76
  x=(a-r*10.0)/a
  pvel(r) = 25.9698 - 16.9341*x
  svel(r) = 20.7689 - 16.5314*x
21
*Calculate the travel time along the ray path for an angle
* of 0.4567 at the base of the crust. This corresponds to an epicentral
* distance of 67 deg (Menahem and Singh p482). The process is then
* repeated for the user defined base of crust.
  origang=0.4567
  deltar=10.
  do i=0,76
    vpint(i)=0.
    vsint(i)=0.
    temp(i)=0.
    time(i)=0.
  enddo
  rayp=sin(origang)*(a-40.)/pvel(4)
  do r=1,76
    dum1=sqrt(1./svel(r)**2.-(rayp/(a-r*10.))**2.)*deltar
    vsint(r)=vsint(r-1)+dum1
    dum2=sqrt(1./pvel(r)**2.-(rayp/(a-r*10.))**2.)*deltar
    vpint(r)=vpint(r-1)+dum2
  enddo
  do r=1,76
    temp(r)=vsint(r)-vpint(r)
  enddo

  rayp=sin(newang)*(a-40.)/pvel(4)
  do r=1,76
    dum1=sqrt(1./svel(r)**2.-(rayp/(a-r*10.))**2.)*deltar
    vsint(r)=vsint(r-1)+dum1
    dum2=sqrt(1./pvel(r)**2.-(rayp/(a-r*10.))**2.)*deltar
    vpint(r)=vpint(r-1)+dum2
  enddo
  do r=1,76
    time(r)=vsint(r)-vpint(r)-temp(r)
  enddo
86 format(14,3x,f8.3)
do 85 r = 0,76,4

```

```

85      write(20,86) r,time(r)
      close(20)
      goto 13
      end

```

```

*****

```

### Program Pcstack

\*A program to delay and sum many seismic traces for a single  
\* station.

```

      parameter (nlast = 1850,ndepth=20,nseis=10)

```

```

      real tdelay(nseis,ndepth),v1(nlast),v(nseis,nlast),
      .work(nlast-400),v2(nlast-400)
      real dt,avg
      common /temp1/v,/temp2/tdelay,v1,work
      integer plomon,plopri,out,i,j,k,l,nse,time,points
      character*12 name1(nseis),name2(nseis),list1*12,list2*12
      character ch1*3,ch2*2,ch3*5,ch8*8,res*1,fn*20,ff*60

```

\*Constants for plot88. The name nomenclature as used in FILON  
\* is used here.

```

*Number of monitor = plomon,number of printer = plopri.
      data plomon/91/,plopri/5/,xmaxwi/42.0/ymaxwi/12.0/
      data tlengt/18.0/,ylengt/6.0/
      ch8='

```

\*Define the sampling period.  
dt = 0.07

```

10  format(i2)
100 format(a)
101 format(f8.3)
102 format(13x,f10.3)
104 format(f8.3,2x,f8.3)
105 format(10x,f8.3)
106 format(a60)
107 format(a12)
108 format(7x,f8.3)

```

```

      write(*,*) 'Do you wish to go straight to graphics'
      read(*,100) res
      if(res.eq.'y') goto 145
      write(*,*) 'Enter the station name eg. BPI'
      read(*,100) ch1
      write(*,*) 'Enter the name of the H-comp file list'
      read(*,107) list1
      open(200,file = list1)
      write(*,*) 'Enter the name of the time-delay file list'
      read(*,107) list2
      open(201,file = list2)

```

\*Enter the number of seismograms

```

write(*,*) 'How many seismograms are to be stacked'
read(*,*) nse

*Enter the H component seismogram data. These files are generated in
* program FILON. All data are stacked relative to an origin coinciding
* with a matrix address j = 200.
do 30 i=1,nse
    write(*,*) 'Entering seismogram filename ',i
    read(200,100) name1(i)
30    write(*,100) name1(i)
    close(200)

*Enter the name of the time delay files. Note these files must be
* entered in an order so that they correspond with the respective
* seismogram
do 40 i=1,nse
    write(*,*) 'Entering time-delay file ',i
    read(201,100) name2(i)
40    write(*,100) name2(i)
    close(201)

*Read in the two data sets
*The stacked H component seismograms-
do 50 i=1,nse
    open(i,file = name1(i))
    do 55 j=1,nlast-2
55        read(i,102) v(i,j)
50    close(i)
* and the time delays.
do 60 i=1,nse
    open(i,file = name2(i))
    do 65 j=1,ndepth
65        read(i,108) tdelay(i,j)
60    close(i)
    write(*,*) 'Data input complete'

*Convert the time delays to data point delays.
do 70 i=1,nse
    do 75 j=1,ndepth
75        tdelay(i,j) = (tdelay(i,j)/dt)
70    continue

*Calculate the average to 'normalise' the weight of each seismogram
write(*,*) 'Stacking commenced'
avg = 1/float(nse)
*Depth stacking is performed for a number of trial phasing depths.
do 80 i=1,ndepth
    write(ch2,10) (i-1)*4
    ch3=ch1//ch2
    write(*,100) ch3
do 78 l=1,nlast-2
78        v1(l) = 0.0

```

```

do 90 j=1,nse
      time = int(tdelay(j,i))
do 110 k=200,nlast-200
110   v1(k-199) = v(j,k+time)*avg + v1(k-199)
90   continue
      open(i,file = ch3)
      write(i,'(a)') ch2
      do 120 k=1,nlast-400
      tt=(k-1)*0.07
120   write(i,104) tt,v1(k)
      close(i)
80   continue

```

## \*Graphics applications

```

145  write(*,*) 'Do you wish for graphics output of one of
      write(*,*) 'the files ,y(es) or n(o)'
      read(*,100) res
      if(res.ne.'y'.and.res.ne.'n') goto 145
      if(res.eq.'n') goto 500
150  write(*,*) 'Enter filename'
      read(*,100) ch3
      open(50,file = ch3)

      do 160 i=1,nlast-402
160   read(50,105) v2(i)

      write(*,*) 'Enter the title of the graph'
      read(*,106) ff
      fn=ch3//ch8
165  write(*,*) 'Define the output monitor'
      write(*,*) 'Monitor = 1,plotter = 2'
      read(*,*) out
      if(out.ne.1.and.out.ne.2) goto 165
      if(out.eq.1) call plots(0,plomon,plomon)
      if(out.eq.2) call plots(0,0,plopri)

      points=nlast-400

      call pisel(out,work,v2,points,dt,tlengt,ylengt,xmaxwi,ymaxwi,
      .fn,ff,1,0.0,'n')
      call plot(0.0,0.0,0.999)

170  write(*,*) 'Do you wish to plot another file- y,n)'
      read(*,100) res
      if(res.ne.'y'.and.res.ne.'n') goto 170
      if(res.eq.'y') goto 150
      if(res.eq.'n') goto 500

500  continue

      end

```

```

*****
Program Selsgraf2
***          SEISGRAF          ***
*** Seismic Plotting Program ; Commissioned by De Beers ***
***          G.R.J.Cooper(%@) June'90 G          ***

```

c(%@) - Modified by P A Cattermole to be compatible with the  
c requirements of the current study.

#### \$STORAGE:2

\*This program displays the output of the LF, HF and Rf files  
\*generated by the program which performs P-S conversions.  
\*Any other set of files may be displayed provided that all the files  
\*in a set are of the same length (not exceeding 1500 points) and in the  
\*correct format.

```

Integer Option,Npts(20),Traca,NoTraces
Integer Sport,Smodel,Prport,Prmodel,Plport,Plmodel
Character Header(20)*3
Character*1 Str1
Logical Present

```

```

Common NoTraces,Npts,Header
Common /Device/ Sport,Smodel,Prport,Prmodel,Plport,Plmodel

```

\* Read in hardware configuration

\*The file SGRAF.CFG must be present when Selsgrf2 is run. This file  
\*contains the screen and printer configurations for Plot88.

```
4 format(i3,2x,i3,2x,i3,2x,i3,2x,i3,2x,i3)
```

```

Open(7,File='Sgraf.Cfg')
Read(7,4) Sport,Smodel,Prport,Prmodel,Plport,Plmodel
write(*,4) sport,smodel,prport,prmodel,plport,plmodel
Close(7)

```

```

1 write(*,*) 'Options are'
write(*,*) '1 - Read in data'
write(*,*) '2 - Onscreen plot'
write(*,*) '3 - Hard Copy'
write(*,*) '4 - Exit'
write(*,*) 'Enter option'
read(*,*) option

```

```

if(option.eq.1) call dataread
if(option.eq.2) call screenplot
if(option.eq.3) call hardcopy
if(option.eq.4) STOP

```

```

goto 1
end

```

```
*****
```

Subroutine DataRead

```

Integer Npts(20),Trace,N,NoTraces
Character Header(20)*3,FileName*15,Str1*1,name1*15
Real Time(20,1500),Amp(20,1500)
Logical Present

```

```

Common NoTraces,Npts,Header
Common /X/ Time
Common /Y/ Amp

```

\*In this subroutine the data is read into the program. The title that  
 \*will be accorded to each graph is the same as the filename. A check  
 \*routine is included to ensure that the file to be read in exists.

```

write(*,*) ' READ IN SEISMIC DATA '
5  write(*,*) 'Enter the filename containing the records to plot'
   read(*,'(a)') name1
   open(200,file=name1)

write(*,*) 'How many traces do you wish to plot ?'
  read(*,*) NoTraces

Do Trace=1,NoTraces
write(*,*) trace
read(200,'(a)') filename
Inquire(File=Filename,Exist=Present)
If (Present.Eqv..False.) then
write(*,*) 'Warning - no file of that name found.'
Goto 5
End If

write(*,*) 'Reading in the data...'
  Header(Trace) = Filename
  Open(6,File=Filename)
  Read(6,'(a)') Header(Trace)
  write(*,'(a)') Header(Trace)
10 Format(A)
   N=0
20 If (Eof(6).Eqv..False.) then
   N=N+1
   Read(6,*,Err=25,End=25) Time(Trace,N),Amp(Trace,N)
   Goto 20
   End If
25 Continue
  Close(6)

  N=N-1
  write(*,*) N
  Npts(Trace)=N
End do

Close(200)

```



Return  
End

Subroutine ScreenPlot

Integer Npts(20),Trace,NoTraces  
Integer Sport,Smodel,Prport,Prmodel,Plport,Plmodel  
Character Header(20)\*3,XI\*20  
Real MinX,MinY,MaxX,MaxY,Length,Height  
Real xx(20),yy(20),zz(20)  
Real Time(20,1500),Amp(20,1500),TempT(1500),TempA(1500)

Common NoTraces,Npts,Header  
Common /X/ Time  
Common /Y/ Amp  
Common /Temp/ TempT,TempA  
Common /Device/ Sport,Smodel,Prport,Prmodel,Plport,Plmodel

```
10  format(a)
    If (Sport.Eq.97) then      I Ega
    MinX=0.6
    MinY=0.6
    Length=8.2
    Height=6.4
    MaxX=9.4
    MaxY=7.5
    Else if (Sport.Eq.99) then  I Cga
    Leng th=6.9
    Height=4.9
    MinX=0.6
    MinY=0.6
    MaxX=8.0
    MaxY=5.9
    Else                        I Hgc
    MinX=0.6
    MinY=0.6
    Length=7.2
    Height=4.5
    MaxX=8.25
    MaxY=5.45
    End If
```

\*This subroutine produces a rough copy of the graphs on the screen.

\*It is here that the spacing between each graph and axis scale should  
\*be determined.

\*Enter the spacing between each graph

\*NOTE!!!!

\*The spacing between each graph also determines the Y axis length of

\*each graph. Only a limited number of graphs can be produced on an

\*A4 sheet. Hence if two graph sets (on separate pieces) of paper are

\*to be compared directly it is vital that the spacing and scaling

\*factors used are the same for each set.

```

write(*,*) 'Enter the spacing between each graph.'
write(*,*) 'Values between 0.25 and 1.0 are recommended.'
read(*,*) space
write(*,*) 'Calling plots'
Call Plots(0, Sport, Smodel)
write(*,*) 'Plots called ', sport, smodel

```

\*The absolute difference between the maximum and minimum amplitude  
\*for each graph is calculated for scaling purposes.

```

do Trace=1, NoTraces
  xx(Trace)=Amp(Trace,1)
  yy(Trace)=Amp(Trace,1)
  do i=1, Npts(Trace)
    if(Amp(Trace,i).gt.xx(Trace)) then
      xx(Trace)=Amp(Trace,i)
    endif
    if(Amp(Trace,i).lt.yy(Trace)) then
      yy(Trace)=Amp(Trace,i)
    endif
  end do
end do

```

```

do Trace=1, NoTraces
  zz(Trace)=xx(Trace)-yy(Trace)
  write(*,*) Trace, zz(Trace)
end do

```

\*The user can scale the Y axis using any graph. The scaling factor for  
\*all H, R and L component graphs will always be approximately the same.  
\*All other graphs Y axes will be scaled relative the values entered.  
\*Once again these values should be kept the same if other graphs  
\*produced on a different sheet of paper are to be compared.

```

write(*,*) 'Scale with Trace?'
read(*,*) j
write(*,*) j
  do l=1, Npts(j)
    TempA(l) = Amp(j,l)
  end do
write(*,*) 'Entering scale'
call Scale(TempA, space*2, Npts(j), 1)
call Scale(TempT, Length, Npts(j), 1)

```

```

First=TempA(Npts(j)+1)
Delta=TempA(Npts(j)+2)
Frist=TempT(Npts(j)+1)
Detia=TempT(Npts(j)+2)

```

```

write(*,*) 'First =   Delta ='
write(*,*) first, delta
write(*,*) 'Enter your first and delta'

```

```

read(*,*) first,delta

Do Trace=1,NoTraces
do i=1,Npts(Trace)
  TempA(i)=Amp(Trace,i)
  TempT(i)=Time(Trace,i)
end do
  TempA(Npts(Trace)+1)=first
  TempA(npts(Trace)+2)=Delta
  TempT(npts(Trace)+1)=-20.0
  TempT(npts(Trace)+2)=17.5

aaa=float(Trace)-0.5

if(trace.eq.1) then
  Call Plot(0.5,aaa,-3)
  XI='
Call Staxis(0.1,0.1,0.1,0.01,1)
Call Axis(0.0,0.0,XI,-10,Length,0.0,-20.0,17.5)
else
  call plot(0.0,space,-3)
endif

Call Staxis(-0.12,0.15,0.1,-0.0,1)
Call Axis(0.0,0.0,Header(Trace),3,1.0,90.0,first,delta)
Call Line(TempT,TempA,Npts(Trace),1,0,0)
End Do

Call Plot(0.0,0.0,999)
Return
End

Subroutine HardCopy

Integer Npts(20),Trace,Ioport,Hmodel,NoTraces
Integer Sport,Smodel,Prport,Prmodel,Plport,Plmodel
Character Header(20)*3,chr*20
Real MinX,MinY,MaxX,MaxY,Length,space,xx(20),yy(20),zz(20)
Real Time(20,1500),Amp(20,1500)
Real TempT(1500),TempA(1500)

Common NoTraces,Npts,Header
Common /X/ Time
Common /Y/ Amp
Common /Temp/ TempT,TempA
Common /Device/ Sport,Smodel,Prport,Prmodel,Plport,Plmodel

write(*,*) 'Printer output'
write(*,*) 'Printer options must be set in the SGRAF.CFG file'

Pr=1

```

```

If (Pr.Eq.1) then      | Printer output
  Ioport=PrPort
  Hmodel=PrModel
  Length=5.5
  MaxX=9.5
  MinX=0.6
  MinY=0.6
  MaxY=7.7
Else                  | Plotter output
  MinX=0.6
  MinY=0.6
  Ioport=PIPort
  Hmodel=PIModel
  MaxY=9.5
  Length=8.0
  MaxX=9.5
End If

write(*,*) 'Enter the spacing between each graph.'
write(*,*) 'Values between 0.25 and 1.0 are recommended.'
read(*,*) space

call Plots(0,Ioport,Hmodel)

call Simplx
DeltaY=0.4

do Trace=1,NoTraces
  xx(Trace)=Amp(Trace,1)
  yy(Trace)=Amp(Trace,1)
  do I=1,Npts(Trace)
    if(Amp(Trace,I).gt.xx(Trace)) then
      xx(Trace)=Amp(Trace,I)
    endif
    if(Amp(Trace,I).lt.yy(Trace)) then
      yy(Trace)=Amp(Trace,I)
    endif
  end do
end do

do Trace=1,NoTraces
  zz(Trace)=xx(Trace)-yy(Trace)
  write(*,*) Trace,zz(Trace)
end do

write(*,*) 'Scale with Trace?'
read(*,*) j
write(*,*) j
do I=1,Npts(j)
  TempA(I) = Amp(j,I)
  TempT(I) = Time(j,I)
end do

```

```

call Scale(TempA,space*2.0,Npts(j),1)
call Scale(TempT,6.5,Npts(j),1)

First=TempA(Npts(j)+1)
Delta=TempA(Npts(j)+2)
Frist=TempT(Npts(j)+1)
Delta=TempT(Npts(j)+2)
write(*,*) 'First =      Delta ='
write(*,*) first,delta
write(*,*) 'Enter your first and delta'
read(*,*) first,delta

    Call Plot(MaxX-0.5,0.5,-3)
    chr='
Call Staxis(0.1,0.1,0.1,0.01,1)
Call Axis(0.0,0.0,chr,-10,Length,90.0,frist,delta)
Call Plot(-space,0.0,-3)

```

```

Do Trace=1,NoTraces
do i=1,Npts(Trace)
    TempA(i)=-Amp(Trace,i)
    TempT(i)=Time(Trace,i)
    end do
    TempA(Npts(Trace)+1)=first
    TempA(npts(Trace)+2)=Delta
    TempT(npts(Trace)+1)=Frist
    TempT(npts(Trace)+2)=Delta

Call Plot(-space,0.0,-3)
Call Symbol(space*0.45,0.0,0.1,Header(Trace),90.0,15)
Call Staxis(-0.12,0.15,0.1,-0.0,1)
Call Axis(0.0,2.0,chr,-10,1.0,0.0,frist,delta)
Call Line(TempA,TempT,Npts(Trace),1,0,0)
End Do
Call Plot(0.0,0.0,999)
Return
End

```

c\*\*\*\*\*

```

    Program Stk467
cA program to stack stacked records generated using program postack
real depth(2000),data(2000,5),ans(2000)
real tmp
integer dpos
character*12 name(5)
write(*,*) 'How many stacked seismograms do you wish to stack'
read(*,*) n
write(*,*) 'Enter', n, ' seismogram names'
open(10,file='stack.out',status='unknown')
do i=1,n
    read(*,'(a)') name(i)

```

```

open(i,file=name(i),status='unknown')
enddo
do i=1,n
c dpos - the phasing depth being stacked. This is appended at the beginning of the file in
c pstack
    read(i,*) dpos
    do j=1,2000
        read(i,*,e1.d=999)depth(j),data(j,i)
    enddo
999    continue
enddo
cStack and average each output trace
do j=1,2000
    tmp=0.
    do i=1,n
        tmp=tmp+data(j,i)
    enddo
    ans(j)=tmp/n
enddo
write(10, '(i4)')dpos
do j=1,rd
    write(10, '(f8.3,f10.3)')depth(j),ans(j)
enddo
do i=1,n
    close(n)
enddo
close(10)
stop
end

```



**Author: Cattermole Paul Andrew.**

**Name of thesis: Upper mantle discontinuities beneath South Africa- results of the analysis of P-to-S converted phases.**

***PUBLISHER:***

University of the Witwatersrand, Johannesburg

©2015

***LEGALNOTICES:***

**Copyright Notice:** All materials on the University of the Witwatersrand, Johannesburg Library website are protected by South African copyright law and may not be distributed, transmitted, displayed or otherwise published in any format, without the prior written permission of the copyright owner.

**Disclaimer and Terms of Use:** Provided that you maintain all copyright and other notices contained therein, you may download material (one machine readable copy and one print copy per page) for your personal and/or educational non-commercial use only.

The University of the Witwatersrand, Johannesburg, is not responsible for any errors or omissions and excludes any and all liability for any errors in or omissions from the information on the Library website.